Expanding the bionanotechnology toolbox using an engineered bacteriophage M13 platform

by

Anthony Petrie

A thesis
presented to the University of Waterloo
in fulfilment of the
thesis requirement for the degree of
Master of Science
in
Chemistry

Waterloo, Ontario, Canada, 2014

I hereby declare that I am the sole author of this thesis. This is a true copy of the thesis, including any required final revisions, as accepted by my examiners.

I understand that my thesis may be made electronically available to the public.

Abstract

M13 is a filamentous virus which has received recent attention as a component for device and material applications. M13 phages have measurements of approximately 6 nm in width and 900 nm in length. M13 is composed of the coat proteins, pIII, pVI, pVII, pVIII, pXI, of which, the most abundant coat protein, pVIII is present in approximately 2700 copies. In order to further develop M13 as a well-characterized nano-scale scaffold, azide-containing M13 phages capable of bioorthogonal reactions were produced. The approach taken in this work was to metabolically incorporate the unnatural amino acid *L*-azidohomoalanine into the pVIII major coat protein of M13. The positioning of *L*-azidohomoalanine was accomplished using site-directed mutagenesis and the characterization of several M13 mutant strains was carried out. For *L*-azidohomoalanine incorporation, appropriate media conditions had to be developed and tested. It was found that having both *L*-methionine, and its analogue, *L*-azidohomoalanine, in growth media was required to obtain both high M13 yields and *L*-azidohomoalanine incorporation. Two bioorthogonal approaches to labelling the resultant M13-azide constructs were examined: the modified Staudinger ligation and the strain-promoted azide-alkyne cycloaddition reaction. Bioconjugation of M13-azide phages with 5(6)-carboxytetramethylrhodamine, a fluorescent dye molecule, resulted in an estimate of 340 reactive azide groups per phage for the best mutant constructs, A9M and S13M. Transmission electron microscopy confirmed that the architecture of M13 mutant strains developed here were not impacted by bioconjugation of biotin to M13-azide constructs.

Considerable work has been carried out on the pIII minor coat protein of M13 as the functional handle of M13. Rather than be used in place of the methodologies currently used for manipulation of M13, the methods examined in this thesis work are expected to be complementary to those approaches. This is expected to expand upon to methodologies by which researchers currently manipulate and organize structures on the nano-scale.

Acknowledgements

I am immensely grateful for all of the work that Dr. John Honek has put into helping me throughout the course of this project. In particular, I feel like I can say that I have been exposed to and converted to the intersecting field of bionanotechnology through his enthusiasm. I am very glad to have been given the opportunity to work on this project as it has been very satisfying getting it to where it now is.

I would like to thank Dr. Elisabeth Daub for teaching me the microbiological skills required for this project and help in overcoming some of the challenges encountered. I learned a lot of very useful "tricks-of-the-trade" that one would be hard-pressed to find in any manual.

The members of the Honek group whom I would like to thank as well include those I have worked alongside and those who have previously made contributions that motivated this work: Anton van der Ven, Dr. Zhengding Su, Dr. Henry Duewel, Sarah Borg, Natalie Koay, Chris Rowan, David Kim, and Ewa Sitarska.

I would also like to extend thanks to Dr. Richard Smith for giving me the opportunity to work on the instruments in the University of Waterloo Mass Spectrometry Facility. Additionally, the training and help provided by Adrienne Boone and Mishi Groh with regard to transmission electron microscopy was very valuable.

Lastly, I would like to thank my partner, Kerith, for helping me in little ways every day and supporting me when I needed it.

Table of Contents

List of Figures

List of Tables

List of Abbreviations

AA	Amino acid
AARS	Amino acyl tRNA synthetase
Ac	*L*-allylcysteine
Aha	*L*-azidohomoalanine
Ala	Alanine
AMP	Adenosine monophosphate
Anl	*L*-azidonorleucine
Arg	Arginine
Asn	Asparagine
Asp	Aspartate
ATP	Adenosine triphosphate
AuNP	Gold nanoparticle
bp	Base pair
BSA	Bovine serum albumin
CCD	Charge-coupled device
CF	Correction factor
CGSC	Coli Genetic Stock Center
CNT	Carbon nanotube
CuCCA	Cu(I)-catalyzed [3+2] cycloaddition
Cys	Cysteine
ddH_2O	Distilled deionized water
Dfm	*L*-difluoromethionine
DIBAC	Aza-dibenzocyclooctyne
DIBAC-biotin	biotin-PEG_4-aza-dibenzocyclooctyne
DIBAC-TAMRA	5(6)-Carboxytetramethylrhodamine-PEG_4-aza-dibenzocyclooctyne
DMSO	Dimethyl sulfoxide
DNA	Deoxyribonucleic acid
dNTP	Deoxyribonucleotide triphosphate
dsDNA	Double-stranded deoxyribonucleic acid
ESI	Electrospray ionization
ESI-TOF MS	Electrospray ionization time of flight mass spectrometry
F-factor	Fertility factor
Gln	Glutamine
Glu	Glutamate
Gly	Glycine
Hag	*L*-homoallylglycine
His	Histidine
Hpg	*L*-homopropargylglycine
Ile	Isoleucine
IPTG	isopropyl β-*D*-1-thiogalactopyranoside
LB	Luria broth
Leu	Leucine
Lys	Lysine
M9MM	M9 minimal media
MetRS	Methionyl-tRNA synthetase
MetSO	Methionine sulfoxide
MQH_2O	Ultra-pure 18 MΩ·cm resistivity water
MS	Mass spectrometry
MWCO	Molecular weight cut-off

NMR	Nuclear magnetic resonance
PBS	Phosphate-buffered saline
PDB	Protein Data Bank
PEG	Polyethylene glycol
Pfu	Plaque forming unit
Pfu	*Pyrococcus furiosus*
Phe	Phenylalanine
PPi	pyrophosphate
Pro	Proline
SA-AuNP	Streptavidin 5 nm gold nanoparticle
SDS-PAGE	Sodium dodecyl sulfate polyacrylaminde gel electrophoresis
SeMet	*L*-selenomethionine
Ser	Serine
SPAAC	Strain-promoted azide-alkyne cycloaddition
ssDNA	Single-stranded deoxyribonucleic acid
TAMRA	5(6)-Carboxytetramethylrhodamine
TAP	triarylphosphine
TAP-biotin	EZ-link® phosphine-PEG_3-biotin
TBS	Tris-buffered saline
TEM	Transmission electron microscopy
Tfm	*L*-trifluoromethionine
THPTA	Tris(3-hydroxypropyltriazolylmethyl)amine
Thr	Threonine
TMB	Trans-membrane
Tris	Tris(hydroxymethyl)aminomethane
tRNA	Transfer ribonucleic acid
Trp	Tryptophan
Tyr	Tyrosine
UAA	Unnatural amino acid
Val	Valine
w/v	Weight/volume
Wt	Wild-type

1. Chapter 1 - Introduction

1.1 Bionanotechnology

Nanotechnology involves finely manipulating structures at the nano-scale allowing for diverse designs and introduction of a greater variety of chemical functionalities for the fabrication of novel devices (1). Bionanotechnology uses biomolecules such as proteins and DNA as key components in these technological applications. One particular reason for their usefulness is that biomolecules can be manipulated very precisely through molecular biological methods. Some important biotechnological applications that are actively under study include the development of sensors, vehicles for drug delivery and novel ways of producing energy (2-4). "Bottom-up fabrication" is an approach where smaller components come together into a larger structure. As an approach, bottom-up fabrication schemes, while complex and challenging, offer better control over the function and properties of more sophisticated devices (1). Utilizing biological molecules as nano-scale scaffolds are an available toolset to make these approaches work.

In particular, virus-based scaffolds have generated intense interest as technological components. Among the viruses that have been used in nanotechnology are cowpea mosaic virus, tobacco mosaic virus and bacteriophage M13, each with unique architectures (5). The filamentous virus M13, for example, has found use in the fabrication of nano-wires (6, 7), functional materials (8-11), and novel approaches to device fabrication for new solar cells and piezoelectric batteries (9, 10, 12). Utilizing bacteriophage M13 as a material has several advantages including that its structure is well-studied and it can be easily manipulated by altering its genome. M13 is composed of several coat proteins that can be engineered separately from each other, allowing multi-valency. The self-assembly of M13 phages is an efficient process that occurs in the absence of harmful organic solvents, making this a green approach to device design (10). Virus-based scaffolds, as an active area of research, will ultimately give engineers and chemists new tools to work with on the nano-scale.

1.2 Bacteriophage M13 biology

1.2.1 Bacteriophage M13 structure

M13 is a filamentous bacteriophage of the Ff bacteriophage family that is specific for bacteria that contain the fertility factor (F-factor) (13). The F-factor is a plasmid that encodes for pili, filamentous structures used by the bacterium to seek other bacteria for conjugation which is the transfer of genetic material. Additionally, these pili are used by Ff bacteriophages as a receptor to initiate infection (14). This requirement makes M13 infection specific to F-factor containing bacteria. Bacteriophage M13 has a well-defined architecture that is 6 nm in width and has variable length that is dependent upon the amount of single-stranded DNA encapsulated inside M13 (**Figure 1.1**) (13). For wild-type (**Wt**) M13 the typical length is 900 nm (15).

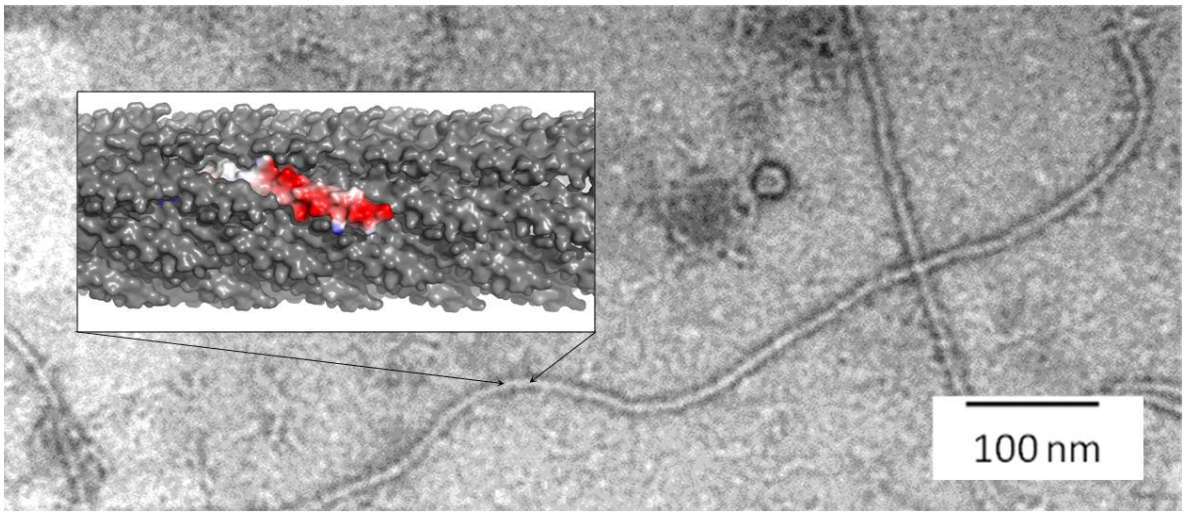

Figure 1.1: Transmission electron microscopy (TEM) image of bacteriophage M13. The inset shows a fibre diffraction structure determined for the packing M13 coat protein pVIII. The structure came from PDB:1IFJ (16)**. The micrograph was produced at the University of Waterloo, Department of Biology TEM facility by Anton van der Ven.**

Bacteriophage M13 is made up of five different coat proteins that encapsulate its single-stranded circular DNA genome (13). As a result of its very stable structure, M13 is tolerant to heat up to 90 ^{o}C, and can resist non-ionic detergents, various proteases, pH changes, and high salt concentrations (17). The four minor coat proteins, pIII, pVI, pVII and pIX, are all present in five copies per phages (**Figure 1.2**). The coat proteins are arranged on assembled M13, such that pIII and pVI are at the opposite pole as pVII and pIX. Spanning the space between is the major coat protein pVIII which is present in approximately 2700

copies and helically arranged around the viral DNA (16). The other genes in the M13 genome that do not encode for coat proteins, encode other proteins necessary for the M13 replication cycle (15).

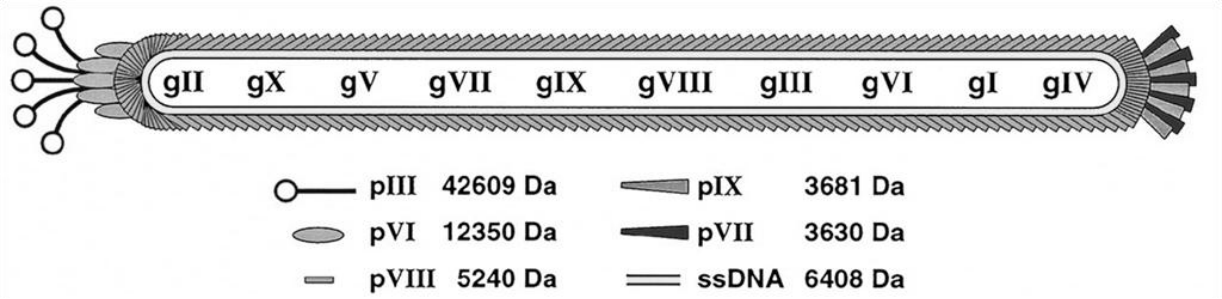

Figure 1.2: Cartoon structure of fd filamentous phage. Image from (18)**.**

1.2.2 Bacteriophage M13 replication cycle

M13 replication has been most well-studied in *Escherichia coli*. While not truly lysogenic, M13 is able to replicate episomally without lysis of its host bacterium. Infected *E. coli* are able to continuously extrude M13 phages resulting in some of the highest yields of any phage at up to 10^{13} plaque forming units (**pfu**) per mL of culture (15). Infection of *E. coli* by M13 starts with binding to the tip of the F-pili which periodically extend and retract, bringing the bound M13 virus close to the bacterial outer membrane (15, 19). The second receptor recognized by pIII is the TolA complex which is bound by M13 in the periplasm of the bacterium (**Figure 1.3**). This binding event is essential for release of M13 into the cell (20). The major coat protein pVIII inserts into the inner membrane at this time and the M13 single-stranded DNA genome is injected into the cell (21).

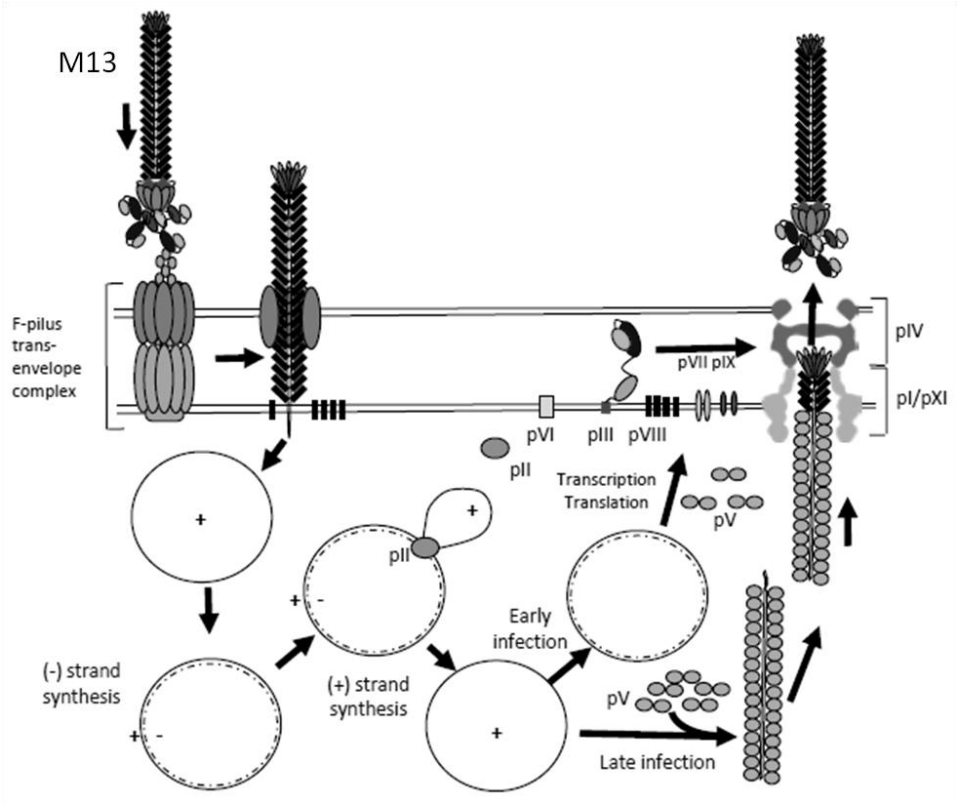

Figure 1.3: Cartoon representation of Ff bacteriophage replication. The image is from (15)**.**

The ssDNA M13 genome is recognized as a substrate by host DNA polymerases and the negative strand is synthesized to produce the double-stranded replicative form of M13 DNA. The M13 protein pII synthesizes additional positive copies of the M13 genome. Using the replicative form of M13 DNA, the host's translational enzymes synthesize the additional proteins required for M13. The proteins pI, pIV and pXI form a membrane-spanning pore through which the M13 assembles and extrudes (**Figure 1.3**). The cytosolic protein pV binds to single-stranded positive M13 DNA guiding it to this pore complex. As it is extruded, the phage coat proteins assemble around the DNA template. When the end of the DNA is reached, the phage is capped by proteins pIII and pVI (15).

1.2.3 M13 Phage Display

Phage display is a very powerful technique whereby peptides with affinity for a particular molecule or material can be discovered. Early examples of phage display were done on coat protein pIII, where a peptide fragment from the restriction endonuclease EcoRI was inserted between two domains on

pIII (22). Later this technique demonstrated that epitopes fused with pIII were recognized by antibodies and did not impair M13 function (23). This technique has also been extended to the display of peptides on the exposed regions of pVIII and pVI (24). By having a library of billions of clones of M13 with randomized displayed peptides one can isolate only those that have affinity for a particular target and through DNA sequencing identify the peptide (**Figure 1.4**). The key to this technology is that infectivity of the phages remains intact after isolating, allowing for subsequent infection of bacteria and amplification of those clones followed by DNA sequencing (24). One of the limitations of phage display is that it is most effective with short peptides. As the length of the randomized peptide increases, the number of possible permutations of a single peptide of fixed length cannot be represented in a library of 1 billion clones (24).

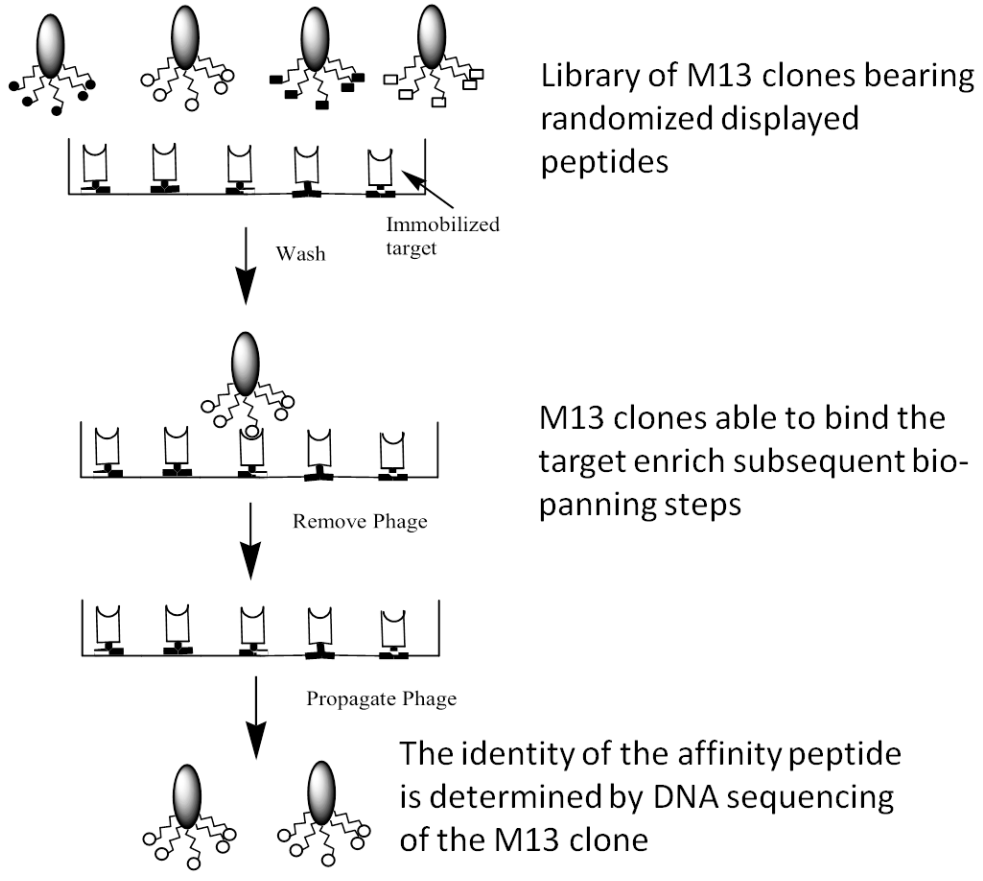

Figure 1.4: A generic overview of bio-panning. Some of the M13 phages bind with various affinities to the target. After, non-specifically bound phages are washed away, the more tightly-bound phages are eluted to re-infect *E. coli*. Several rounds of amplification using increasingly harsh conditions enrich the phage pool in one or more clones that interact with the target.

The process of bio-panning is not limited to finding interactions with biological targets. Phage display has been used to great effect as a technique to discover peptides that have affinity for materials as well. Phage display libraries have been used to find new peptide motifs that bind specifically to carbon nanotubes (**CNTs**) for example (25, 26). Additionally, peptides that can bind to semi-conductor materials have also been discovered using this technique (27). The power of phage display to find peptides bearing affinity for particular targets comes from the diversity of the phage library population itself. Given appropriate selection conditions, phage display has been suggested as something that can outcompete rational design given that a library of phages are sufficiently diverse (24).

1.2.4 M13 pVIII major coat protein

The most abundant coat protein of M13 is the major coat protein pVIII. The protein pVIII is synthesized as pro-pVIII, a 73 amino acid protein with an N-terminal signal sequence to direct it to the bacterial cell membrane (15). At the cell membrane it is cleaved to mature pVIII by leader peptidase, an endogenous *E. coli* membrane protein (28). Mature pVIII is 50 amino acids long and has three major structural domains: residues 1-20 consist of an amphipathic region, residues from 21-39 compose a hydrophobic transmembrane (**TMB**) region, and residues 40-50 compose the DNA-binding region (**Figure 1.5**). The amphipathic region is composed of a solvent-exposed face and an alanine-rich face responsible for hydrophobic interaction between other pVIII in assembled M13 (29). There is strict conservation found in the C-terminal region that is responsible for binding to DNA (29). Mutagenesis studies on pVIII have demonstrated that it is overall highly tolerant to mutations. A minimalist pVIII was constructed where all amino acids except for 9 amino acids were mutated to alanine and retained the ability to incorporate into M13 (30). This demonstrates flexibility and opens up some possibilities for making necessary mutations to M13.

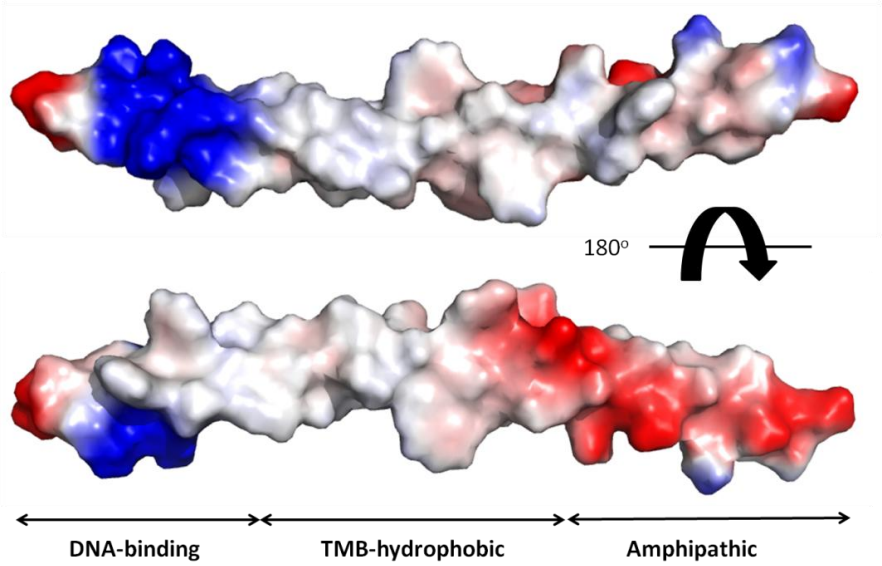

Mkkslvlkasvavatlvp**M**lsfa | aegddpak**a**afnslq**a**sateyigyawa**M**vvvivgatigiklfkkftskas
cut site

Figure 1.5: Structure of pVIII from M13. The surface potential was generated using the vacuum electrostatics function in PyMol (The PyMOL Molecular Graphics System, Version 1.3 Schrödinger, LLC). Blue and red represent positive and negative surface potentials respectively. Based on PDB: 1IFJ (16)**.**

Modification of pVIII has led to interesting applications of M13 in technology and materials science. For example, by genetically engineering M13 to position an exposed tyrosine residue onto pVIII followed by chemical modification, Murugesan *et al.* were able to create photo-responsive nanowire-like structures (11). Extra glutamate residues have been introduced to pVIII to better bind Ag^+ particles electrostatically. These M13 phages were then cross-linked and used to create fibres with antibacterial properties due to the presence of silver (31). Using the same negatively charge M13 mutant, binding of gold nanoparticles (**AuNPs**) increased light absorption in a dye-sensitised solar cell that used M13 as a template structure in the fabrication (12). Utilizing pVIII gives the advantage of thousands of available functional groups per M13 phage and, in combination with the filamentous geometry of M13, has allowed for these novel applications.

1.3 Protein expression with unnatural amino acids

Unnatural amino acids (**UAAs**) are amino acids which exist outside of the 20 canonical amino acids. Reasons for expanding the genetic code to include UAAs include their use as probes to study

protein structure, as bioorthogonally-reactive labels for protein modifications, and to change protein properties, such as enhancing fluorescence in green fluorescent protein (32-36). UAA incorporation is accomplished by manipulating the translational machinery of the microorganism. This is accomplished in two ways typically: (i) through site-specific UAA incorporation where an infrequently used codon is repurposed or (ii) by residue specific incorporation, where an UAA utilizes an existing amino acid codon.

1.3.1 Site-specific unnatural amino acid incorporation

One approach to placing a UAA into a protein is through site-specific incorporation. The typical approach is to introduce an amber stop codon (TAG) in the DNA that codes for the residue position of interest. Normally, this would result in a truncated protein at that position by recognition of the stop codon by prokaryotic release factors (37). By having an UAA attached to suppressor-tRNA instead, a full-length protein is produced with an UAA at that position only (38). These early studies on site-specific incorporation relied on synthesizing the UAA-tRNA *in vitro* and also carrying out protein translation *in vitro*. Normally, attachment of amino acids to tRNA is accomplished by amino acyl tRNA synthetases (**AARS**; **Figure 1.6**). This limitation was overcome by engineering an orthogonal AARS from yeast that catalysed attachment of an UAA to yeast suppressor tRNA (39). Site-specific UAA incorporation was later applied to incorporation of UAAs into M13 proteins utilizing an orthogonal AARS/tRNA pair from *Methanococcus jannaschii* to allow phage display which could utilize an expanded amino acid code including a number of tyrosine analogues (40). An obvious strength to using this approach is that one can precisely position the UAA using an amber stop codon. Some of the drawbacks to this approach include truncated protein products that can occur when the orthogonal suppressor tRNA fails to compete with release factor-1 (41). Despite the strengths of this approach, it can often involve extensive modifications to the host microorganism, and the translational machinery.

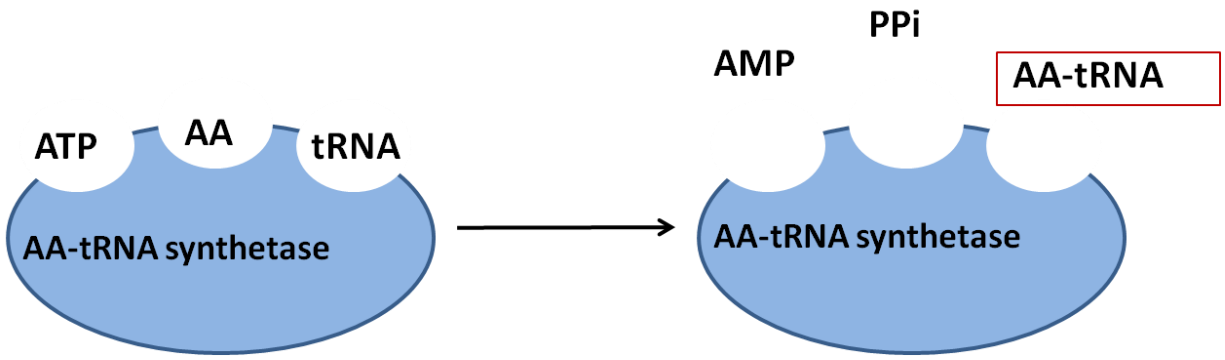

Figure 1.6: Schematic for charging amino acids (AA) onto transfer-RNA (tRNA). Adenosine triphosphate (ATP) is reacted to adenosine monophosphate (AMP) and pyrophosphate (PPi) during the AARS catalysed reaction.

1.3.2 Residue-specific unnatural amino acid incorporation

Residue-specific incorporation of UAAs utilizes the host microorganism's translational machinery, unlike site-specific incorporation where orthogonal AARS are introduced. Methionyl-tRNA synthetase (**MetRS**) in particular is applicable to this approach due to its apparent flexible active site (42). If an UAA is close enough in structure and chemistry to a canonical amino acid, it can be charged onto tRNA by the corresponding AARS (35, 43, 44). Well-known methionine analogues that are documented to incorporate into proteins in place of methionine include *L*-difluoromethionine (**Dfm**), *L*-trifluoromethionine (**Tfm**), *L*-Azidohomoalanine (**Aha**), *L*-homopropargylglycine (**Hpg**), *L*-homoallylglycine (**Hag**), *L*-allylcysteine (**Ac**) and *L*-selenomethionine (**SeMet**) are (**Figure 1.7**) (32, 35, 44-47). Dfm and Tfm are useful as sensitive ^{19}F nuclear magnetic resonance (**NMR**) probes for proteins (32, 45). On the other hand, analogues such as Aha and Hpg provide useful reactive chemical handles to proteins (35, 44, 48). In comparison to Hpg, Aha is a more desirable analogue given that a wider number of chemical reactions can be carried out with it including both Cu(I)-catalysed and Cu(I)-free cycloadditions which are well-known click chemistry tools (49-51).

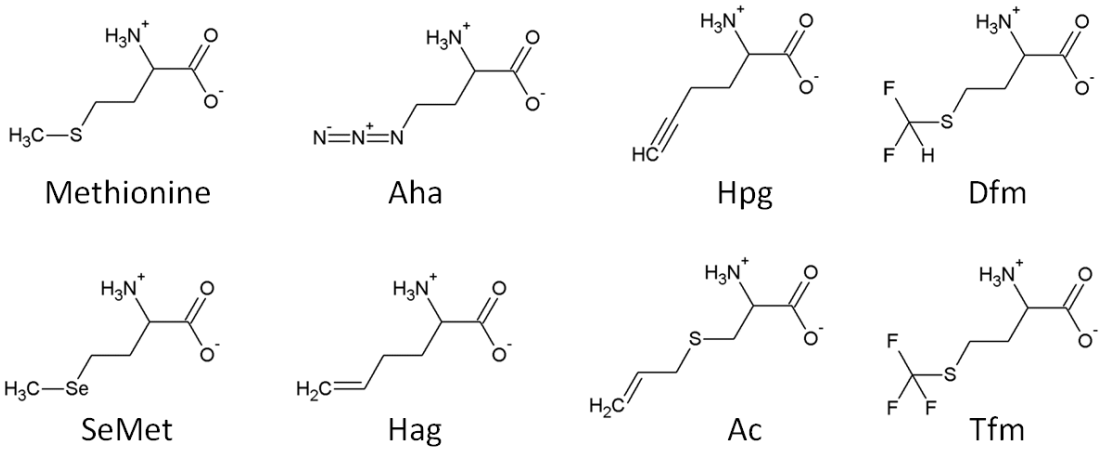

Figure 1.7: Chemical structures of methionine analogues.

The catalytic efficiencies of MetRS with Hpg and Aha as substrates are at least two orders of magnitude less than that of methionine. Since methionine will be the preferred substrate for MetRS, the use of methionine auxotrophs of *E. coli*, strains of *E. coli* that have a genetic block in the biosynthetic pathway to methionine, is necessary for this type of incorporation (35). Additionally, it has been found that over-expession of MetRS helps with incorporation of the UAA in proteins (42). With this in mind, methionine also needs to be mostly removed from any bacterial growth media for successful incorporation of these analogues. Additionally, while an AARS may only recognize a subset of analogues, its active site can be mutated to accept a wider range of substrates as was demonstrated with leucyl-tRNA synthetase (52). Residue specific UAA incorporation offers a powerful technique to modify a protein without extensively modifying the translational machinery of the host organism.

1.4 Bioconjugation strategies with unnatural amino acids

1.4.1 Azide-alkyne [3+2] cycloaddition

The most chemically flexible methionine analogue to incorporate is Aha. It is capable of several different reactions of varying biocompatibility. Likely the least biocompatible of these is the Cu(I)-catalyzed [3+2] cycloaddition (**CuCCA**) due to the tendency of Cu(I) to induce oxidative stress in the cellular environment (53). Recent insight into the role of Cu(I) in the mechanism of the CuCCA reaction though, may lead to future improvements to this chemistry (54). The product of this ligation is a triazole

linking two groups together (**Figure 1.8**) (55). Two main approaches to generate Cu(I) are commonly seen: (i) *in situ* generation of Cu(I) and (ii) direct addition of Cu(I) as $CuBr_{(s)}$ (56). *In situ* generation of Cu(I) has been successful for labelling RNA and protein. In this approach a Cu(I) ligand is necessary to accelerate the reaction as well as a reducing agent, such as ascorbate, to reduce Cu(II) to Cu(I) (56). Additionally, direct addition of CuBr has been used to post-translationally label a protein with a biologically relevant sugar molecule (57).

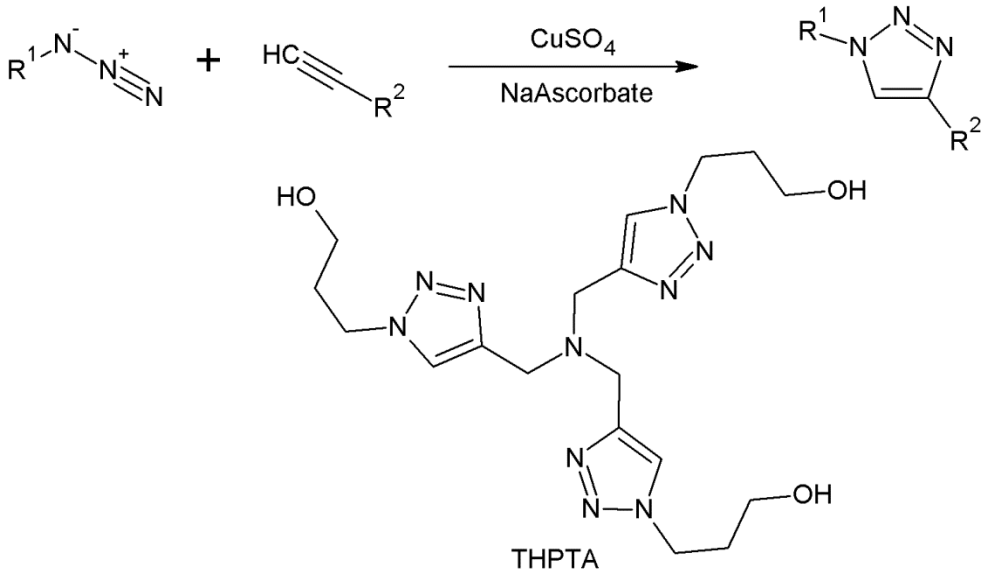

Figure 1.8: Generic reaction scheme for Cu(I)-catalyzed [3+2] cycloaddition. Tris(3-hydroxypropyltriazolylmethyl)amine (THPTA) is a Cu(I) ligand. Reaction conditions are from (56)**.**

1.4.2 Modified Staudinger ligation

The modified Staudinger ligation is another type of ligation chemistry that can be done with Aha-labelled protein and a triarylphosphine (58). The mild conditions of this reaction have allowed it to be used with success in labelling live mammalian cells (**Figure 1.9**). In that study, a biotinylated-phosphine was conjugated to an azide-labelled glycoprotein in a mammalian cell membrane. A drawback noted by the authors was that the triarylphosphine itself did not dissolve well in water. To address this, the authors used polyethylene glycol (**PEG**) to link biotin to the phosphine (50). Recently a traceless Staudinger ligation has been introduced as a technique that can join two peptides, leaving only an amide bond (59). While the Staudinger ligation effectively and specifically reacts with azides, the inability to greatly

improve the kinetics of the reaction motivated Bertozzi and coworkers to try different approaches to bioorthogonal labelling using strained cyclooctynes (60).

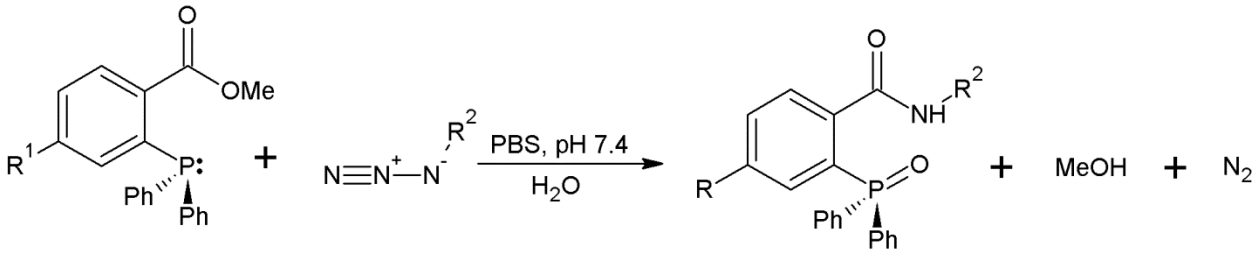

Figure 1.9: Reaction scheme for the modified Staudinger ligation. Reaction conditions from (50)**.**

1.4.3 Strain-promoted azide-alkyne cycloaddition

The Cu(I)-free strain-promoted azide-alkyne cycloaddition (**SPAAC**) reaction is similar to the Staudinger ligation in terms of biocompatibility and specificity. The SPAAC approach utilizes a strained cyclooctyne to drive the reaction forward (**Figure 1.10**). Early approaches to using the SPAAC reaction to label biomolecules utilized 3-alkoxy-cyclooctynes which reportedly react with a similar rate to the modified Staudinger ligation (61). The mild conditions for this reaction were suitable for labeling live mammalian cells with quantum dots (62). Improvements to reaction rate and water solubility inspired a series of related compounds for SPAAC reactions. Aza-dibenzocyclooctynes have been reported to have better water solubility and increased reaction rates (**Figure 1.11**) (51). Given the mild conditions and specificity, either the Staudinger ligation or the SPAAC reaction are expected to be compatible with labelling viruses with incorporated azides.

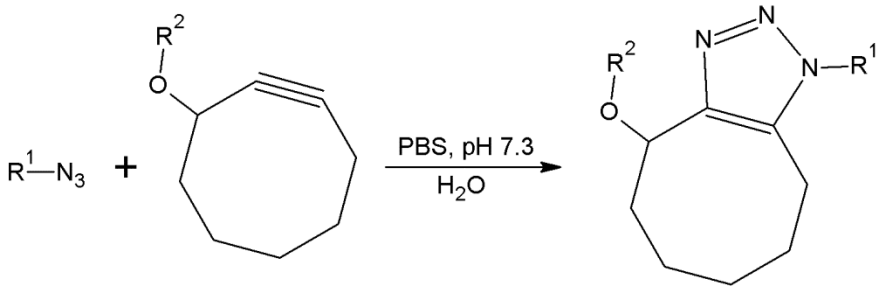

Figure 1.10: Reaction scheme for Cu(I)-free SPAAC reaction. Reaction conditions from (62)**.**

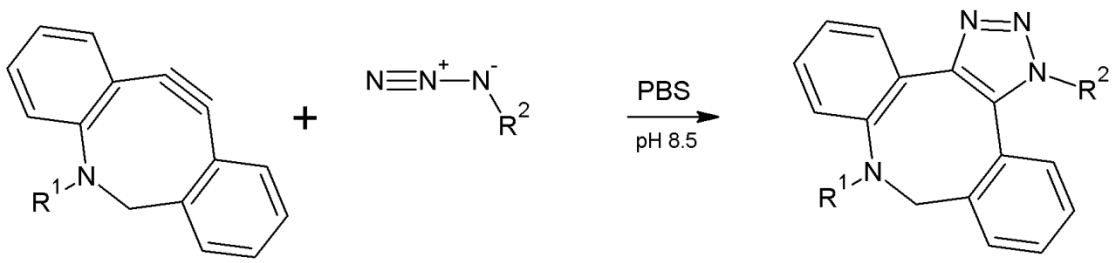

Figure 1.11: Generic reaction scheme for Cu(I)-free SPAAC reaction with aza-dibenzocyclooctyne reagents. PBS=phosphate buffered saline. Reaction conditions are from (51)**.**

1.5 Research goals

Given the recent technological applications of bacteriophage M13, the research described here involves expanding upon the conjugation capabilities of M13. The usefulness of M13 as a tool for nanotechnology comes partially from its filamentous structure, which lends itself to the formation of well-structured thin films and matrices (9, 12). Also important is the ability to separately manipulate each of the five coat proteins of M13 through genetic modification. In this way one can controllably engineer affinity for biological and inorganic components onto M13.

There has been very little research involving the incorporation of azides into pVIII. Work done with UAA incorporation into M13 has been reported for the minor coat protein pIII though (63). For example, UAA incorporation was combined with phage display in order to expand the sequence possibilities when bio-panning (40). Similarly, phage display using an Hpg-encoded library has been applied to optimizing the substrate for a palladium-mediated cross coupling reaction (64). Expanding upon the idea of multi-valency as a key aspect of a good nano-scale molecular scaffold, in this research, the incorporation of Aha into the pVIII major coat protein via residue specific UAA incorporation was explored. Since Aha offers a highly specific handle to M13 via the azide functional group, one could carry out bioconjugation reactions without cross-reactivity.

First, bacteriophage M13 had to be engineered in order to accommodate Aha at a position that was rationally designed. This would involve the production of a series of mutants that placed methionine residues at positions of better solvent-accessibility on pVIII. The viability of these mutants was assessed and confirmation that Aha could incorporate into pVIII was obtained. The resulting engineered M13-Aha

phages were then characterized for their reactivity and capability as nano-scale scaffolds with small molecules and larger inorganic particles as case examples.

2. Chapter 2 - Materials and Methods

2.1 Growth Media

Unless specified, any buffers or growth media used in this thesis work were prepared using distilled, de-ionized water (**ddH_2O**). Growth media was either sterilized by autoclaving or by filtration through a 0.2 micron filter.

2.1.1 Luria Broth

Luria Broth (**LB**) was used for the routine growth and maintenance of *E. coli* strains and M13 phages (**Table 2-1**). Tetracycline was used at a final concentration of 8 µg/mL for the growth of tetracycline-resistant bacteria in liquid media. Kanamycin was used at a final concentration of 50 µg/mL for the growth of kanamycin-resistant bacteria in liquid media. Solid LB media was prepared by dissolving 15 g/L agar into liquid media and pouring into plastic Petri plates after autoclaving. For top LB agar 7.5 g/L agar was dissolved into LB media autoclaved. For the growth of tetracycline-resistant bacteria on solid media tetracycline was used at a final concentration of 12 µg/mL. For the growth of kanamycin-resistant bacteria on solid media kanamycin was used at a final concentration of 20 µg/mL.

Table 2-1: Growth media protocols.

Media	Components
Luria Broth Media	1 % peptone (w/v) 0.5 % yeast extract (w/v) 1 % NaCl (w/v)
M9 Minimal Media	40 mM Na_2HPO_4 22 mM KH_2PO_4 60.7 mM NaCl 75.7 mM $(NH4)_2SO_4$ **The following were added after autoclaving individually:** 1 mM $MgSO_4$ 0.1 mM $CaCl_2$ 2 g/L *D*-glucose **The following was added after passing through a 0.2 micron filtration membrane:** 0.1% thiamine.HCl (w/v)

2.1.2 M9 minimal media

M9 minimal media (**M9MM**) was used as a defined media for producing M13 phages in different concentrations of *L*-methionine or for the incorporation of *L*-azidohomoalanine (**Aha**; Bachem, Torrance, USA). Solid M9MM was prepared by dissolving 15 g/L agar into liquid M9MM and pouring into plastic Petri plates after autoclaving. The following *L*- amino acids were added to further supplement the M9MM (concentration in parentheses as µg/mL): Phe (50), Lys (50), Arg (125), Gly (10), Val (35), Ala (42), Trp (20), Thr (35), Ser (420), Pro (230), Asn (48), Asp (52), Gln (730), Glu (935), Tyr (18), Ile (40), Leu (40), His (50) and Cys (50).

2.2 Bacterial strains

2.2.1 *E. coli* K12 ER2738

This strain was purchased from New England Biolabs (New England Biolabs, Whitby, Canada) and used for the growth and maintenance of M13 and M13 mutants. This strain was also used for the mutagenesis of M13 DNA and other molecular biology work. The strain *E. coli* K12 ER2738 is a *FhuA2* version of *E. coli* NM522 (65). The genotype of *E. coli* K12 ER2738 is F' *proA*$^{+}$*B*$^{+}$ *lacI*^{q} *Δ(lacZ)M15/ Δ(lac-proAB) glnV thi-1 Δ(hsdS-mcrB)5 FhuA2*.

2.2.2 Generation of *E. coli* methionine auxotroph strains

E. coli K12 MetA

This strain is a *ΔmetA780::kan* knock-out mutant of *E. coli* K12 ER2738. This strain was produced via a $P1_{vir}$ transduction with DNA from JW3973-1 (Sex: F- Chromosomal markers: *Δ(araD-araB)567, ΔlacZ4787(::rrnB-3), λ*$^{-}$, *rph-1, ΔmetA780::kan, Δ(rhaD-rhaB)568, hsdR514*) from the Coli Genetic Stock Center (**CGSC**) (66).

In short, an overnight culture of JW3973-1 grown in LB media with 50 µg/mL kanamycin was diluted 100-fold into LB with 15 mM $MgCl_2$, 5 mM $CaCl_2$ and 0.1% (w/v) glucose and grown for 1 hour at 37^{o}C with shaking. To 5 mL of this culture, 100 µL of $P1_{vir}$ phage was added. Lysis was observed at about 2 hours into the infection, noted by slight clearing of turbidity. A few drops of

chloroform were added to completely lyse cells. Chloroform was removed and the sample was pelleted at 15000 *g* for 2 minutes to remove cell debris and the supernatant was retained overnight at 4 ^{o}C.

A 2 mL overnight culture of *E. coli* K12 ER2738 grown in LB media with 8 µg/mL tetracycline was centrifuged at 3200 *g* for 2 minutes. The pellet was resuspended in 400 µL of LB with 100 mM $MgSO_4$ and 5 mM $CaCl_2$. Three reactions were set up: **1)** 100 µL of undiluted $P1_{vir}$ lysate and 100 µL ER2738, **2)** 100 µL 1:10 diluted $P1_{vir}$ lysate and 100 µL ER2738, and **3)** 100 µL $P1_{vir}$ lysate and 100 µL LB media. These were incubated for 30 minutes at 37 ^{o}C. Then 200 µL of 1 M sodium citrate (pH 5.5) and 1 mL LB were added and incubated at 37 ^{o}C for 1 hour. Cells were pelleted by centrifugation at 3200 *g* for 5 minutes and resuspended in 200 µL 1 M sodium citrate (pH 5.5) and 1 mL LB. Last, 200 µL of cells were spread-plated onto LB agar plates with 20 µg/mL kanamycin and 12 µg/mL tetracycline. Single colonies were picked and re-streaked twice more to remove $P1_{vir}$ by dilution. The final isolates were stored at -80 ^{o}C in 20% glycerol LB and will be referred to as ER2738 MetA. The success of the transduction was determined by spread plating ER2738 MetA onto M9MM agar plates and adding a few crystals of *L*-methionine to one side of the plate. Additionally, retention of the bacterial F' genotype was confirmed by spot plating 10 µL of M13 onto a lawn of ER2738 MetA.

***E. coli* K12 MetE**

This strain is a *ΔmetE774::kan* knock-out mutant of *E. coli* K12 ER2738. This strain was produced via a $P1_{vir}$ transduction with DNA from JW3805-1 (Sex: F- Chromosomal markers: Δ(araD-araB)567, ΔlacZ4787(::rrnB-3), λ-, rph-1, ΔmetE774::kan, Δ(rhaD-rhaB)568, hsdR514) from CGSC (66).

The $P1_{vir}$ transduction was carried out as above and the resulting strain was characterized as above. This mutant will be referred to as ER2738 MetE.

2.3 Generating mutant M13 strains

2.3.1 $M13_{M\text{-}5/28L}$ strain

Naturally occurring methionine residues at positions -5 and 28 (mature pVIII numbering) of pVIII protein of M13 were mutated to leucine. M13KE (New England Biolabs, Whitby, ON, Canada)

was the starting plasmid for these mutations. Site-directed mutagenesis of M-5L and M28L were carried out sequentially using the forward and reverse primers in **Table 2-2**. The site-directed mutagenesis reactions were set up using the component concentrations as described in **Table 2-3**. To carry out 13 rounds of site-directed mutagenesis, the temperatures and times indicated in **Table 2-4** were used. To initiate the reaction Pfu polymerase (ThermoScientific, Ottawa, Canada) was added once the temperature of the thermal cycler had reached 95 ^{o}C.

Table 2-2: Summary of primer sequences used for site-directed mutagenesis of M13KE. Primers were purchased from Sigma-Aldrich (Sigma-Aldrich, Oakville, Canada).

Primer name	Primer Sequence
M-5L forward	5'-GTT GCT ACC CTC GTT CCG CTG CTG TCT TTC GCT GCT GAG-3'
M-5L reverse	5'-CTC AGC AGC GAA AGA CAG CAG CGG AAC GAG GGT AGC AAC-3'
M28L forward	5'-ATC GGT TAT GCG TGG GCG CTG GTT GTT GTC ATT GTC GGC-3'
M28L reverse	5'-GCC GAC AAT GAC AAC AAC CAG CGC CCA CGC ATA ACC GAT-3'
A9M forward	5'-GGT GAC GAT CCC GCA AAA ATG GCC TTT AAC TCC CTG C-3'
A9M reverse	5'-GCA GGG AGT TAA AGG CCA TTT TTG CGG GAT CGT CAC C-3'
S13M forward	5'-GCA AAA GCG GCC TTT AAC ATG CTG CAA GCC TCA GCG ACC-3'
S13M reverse	5'-GGT CGC TGA GGC TTG CAG CAT GTT AAA GGC CGC TTT TGC-3'
A16M forward	5'-GGC CTT TAA CTC CCT GCA AAT GTC AGC GAC CGA ATA TAT CGG-3'
A16M reverse	5'-CCG ATA TAT TCG GTC GCT GAC ATT TGC AGG GAG TTA AAG GCC-3'

Table 2-3: Site-directed mutagenesis reaction mixture for M-5L and M28L mutations.

Site-directed mutagenesis components (50 µL reactions)
39 µL ddH_2O
5 µL 10x Pfu buffer with $MgSO_4$ (ThermoScientific, Ottawa, Canada)
1 µL 10 mM dNTP
2 µL 5 pmol/µL each forward/reverse primer
2 µL of ~10 ng/µL template
1 µL of 2.5 U/µL Pfu polymerase

Table 2-4: Thermal cycler settings for site-directed mutagenesis reactions.

Site-directed mutagenesis thermal cycler settings			
Stage	**Cycles**	**Temperature**	**Time**
1	cycle 1	95 ^{o}C	30 sec
2	cycle 2-12	95 ^{o}C	30 sec
		55 ^{o}C	1 min
		68 ^{o}C	8 min
3	cycle 13	68 ^{o}C	10 min

The finished site-directed mutagenesis reactions were digested with 1 µL of FastDigest DpnI (ThermoScientific, Ottawa, Canada) for 1 hour at 37 ^{o}C. After digestion, competent *E. coli* ER2738 were transformed with the M-5L mutant DNA. To 100 µL of competent ER2738 cells, ~40 ng of DNA was incubated on ice for 30 minutes. These were then heat-shocked at 42 ^{o}C for 2 minutes and then recovered on ice for 5 minutes. Next, 1 mL of LB media was added and tubes were incubated for 45 minutes at 37 ^{o}C with shaking. Then, 500 µL of this outgrowth was mixed with 200 µL mid-log (A_{600} ~ 0.6) ER2738 *E. coli* and 3 mL melted LB top agar (7.5% agar). These plates were grown overnight at 37 ^{o}C and plaques were counted the following day. Single plaques were amplified by scrapping into a 1:100 diluted overnight culture of *E. coli* ER2738 and growing at 37 ^{o}C for 4.5 hours. The cells were pelleted by centrifugation at 3200 *g* for 5 minutes and processed using GeneJET Plasmid Miniprep kit (ThermoScientific, Ottawa, Canada) as per the manufacturer's instructions to obtain purified M13 dsDNA. The resulting M13-containing supernatant was stored at -20 ^{o}C in 50% glycerol. Successful mutation was confirmed by DNA sequencing (Mobix Lab, McMaster University, Hamilton, Canada).

The above procedure was repeated for M28L using the resulting M13KE-p$VIII_{M\text{-}5L}$ as a starting point. The resulting M13KE plasmid had the mutations M-5L and M28L both present and is denoted M13KE-p$VIII_{M\text{-}5/28L}$.

2.3.2 Construction of single methionine M13 mutants.

A series of single methionine mutants (p$VIII_{A9M}$, p$VIII_{S13M}$ and p$VIII_{A16M}$) were then constructed. M13KE-p$VIII_{M\text{-}5/28L}$, described in **section 2.3.1**, was the starting point for the single methionine mutants. Site-directed mutagenesis was carried out using the forward and reverse primers as

indicated in **Table 2-2**. The site-directed mutagenesis components for these mutations included dimethyl sulfoxide (**DMSO**) as described (**Table 2-5**). Each of these mutants were transformed into *E. coli* K12 ER2738 as described above in **section 2.3.1**. Successful transformants were selected for by plaque formation and the dsDNA was obtained as described in **section 2.3.1**. The resulting plasmids are denoted M13KE-pVIII$_{A9M}$, M13KE-pVIII$_{S13M}$, and M13KE-pVIII$_{A16M}$ respectively. Sequences of plasmids were confirmed by DNA sequencing (Mobix Lab, McMaster University, Hamilton, Canada).

Table 2-5: Site-directed mutagenesis reaction mixture for A9M, S13M and A16M mutations.

PCR conditions with DMSO (50 µL reactions)
37.75 µL ddH_2O
1.25 µL 100% DMSO
5 µL 10x Pfu buffer with $MgSO_4$ (ThermoScientific, Ottawa, Canada)
1 µL 10 mM dNTP
2 µL 5 pmol/µL each forward/reverse primer
2 µL of ~10 ng/µL template
1 µL of 2.5 U/µL Pfu polymerase

2.4 Growth of M13 strains

2.4.1 M13 quantification

M13 was quantified by determining titre in plaque forming units (**pfu**) per mL. This was accomplished using an overlay plating method. Mid-log phase *E. coli* ER2738 were mixed with melted LB top agar (7.5% agar) which was poured over top of an LB agar (15% agar) plate with 12 µg/mL tetracycline. Once the overlay was solidified, 10 µL of diluted phages were spotted onto the plate. After growing overnight at 37 ^{o}C, zones of turbidity (clearing) were considered a single pfu.

2.4.2 Comparative growth of M13 strains

An overnight culture of *E. coli* ER2738 grown with 8 µg/mL tetracycline was diluted 100-fold into LB media and then infected with 10^6 pfu/mL of the M13 strain. Phages were amplified for 4.5 hours at 37 ^{o}C, at which point the *E. coli* ER2738 were removed by centrifugation at 3200 *g* for 5 minutes. Phages were diluted into 1x phosphate-buffered saline (**1x PBS**; 10 mM Na_2HPO_4, 1.8 mM KH_2PO_4, 137 mM NaCl, 2.7 mM KCl, pH 7.4) before spot-plating as described in **section 2.4.1** to

obtain a titre. Titre of M13 strains were compared with Wt M13 to obtain a measure of comparative growth.

Similarly, in testing the ability of these M13 strains to produce under methionine-limited conditions, an overnight culture of ER2738 MetE grown with 8 µg/mL tetracycline was diluted 100-fold in LB media and grown until an A_{600} of 1 at 37 ^{o}C. At this time, the cells were pelleted by centrifugation at 3200 *g* for 5 minutes, and washed once with M9 media salts (40 mM Na_2HPO_4, 22 mM KH_2PO_4, 60.7 mM NaCl, 75.7 mM $(NH_4)_2SO_4$). The cells were again pelleted by centrifugation at 3200 *g* for 5 minutes and resuspended in the final M9 media solution with a defined quantity of *L*-methionine or Aha. At this point, the culture was infected with 10^6 pfu/mL of M13 strain and grown for 4.5 hours with shaking at 37 ^{o}C. The *E. coli* were removed by centrifugation at 3200 *g* for 5 minutes and the phage-containing supernatant was assayed to determine the titre as in **section 2.4.1**.

2.4.3 Small scale purification of M13 phages with Aha

Incorporation of Aha into M13 used media-shift expression, adapted from the method described by van Hest *et al.* (44). An overnight culture of *E. coli* ER2738 MetE grown with 8 µg/mL tetracycline was diluted 100-fold into 25 mL LB media and grown until mid-log phase (A_{600}=1) at 37 ^{o}C with shaking. The media was exchanged as described above in **section 2.4.2**. The final concentration of *L*-methionine in the media was 235 µM, and for Aha incorporation, 10 mM Aha was also included. *L*-cysteine and *L*-methionine were freshly added to the media, and not stored in solution as described in **section 2.1.1**, to limit air oxidation of the sulfur. These cultures were infected with 10^6 pfu/mL of the M13 strain and grown for 4.5 hours at 37 ^{o}C. *E. coli* ER2738 MetE were removed by centrifugation and the top 20 mL of the supernatant was retained. To the supernatant was added 5 mL of 20% PEG8000/2.5M NaCl to precipitate the phages overnight at 4 ^{o}C. The precipitated phages were pelleted by centrifugation at 12000 *g* for 15 minutes. The pellet was gently resuspended in 1 mL of sterile 1x PBS and then precipitated for an additional 15 minutes on ice after adding 200 µL of 20% PEG8000/2.5M NaCl. Phages were pelleted at 15000 *g* in a microcentrifuge for 10 minutes. The supernatant was removed and the pellet retained. The pellet was resuspended in 200 µL of 1x PBS by

gentle pipetting. If the solution was cloudy, it was centrifuged at 15000 *g* for an additional 1 minute and the supernatant containing solubilised phages was retained.

2.5 ESI mass spectrometry of intact M13 phages

Intact M13 phages could be directly analyzed by electrospray ionization (**ESI**) mass spectrometry. M13 was exchanged into ultra-pure (18 MΩ·cm resistivity) water using a Pall Nanosep® 10 kDa MWCO column and concentrated to approximately $1x10^{13}$ pfu/mL (approximately 40 µM of pVIII subunits). This was further diluted to about 1 µM of pVIII subunits in appropriate solvent for the ESI MS. ESI-TOF spectra were run in 1:1 H_2O:MeCN 0.2 % formic acid on a Micromass Q-TOF Ultima Global (Waters, Milford, Mass., USA) equipped with a nano ESI source. Additionally, a ThermoScientific Q-Exactive Orbitrap equipped with an ESI source was also used to collect spectra. On this instrument, spectra were run in 1:1 H_2O:MeOH 0.1 % formic acid due to better stability of total ion count on the instrument. Raw spectrum deconvolution was carried out using MassLynx™ 4.0 Global software for data obtained on the Micromass Q-TOF, and using Xcaliber™ 2.2 SP1.48 for data obtained on the Q-Exactive.

2.6 Strain-promoted azide-alkyne cycloaddition with M13-Aha

M13 strains grown with Aha as described in **section 2.4.3** were reacted with 5(6)-Carboxytetramethylrhodamine-PEG_4-aza-dibenzocyclooctyne (**DIBAC-TAMRA;** Click Chemistry Tools, Scottsdale, AZ, USA). A stock solution of DIBAC-TAMRA was prepared as a 5 mM stock in 100% DMSO and was stored at -20 ^oC. Additionally, M13 strains grown with Aha were reacted to biotin-PEG_4-aza-dibenzocyclooctyne (**DIBAC-bioin;** Click Chemistry Tools, Scottsdale, AZ, USA). A stock solution of DIBAC-biotin was prepared as a 5 mM stock in 100% DMSO and was stored at -20 ^oC.

For DIBAC-TAMRA labelling, M13 phages ($1x10^{13}$ pfu/mL) were reacted with 30 µM DIBAC- TAMRA (Click Chemistry Tools, Scottsdale, AZ, USA) in 1x PBS buffer for 24 hours at 23^oC. For DIBAC-biotin labelling, M13 phages ($1x10^{13}$ pfu/mL) were reacted with 30 µM DIBAC-

biotin (Click Chemistry Tools, Scottsdale, AZ, USA) in 1x PBS buffer for 24 hours at 23^{o}C. Excess label was removed by spin filtration using a Pall Nanosep® 10 kDa MWCO column (Sigma-Aldrich, Oakville, Canada) and washing with 1x PBS. Spin filtration was carried out as per the manufacturer's protocols and repeated for a total of 3 washes with 500 µL 1x PBS. Absorbance spectra of TAMRA-labelled M13 were read on a SpectraMax M5 spectrophotometer (Molecular Devices, Sunnyvale, CA, USA) scanning from 240-650 nm.

2.7 Modified Staudinger ligation with M13-Aha

M13 strains grown with Aha as described in **section 2.4.3** were reacted via the modified Staudinger ligation using EZ-link® phosphine-PEG$_3$-biotin (**TAP-biotin**; ThermoScientific, Ottawa, Canada). A stock solution of TAP-biotin was prepared as a 10 mM stock in 100% DMSO and was stored at -20 ^{o}C.

For TAP-biotin labelling, M13 phages (1x10^{13} pfu/mL) were reacted with 30 µM TAP-biotin (ThermoScientific, Ottawa, Canada) in 1x PBS buffer for 24 hours at 37 ^{o}C. Excess label was removed by spin filtration using a Pall Nanosep® 10 kDa MWCO column (Sigma-Aldrich, Milwaukee, WI, USA) and washing with 1x PBS. Spin filtration was carried out as per the manufacturer's protocols and repeated for a total of 3 washes with 500 µL 1x PBS.

2.8 Transmission electron microscopy of M13 phages

Sample grid preparation was adapted from Ploss, M. and Kuhn, A. (67). M13 samples at 10^{9} pfu/mL in ultra-pure (18 MΩ·cm resistivity) water (MQH$_2$O) were deposited onto a carbon-formvar coated 400 mesh grid (Canemco-Marivac, Gore, Canada) for 1 min followed by 0.1% bovine serum albumin (**BSA**) in Tris-buffered saline (**TBS;** 50 mM tris(hydroxymethyl)aminomethane, 150 mM NaCl) for 10 minutes. Excess BSA was blotted off and 20 µL of a 1:10 dilution of 0.15 mg/mL 5 nm streptavidin-coated gold nanoparticle (**SA-AuNP**) solution (Cytodiagnostics, Burlington, Canada) was added to the grid for 30 minutes. After two washes with MQH$_2$O, the grid was stained for two minutes using 1% uranyl acetate (a generous gift from Dr. Dale Weber, Department of Biology, University of

Waterloo). M13 phages were imaged at 60kV using a CM10 Philips microscope modified with an Advanced Microscopy Techniques image capturing CCD camera (Department of Biology, University of Waterloo). When counting AuNPs associated per M13 only phage particles that could be identified as a single assembly were counted. These excluded cases were multiple phages were entwined together.

3. Chapter 3 - Development of strains and media conditions for Aha incorporation

3.1 Introduction

Recent approaches to developing new nanotechnologies have utilized viruses as scaffolds to allow manipulation and the organization of components at the nano-scale. The goals of this research were to engineer bacteriophage M13 as a nano-scale scaffold capable of facile modification and further develop it for use in technological applications. Through the course of this research, this was accomplished by utilizing residue specific incorporation of the unnatural amino acid (**UAA**), *L*-azidohomoalanine (**Aha**), into the pVIII major coat protein of bacteriophage M13. Aha is an azide-containing analogue of methionine and its incorporation would allow the display of azide functional groups organized along the length of M13. Azide functional groups can be chemically reacted bioorthogonal to other commonly employed chemistries used to label protein scaffolds and would increase the number of different compounds that could be controllably loaded onto the surface of M13.

In order to achieve Aha incorporation into pVIII, two main goals needed to be met initially. First, residue specific incorporation of UAAs relies on the use of auxotrophic bacterial strains. This had to be engineered to be auxotrophic for methionine and also capable of infection by M13. Second, the media growth conditions had to be developed and assessed to balance good yields of M13 with high levels of Aha incorporation. Incorporation of Aha was successfully accomplished and the samples produced here were suitable for further analysis to determine their reactivity via azide specific chemistries.

3.2 Developing methionine auxotrophic bacterial strains

The bacterial strains developed for this project were prepared using a $P1_{vir}$ transduction (68). The goal was to transduce one of the knocked-out methionine biosynthesis genes from the donor strains, JW3973-1 or JW3805-1 *E. coli*, into an F' containing strain designed for M13 amplification (**Figure 3.1**). In JW3973-1 and JW3805-1 the biosynthesis genes that were knock-outs were *metA* and *metE* respectively. In their respective strains, these genes were knocked out by insertion of a kanamycin-resistance gene into the open reading frame of *E. coli* K-12 (66). Tetracycline resistance is conferred by

the F' factor present in the recipient strain, ER2738 *E. coli* (New England Biolabs, Whitby, ON, Canada). Therefore, successful growth of the recipient strains after transduction on solid media containing both kanamycin and tetracycline confirmed presence of the knocked-out gene and the F' plasmid both respectively in the engineered strains. The presence of the F' plasmid was essential to ensure that the resulting engineered strain could be infected by M13.

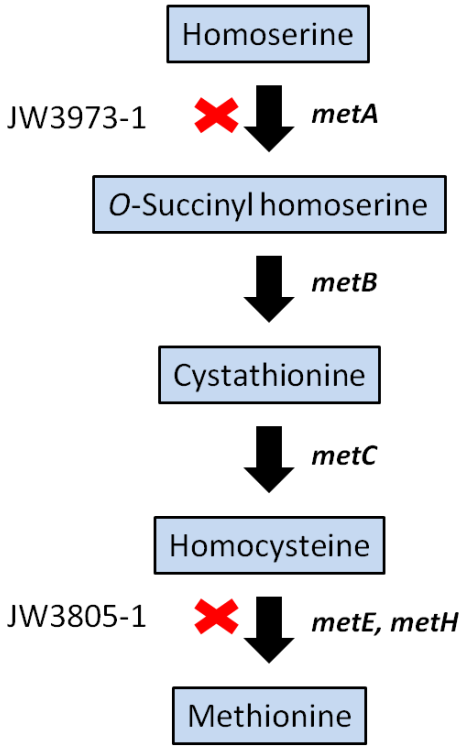

Figure 3.1: Methionine biosynthesis pathway in *E. coli* (69)**. The two steps in the pathway that were knocked-out are highlighted with red with the associated strain designation that contained that knock-out.**

The *E. coli* strains developed here will be referred to as **ER2738 MetA** where *metA* was knocked-out and **ER2738 MetE** where *metE* was knocked-out. Further confirmation of gene knock-out was obtained by culturing each strain on minimal media lacking methionine and observing whether a growth phenotype could be restored in the presence of methionine. ER2738 MetA was able to grow in the absence of methionine which indicated that this strain was able to synthesize its own methionine. *MetA* encodes homoserine *o*-succinyltransferase which catalyzes the synthesis of *o*-succinyl homoserine from *L*-homoserine as a starting metabolite (70). This is an early step in the methionine biosynthesis pathway and further transformations lead to the biosynthesis of methionine. It was not expected that this strain

would be able to grow without methionine. Knock-outs of this gene were reported to be unable to grow in M9 minimal media (71). The possibility of a revertant is unlikely since the strain was able to grow on both tetracycline and kanamycin and therefore should have had the knocked-out gene present as well as the F' factor. It may be possible that an unanticipated compensatory mutation occurred that allowed for functional methionine biosynthesis.

The other strain developed, ER2738 MetE, was unable to grow on minimal media plates in the absence of methionine. *MetE* encodes for the cobalamin-independant homocysteine transmethylase which is the final step in methionine biosynthesis. This enzyme catalyses the synthesis of methionine from homocysteine in the absence of the cofactor cobalamin. An additional gene, *metH*, encodes for methionine synthase, a cobalamin-dependant version of the enzyme, which catalyses the same step in the pathway (72). Future modifications to the growth media should avoid the addition of cobalamin to the culture to prevent synthesis of methionine down this alternate pathway. Since control over the pool of methionine available to the *E. coli* translates to better experimental controllability for UAA incorporation, it was important that the generated organisms were truly auxotrophs of methionine. Therefore, only the strain ER2738 MetE was used for further experiments since it was clear that this strain was unable to synthesize its own source of methionine.

3.3 Developing bacteriophage M13 mutant strains

A series of pVIII mutants of M13 were constructed using site-directed mutagenesis. The necessity of engineering these mutants was in anticipation of the possibility that $pVIII_{WT}$ would be unsuitable for incorporation of Aha based on the previous work by Sarah Borg (73). This was also evident when looking at a fibre diffraction structure of fd phage which shows assembled pVIII coat proteins (16). It was expected that Met28 on mature $pVIII_{WT}$ would be poorly exposed to the solvent (**Figure 3.2**). This was further supported by the low solvent accessible surface area predicted by Marvin *et al.* at Met28 (74). If Aha were incorporated at Met28 on $pVIII_{WT}$ the low solvent accessibility would likely result in poor reactivity of the azide. Since Aha is known to replace methionine in residue specific UAA incorporation experiments, one can control the position of the azide on pVIII through better positioning of methionine

residues (44). Therefore, in anticipation of this accessibility problem, Met28 on $pVIII_{WT}$ was re-positioned. The option to specifically move a functional residue highlights one of the major advantages of using proteins in building more complex nano-materials. Atom scale controllability is possible through genetic modifications to the DNA sequences encoding a particular protein.

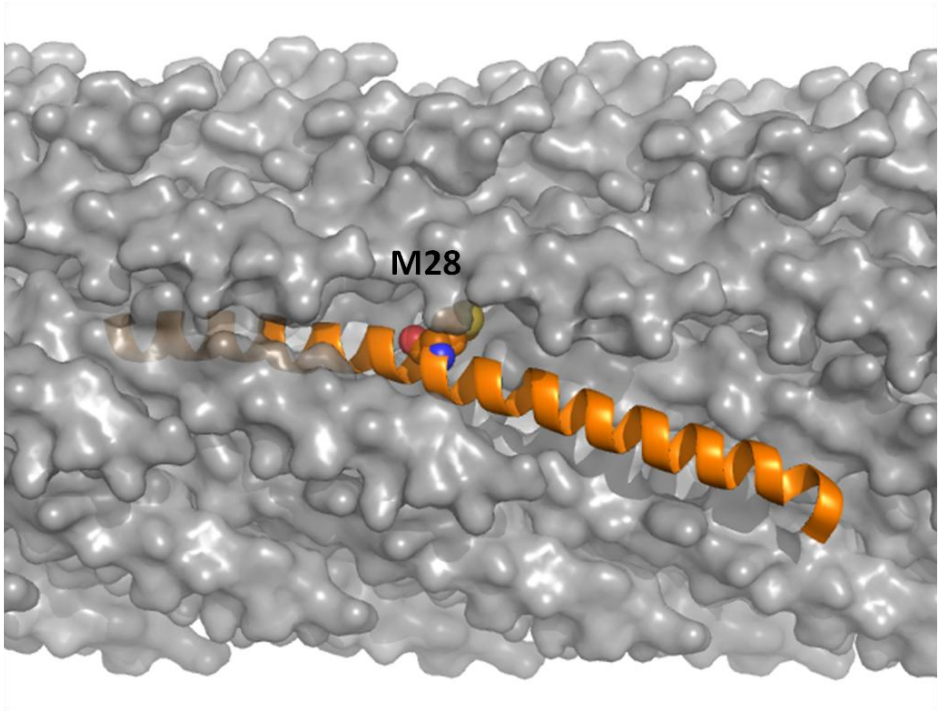

Figure 3.2: Fibre diffraction structure of fd phage highlighting a single pVIII subunit with Met28 highlighted. The PDB:1IFJ structure of fd bacteriophage is shown (16)**.**

In order to maintain better control and simplify the analysis of the M13 constructs, the mutants were designed to only have a single methionine residue. The existing methionine in $pVIII_{WT}$ at position Met28 was mutated to leucine. The residue at Met-5 of pro-pVIII was also mutated to leucine despite not being present after pro-pVIII cleavage by leader peptidase. The start codon methionine at the N-terminus of pro-pVIII was not mutated to avoid issues with translation. This methionine-less mutant was termed $pVIII_{M\text{-}5/28L}$ and was the starting point for a series of single methionine mutants that have re-positioned the methionine residue (**Figure 3.3**). The single methionine mutants were designed with solvent accessibility of the re-positioned methionine, and ultimately of the newly introduced azide group from Aha, in mind. The model by Marvin *et al.* was again used to predict where an engineered methionine residue might be

more exposed (16, 74). The positions at Ala9, Ser13 and Ala16 appeared to be on the external side of the alpha-helical pVIII (**Figure 3**). Methionine was introduced individually at each of these positions to generate $pVIII_{A9M}$, $pVIII_{S13M}$ and $pVIII_{A16M}$ single methionine pVIII mutants as outlined in the methods.

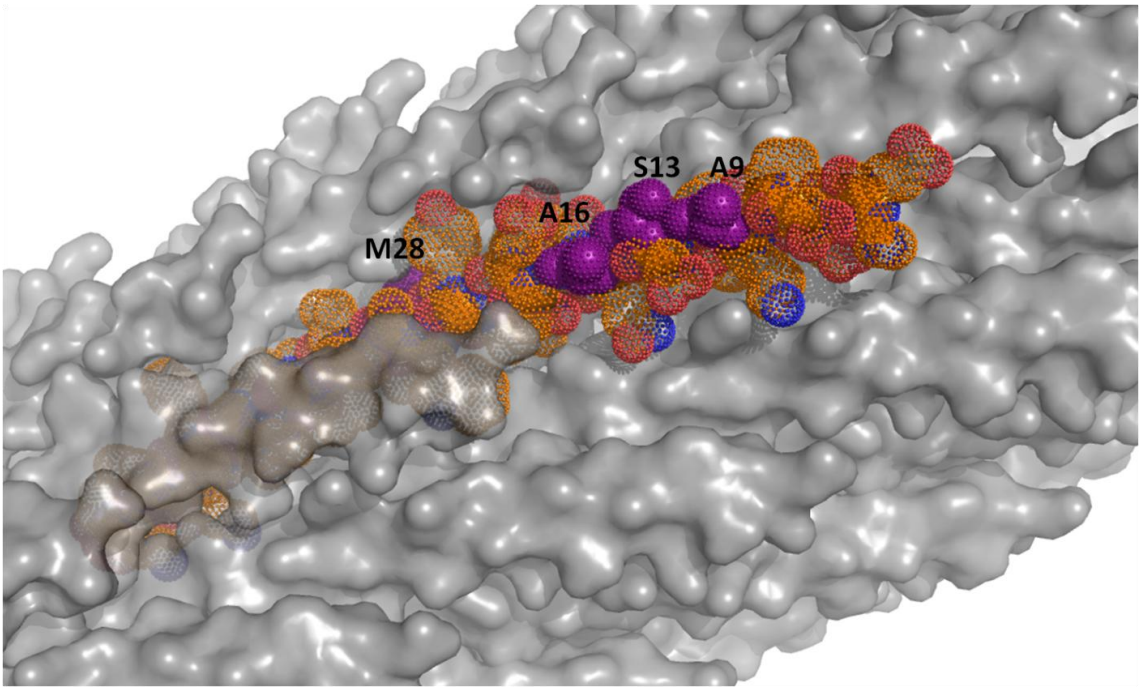

Figure 3.3: Fibre diffraction structure of fd phage highlighting a single pVIII subunit with residues that were mutated to methionine highlighted in purple. The PDB:1IFJ structure of fd bacteriophage is shown (16)**.**

Due to the nature of the single-stranded DNA primers used for site-directed mutagenesis at positions A9M, S13M and A16M of pVIII special consideration was needed. In particular, for S13M and A16M mutations, the primers used had the possibility of self-dimerization and the formation of hairpin structures that might compete with annealing of the primers to the M13 DNA template (**Figure 3.4A**). Using the standard site-directed mutagenesis conditions no product was detected for S13M or A16M mutations. The addition of 2.5% DMSO resulted in the formation of amplified mutant DNA seen at 8.3 kbp (**Figure 3.4B**). The length of the M13 genome is 7.7 kbp, but due to the product being formed as nicked, circular DNA it was not expected to run true to its length. In the case of A9M, some product was detected in the absence of DMSO, but yields were greatly improved after the addition of DMSO. The likely role of DMSO is in reducing secondary DNA structure formation in the primers and template by

disrupting intra-strand re-annealing (75). While the focus of this research was not on molecular biological methods, in relation to engineering M13, this kind of information is useful for future modifications to the N-terminal region of pVIII.

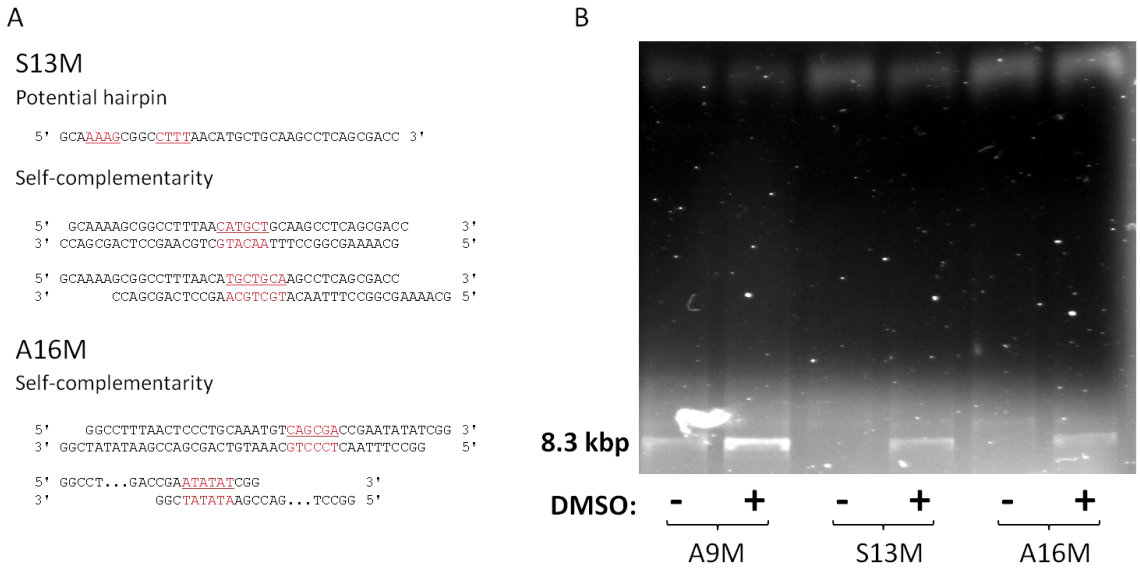

Figure 3.4: Site-directed mutagenesis of single methionine mutants. (A) Predicted secondary structures of primers used in site-directed mutagenesis reactions using OligoCalc (76)**. (B) A 1% agarose gel of the products of 13 rounds of QuikChange® site-directed mutagenesis on M13KE DNA (7666 bp) stained with ethidium bromide. The "-"indicates absence of DMSO and the "+" indicates the presence of 2.5% DMSO.**

3.4 Growth properties of M13 mutants

The viabilities of the engineered M13 strains were tested by comparing the titre of phages at 4.5 hours of amplification with Wt M13 amplification. Titre is a measure of the number of infective M13 particles and is quantified in units of plaque forming units (**pfu**). The ability of mutant pVIII to assemble into M13 phages and the ability of these mutant M13 to re-infect *E. coli* are tested together using this approach. The mutations of M28L or M-5L individually resulted in similar decreases in phage viability at 3.0 and 3.4-fold decreases respectively (**Figure 3.5**). The combination of the two mutations, M-5/28L, did not have a viability that was significantly lower than either mutation individually at 3.7-fold less than Wt M13. It was surprising that the mutation M-5L had such an impact on the viability of M13 given that it does not actually change the mature pVIII protein sequence. The viability lost might indicate processing difficulties of the pVIII pro-peptide to mature pVIII. It is unlikely that the affected step was cleavage of

pro-pVIII by leader peptidase though. At the Met-5 position, methionine can be replaced by any amino except for proline based on consensus sequences recognized by leader peptidase (28). Furthermore it was determined in over-expressed pVIII that cleavage of pro-pVIII to mature pVIII was 100% when Met-5 was mutated to leucine (77). In a randomized mutagenesis study, mutations of M28L were sometimes found accompanied by mutations of Val31 to either leucine or alanine (29). For future modifications to improve M13 strains engineered here, this additional mutation might make for a more viable construct.

Starting from the $pVIII_{M-5/28L}$ mutant, several single methionine mutants were constructed. The mutations that were done were A9M, S13M and A16M. The mutation of A16M caused a significant 7.0-fold decrease in viability compared to Wt M13 (**Figure 3.5**). The mutation of alanine to methionine has the potential to be disruptive given their differing sizes. It is likely that the further from the N-terminus that methionine is introduced; the more likely it is to interfere with the overlapping of adjacent pVIII subunits and disrupt tertiary structure. This might explain why the A9M or S13M mutations did not also result in further losses of viability. They are both further away from the region of pVIII that is involved in inter-subunit interactions.

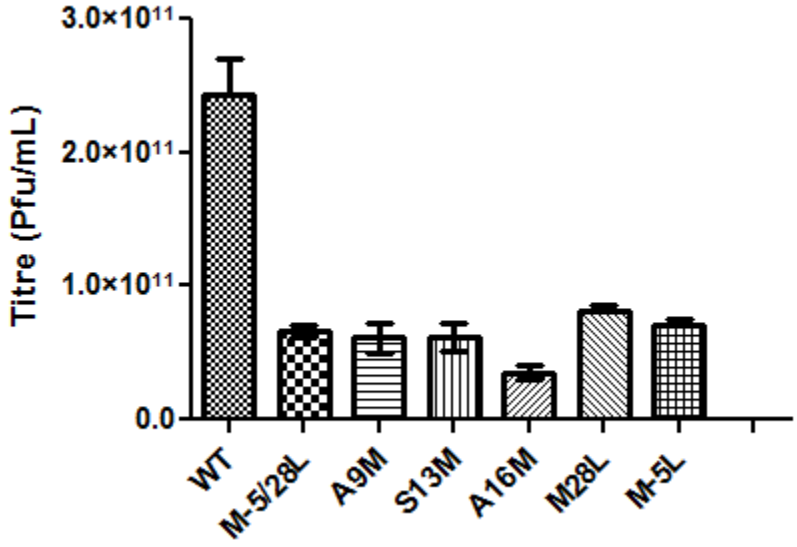

Figure 3.5: Comparative growth of M13 mutants. The viabilities were measured at the quantity of M13 produced after 4.5 hours of amplification in ER2738 *E. coli* as the host bacteria. Results shown are from at least triplicate (n=3) data.

The purified M13 mutants were analysed by SDS-PAGE. Tricine SDS-PAGE was used to resolve the smaller coat proteins such as pVIII (78). The molecular weights of two of the M13 coat proteins could be clearly identified from this type of analysis. The major coat protein, pVIII ran at 7.8 kDa on the gel (**Figure 3.6**). The band with the next greatest intensity ran at 40 kDa. This most likely corresponded to pIII coat protein which has a calculated mass of 43 kDa (79). The additional band seen at 60 kDa might also be pIII, which has been reported to run at a higher apparent molecular weight and so it was not unexpected to also see a band at 60 kDa. It has been suggested that pIII running at 60 kDa is due to a glycine-rich region in its sequence (80). None of the other coat proteins, pVI, pIX and pVII, were clearly identified on the gel. Given that there are many copies of pVIII per M13 phage, visualizing the major coat protein from solubilised M13 phages was quite effective. All pVIII mutants ran similarly on Tricine SDS-PAGE as compared to Wt pVIII. This was expected given that only point mutations were introduced but was confirmed regardless.

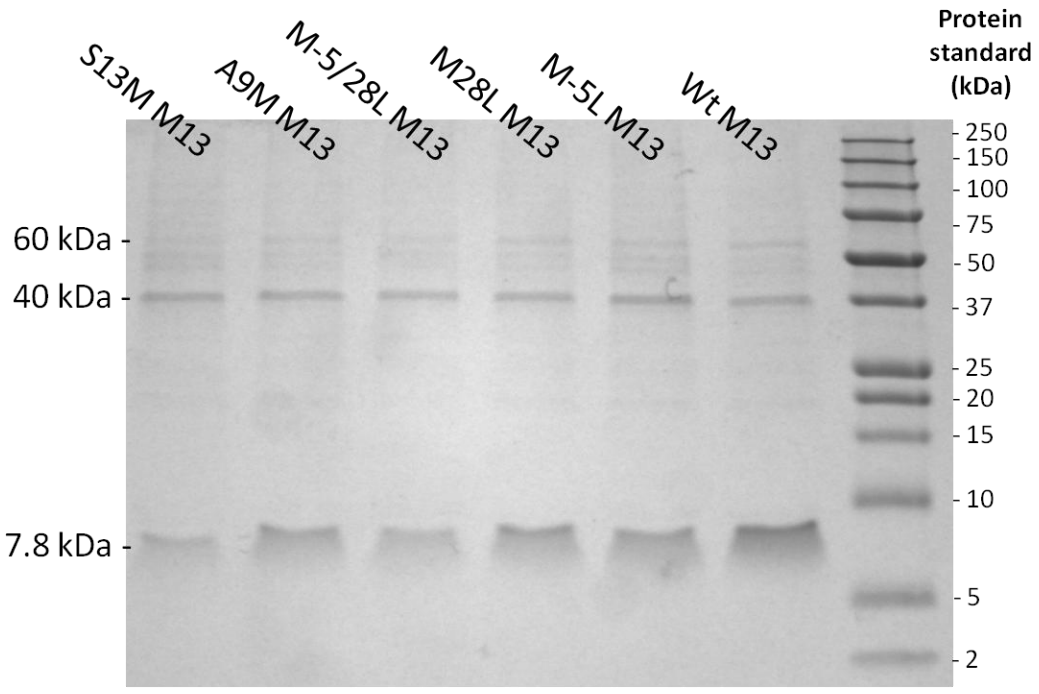

Figure 3.6: Tricine SDS-PAGE of Wt M13 and mutants grown under rich media conditions. The standard run was Precision Plus Protein™ Dual Xtra Standards (Bio-Rad, Hercules, CA). The gel was stained with Coomassie G250.

3.5 Developing growth conditions for Aha incorporation into M13

The growth of the methionine-auxotrophic strain ER2738 MetE was tested under different media conditions. In M9 minimal growth media, the cells were provided with defined resources for growth: glucose as a carbon source and ammonium sulfate as a nitrogen source. This use of chemically defined media was essential so that methionine in the growth media could be a controllable parameter for developing the conditions for residue specific UAA incorporation. The simplest case and starting point was to grow ER2738 MetE in M9 minimal media with only methionine present as a supplement. The growth rate of ER2738 MetE with 340 µM methionine was slow with a doubling time of 90 minutes (**Figure 3.7A**). It was anticipated that the growth rate could be improved by introducing a supplement of the other 19 amino acids. Introducing these additional resources decreased the doubling time to 45 minutes. Since the addition of an amino acid supplement enhanced the growth of ER2738 MetE so well, it was included in all future modifications to the growth media.

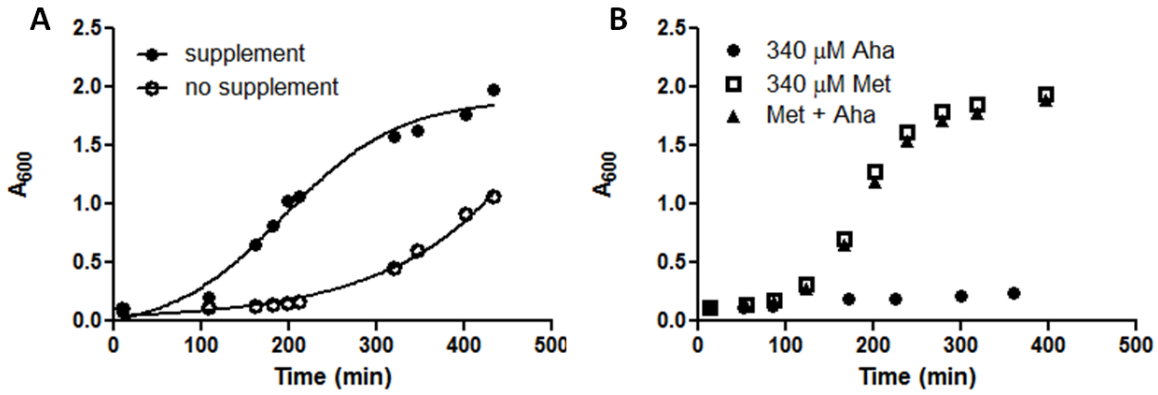

Figure 3.7: ER2738 MetE growth properties in minimal media conditions. Growth of ER2738 MetE was monitored by following the absorbance at 600 nm of the culture. (A) ER2738 MetE grown in M9 minimal media containing 340 µM methionine with and without the addition of an amino acid supplement of the other 19 naturally-occurring amino acids. (B) ER2738 MetE growth in M9 minimal media with different combinations of methionine and Aha as indicated in the legend.

Next, the effect of adding Aha to the culture media on ER2738 MetE growth was tested. Three conditions were used in these experiments: **(i)** Growth in minimal media with amino acid supplement and 340 µM methionine, **(ii)** growth with amino acid supplement where Aha and methionine were added to the growth media in equal quantities at 340 µM, and **(iii)** growth in minimal media with amino acid

supplement and 340 µM Aha only. Under condition **i**, the doubling time was 45 minutes for growth with methionine only (**Figure 3.7B**). Under condition **ii**, ER2738 MetE grew as well as it did under condition **i** with a doubling time of 45 minutes. At 340 µM methionine it seemed that 340 µM Aha does not disrupt the growth of *E. coli* ER2738 MetE. This may have been the result of the low Aha concentrations that were tested early on. Similarly it was found that 2.8 mM Aha did not greatly decrease the growth of *E. coli* MTD123 when grown in combination with methionine (81). The ability of Aha to support the growth of ER2738 MetE on its own was tested as an extreme case. In condition **iii**, it was clear that 340 µM of Aha alone cannot support growth of ER2738 MetE. Since it was evident that ER2738 MetE would not grow well with Aha alone, the methionine requirements for M13 production were explored next.

First, ER2738 MetE was grown to mid-log phase growth in rich LB media before exchanging it into defined M9 media with differing methionine concentrations. At this point, the culture was infected with M13 and phage growth was monitored. At 340 µM methionine, M13 produced exponentially over the course of 21 hours reaching a final yield of $1.6x10^{11}$ pfu/mL (**Figure 3.8A**). At a methionine concentration of 34 µM the production of M13 was no longer detected. This was surprising given that the concentration was only decreased by 10-fold and replication of M13 appeared to be completely abolished. Lastly, M13 was unable to produce in the presence of 2 mM Aha only. As with ER2738 MetE growth, M13 replication required methionine in combination Aha to obtain a detectable increase in titre.

It was important that the minimum methionine requirements for M13 amplification were determined. Ideally, one would only use the minimal amount of methionine required for M13 amplification such that Aha would still have a reasonable chance of incorporation into pVIII over methionine. Over the range of 340 to 34 µM methionine tested, M13 yields were drastically reduced from $1x10^{11}$ pfu/mL at 340 µM methionine to no measured increase in titre at 34 µM methionine (**Figure 3.8B**). Additionally, at a concentration at or below 170 µM methionine, it was found that increasing the growth period from 4.5 hours to 21 hours actually resulted in a decrease of M13 yield overnight. It is possible that decrease of titre overnight was due to depletion of methionine. For Aha incorporation experiments, a concentration of 235 µM was estimated as a suitable concentration of methionine that

would allow for both amplification of M13 as well as allow Aha to have an increased chance at incorporation over methionine.

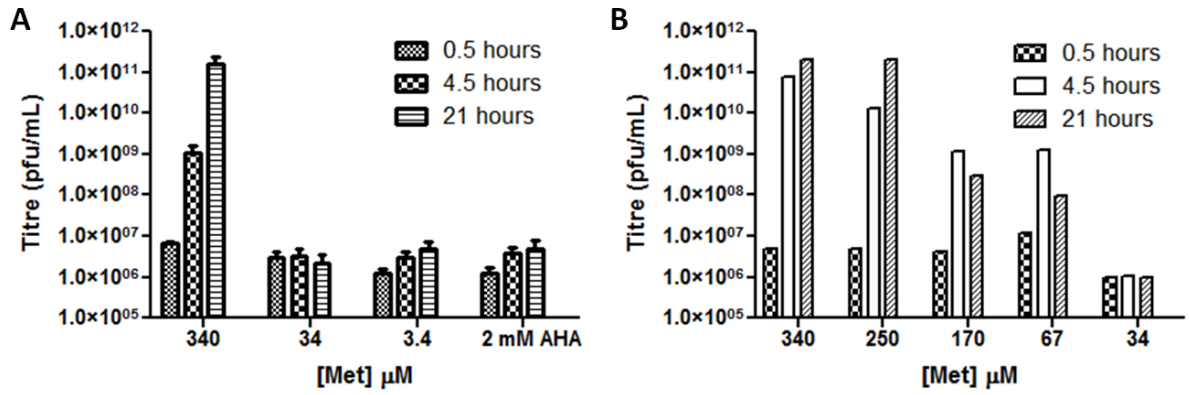

Figure 3.8: M13 replication under differing M9 minimal media conditions. M13 growth was monitored by spot-plating serial dilutions and measuring phage titres. (A) M13 amplification with defined methionine concentrations and Aha alone. Results were from triplicate (n=3) data. (B) M13 amplification with defined methionine concentrations in order to determine the minimal methionine requirements for phage amplification. Results were from a single trial (n=1).

Using M9 media conditions that now included an amino acid supplement and a defined methionine concentration, the impact of Aha incorporation on M13 amplification was examined. A high concentration of 10 mM Aha was chosen to increase the chances of its incorporation into M13 coat proteins. A two-way analysis of variance using different M13 mutants and presence of Aha as the two variables indicated that both the mutant used and the presence of Aha both had a significant effect on the yield of M13 obtained (**Figure 3.9;** $p<0.05$). Between all M13 strains, the addition of 10 mM Aha decreased the yield of M13 obtained. Also, in contrast to the results where M13 strains produced similar yields in rich LB media, here $pVIII_{A9M}$ M13 and $pVIII_{M\text{-}5/28L}$ were produced in the highest yields.

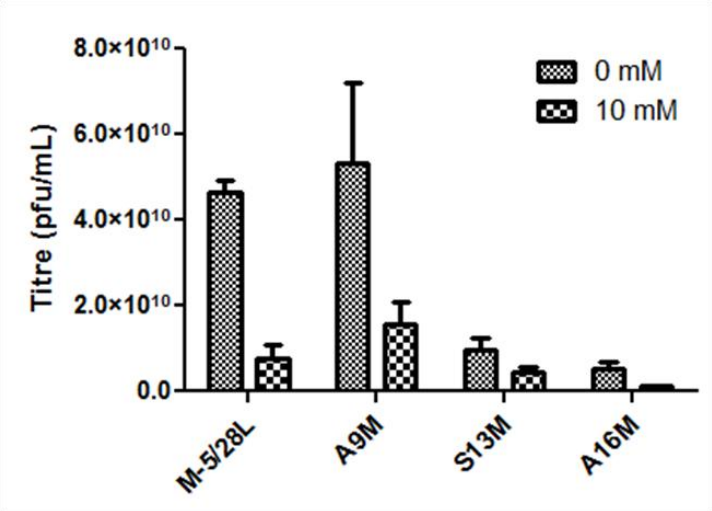

Figure 3.9: M13 replication in the presence of Aha. ER2738 MetE was grown to mid-log phage and exchanged into media containing 235 µM methionine, either with or without the addition of 10 mM Aha. Titre was determined by spot-plating serial dilutions of M13 at 4.5 hours of growth. Results were from at least triplicate (n=3) data.

Two cases can be considered to explain the decrease in M13 yield when grown with 10 mM Aha: (**i**) the incorporation of Aha into M13-encoded proteins directly hinders their normal function, or (**ii**) the incorporation of Aha into endogenous *E. coli* proteins resulted in slowed growth of the host followed by slowed replication of M13. In the first case, destabilization of pVIII in particular was likely not the reason for the observed decrease in yield. A 6.1-fold decrease in M13 yield was observed even for $pVIII_{M\text{-}5/28L}$ M13 grown with 10 mM Aha. This mutant contained no methionine residues, with the exception of the start codon methionine, with which Aha could replace. This does not rule out whether the incorporation of Aha into any of the other proteins produced by M13 caused a decrease in M13 yield (**Table 3-1**). A combination of the above two scenarios likely accounts for the decrease in M13 yield. From a practical point of view, a 2- to 4.4-fold decrease in titre following the addition of 10 mM Aha still yielded appreciable amounts of M13 for further study.

Table 3-1: Number of methionine residues in proteins encoded by the M13 genome.

M13 protein	Number of Met*	Amino acids (% Met)
pI	3	348 (0.86)
pII	6	410 (1.46)
pIII‡	9 (8)	424 (1.89)
pIV	6	426 (1.41)
pV	2	87 (2.30)
pVI	1	112 (0.89)
pVII	2	33 (6.06)
pVIII‡	3 (1)	73 (4.11)
pIX	2	32 (6.25)
pX	3	111 (2.70)
pXI	1	108 (0.93)

***Number in parentheses indicates methionine residues after endogenous protease cleavage.**

In other studies, high percentages of UAA incorporation could be obtained by switching the expression strain into media containing only the UAA of interest (32, 35, 44, 45, 82). In these approaches, the auxotroph *E. coli* strain had the gene for the protein of interest encoded into an expression vector. At the time of media exchange, an inducer of expression such as isopropyl β-*D*-1-thiogalactopyranoside (**IPTG**) was added and protein collected afterwards had levels of incorporation as high as 100% (32). With M13, this kind of approach was found unsuitable, as neither the host ER2738 or M13 could produce well in the complete absence of methionine. Since the strain $pVIII_{A16M}$ M13 produced poorly when grown with 10 mM Aha, it was not pursued further. Both $pVIII_{A9M}$ and $pVIII_{S13M}$ were produced in adequate yields and could be concentrated for further analyses.

3.6 Aha incorporation determined by mass spectrometry

The actual incorporation of Aha into the pVIII coat protein of M13 was assessed through ESI mass spectrometry (**MS**). Intact M13 phages were applied directly without prior denaturation for analysis of the pVIII major coat protein by ESI-MS. Since pVIII is present in 540-fold excess to the other M13 coat proteins (pIII, pVI, pVII and pIX), it is readily detected over those proteins on the mass spectra. For

each of the M13 strains tested, the peaks which were expected on the mass spectra include those corresponding to pVIII with methionine incorporated (**pVIII-Met**) and pVIII where methionine had been replaced by Aha (**pVIII-Aha**). The average molecular mass of Aha is 144 g/mol and the average molecular mass of methionine is 149 g/mol. It was therefore expected that the mass of pVIII where Met had been replaced by Aha would be 5 Da less. The theoretical masses predicted for pVIII-Met and pVIII-Aha peaks are summarized in **Table 3-2**.

Table 3-2: Summary of expected masses of mutant pVIII proteins.

M13 strain	Expected mass of pVIII-Met (Da)	Expected mass of pVIII-Aha (Da)
WT	5238.0	5235.0
M-5/28L	5220.0	N/A
A9M	5280.1	5275.1
S13M	5264.1	5259.1

M13 $pVIII_{A9M}$ samples that were grown in the absence or presence of 10 mM Aha were run on ESI-TOF MS. There was a consistent deviation of 1 Da for all peaks and their expected masses. The major peak was observed at 5279 Da and corresponded to the theoretical mass of $pVIII_{A9M}$-Met (**Figure 3.10**). A secondary peak was observed at 5274 Da. This corresponded well with the theoretical mass of $pVIII_{A9M}$ where Aha has been incorporated in place of methionine (**Table 3-2**). A number of adducts were observed in addition to the $pVIII_{A9M}$-Met and $pVIII_{A9M}$-Aha peaks. Most of these could be identified as common ion adducts such as K^+ or acetonitrile (**Figure 3.11**). The +16 Da peak likely corresponded to the formation of methionine sulfoxide (**pVIII-MetSO**). A9M M13 grown in the absence of Aha had a major peak at 5279 Da, but no peak at 5274 Da. This indicated that for $pVIII_{A9M}$, Aha incorporation occurred only when M13 was amplified in 10 mM Aha. Also of note, the incorporation of Aha was not 100% as the majority of signal on the spectrum came from $pVIII_{A9M}$-Met. The intensity of the $pVIII_{A9M}$-Aha peak was 10.2% of the $pVIII_{A9M}$-Met peak.

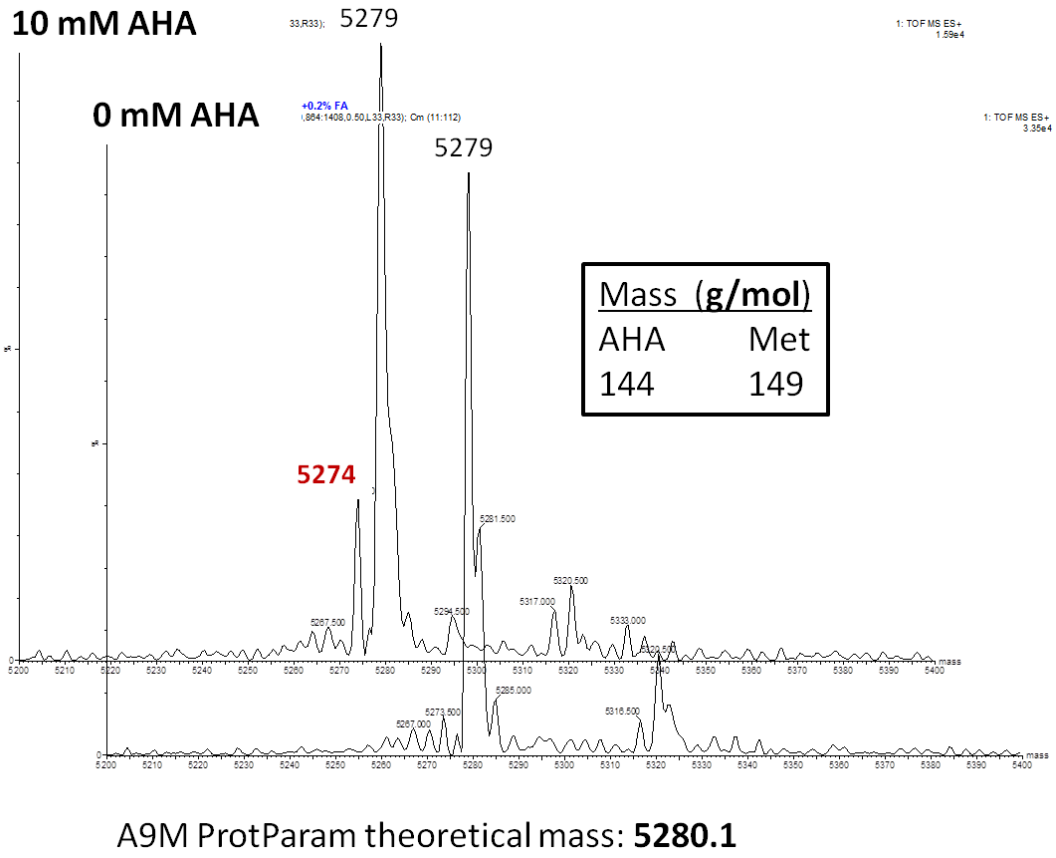

Figure 3.10: Deconvoluted ESI-TOF mass spectrum of $pVIII_{A9M}$ run on a Waters Q-TOF instrument. The raw spectrum was deconvoluted using MassLynx™ 4.0 Global software with a resolution of 0.5 Da.

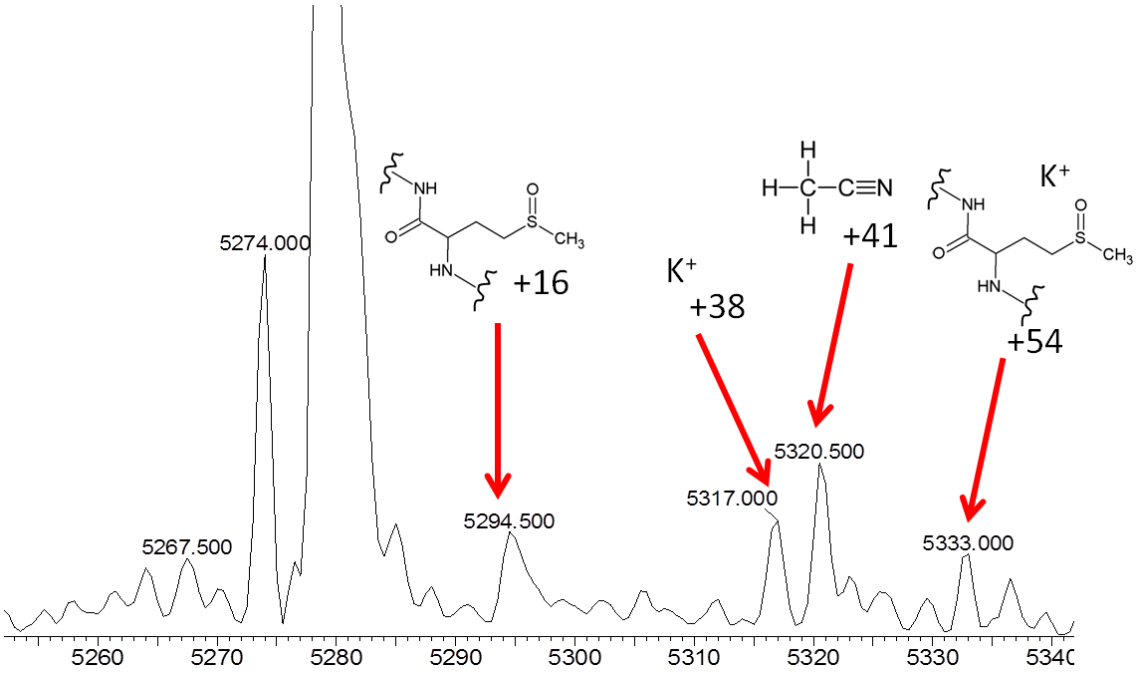

Figure 3.11: Deconvoluted ESI-TOF mass spectrum of pVIII$_{A9M}$ grown in 10 mM Aha and run on a Waters Q-TOF instrument. Commonly seen adducts on ESI-TOF MS of M13.

M13 pVIII$_{S13M}$ that was grown in the absence or presence of 10 mM Aha was analyzed using ESI-TOF MS. The major peak was observed at 5262.5 to 5263 Da (**Figure 3.12**). A peak detected at 5258.5 Da corresponded well with the theoretical mass of pVIII where Aha has been incorporated in place of methionine (**Table 3-2**). The pattern of ion adduct formation was similar to that seen for pVIII$_{A9M}$ where peaks likely corresponding to K^+ and acetonitrile were identified. S13M M13 grown in the absence of Aha had a major peak at 5263 Da, but no clear peak at 5258 Da to indicate Aha incorporation. These spectra showed that for M13 pVIII$_{S13M}$, Aha incorporation occurred when M13 was produced in the presence of 10 mM Aha. Some oxidation of methionine was observed with this mutant as well, perhaps suggesting solvent accessibility of methionine at residue position Met13. As with pVIII$_{A9M}$, the incorporation was not 100% as the major signal on the spectrum came from pVIII$_{S13M}$-Met. The intensity of the pVIII$_{S13M}$-Aha peak was 13.4% of the pVIII$_{S13M}$-Met.

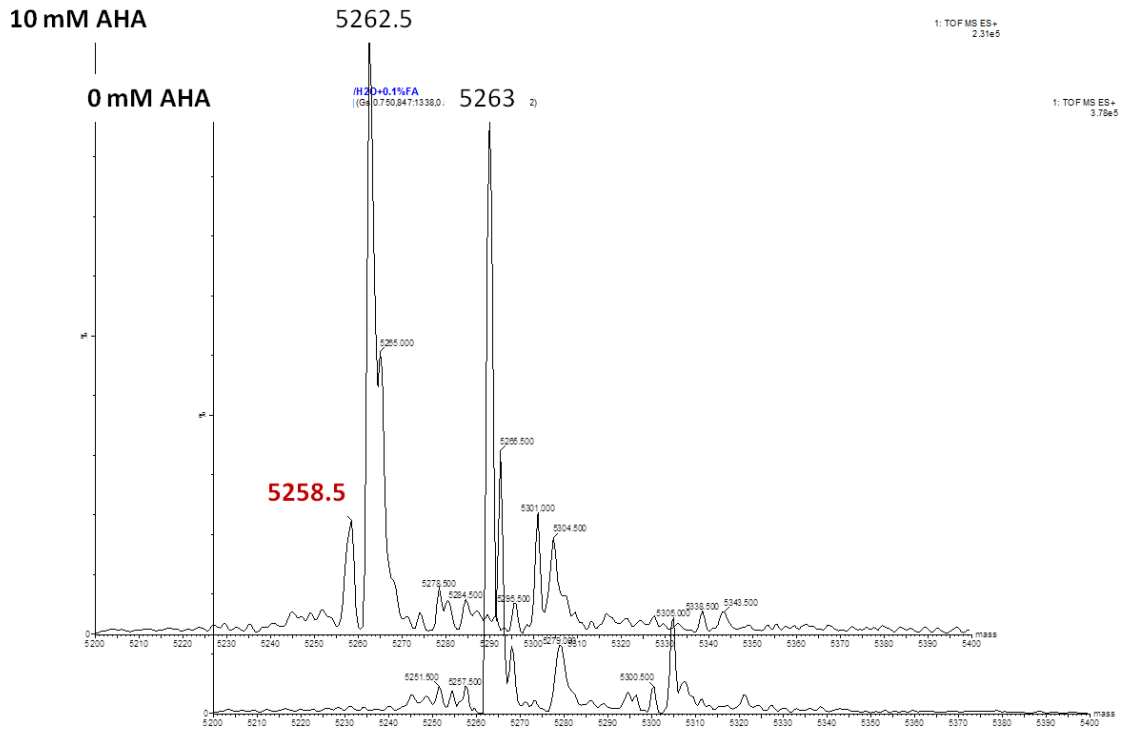

Figure 3.12: Deconvoluted ESI-TOF mass spectrum of $pVIII_{S13M}$ run on a Waters Q-TOF instrument. The raw spectrum was deconvoluted using MassLynx™ 4.0 Global software with a resolution of 0.5 Da.

Wt M13 was also grown in the absence or presence of 10 mM Aha and was analyzed using ESI-TOF MS. The major peak was seen at 5236.5 to 5237 Da which corresponded to the theoretical mass of $pVIII_{WT}$ which is 5238 Da (**Figure 3.13**). In the sample grown in the presence of 10 mM Aha, a secondary peak was seen at 5232.5 Da which corresponded to what would be expected for Aha to replace methionine in pVIII (**Table 3-2**). This indicated that for Wt M13, Aha can replace methionine at the Met28 position. The pVIII-Aha peak was 11.3% of the pVIII-Met peak in this sample. Unlike with $pVIII_{A9M}$ and $pVIII_{S13M}$, the methionine sulfoxide peak at +16 Da was not clearly seen here. This would be consistent with the prediction that Met28 is not very accessible to the solvent and not as readily oxidized. The secondary peak corresponding to pVIII-Aha was also notably absent from the sample grown in the absence of Aha. These results were consistent with Aha incorporation into $pVIII_{WT}$ under 10 mM Aha growth conditions.

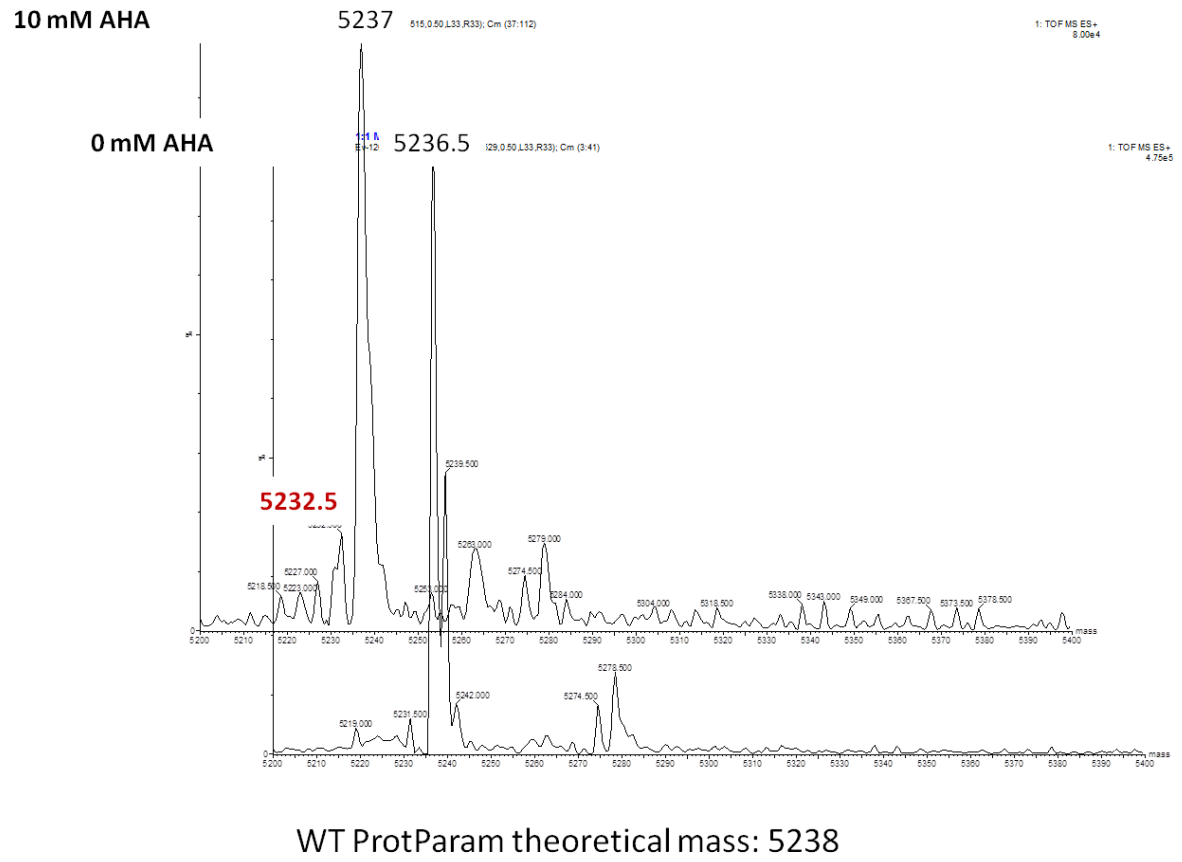

Figure 3.13: Deconvoluted ESI-TOF mass spectrum of pVIII$_{WT}$ run on a Waters Q-TOF instrument. The raw spectrum was deconvoluted using MassLynx™ 4.0 Global software with a resolution of 0.5 Da.

The control strain, M13 pVIII$_{M\text{-}5/28L}$, was also grown in the presence or absence of 10 mM Aha and run on ESI-TOF MS. Given the lack of any methionine on mature pVIII$_{M\text{-}5/28L}$, it was expected that both samples produced with and without Aha would have similar mass spectra. With the exception of extra noise in the 10 mM Aha spectra likely due to the lower concentration of that sample, the two spectra were very similar (**Figure 3.14**). For the pVIII$_{M\text{-}5/28L}$ samples the major peaks were seen at 5218.5 to 5219 Da and corresponded to the theoretical mass of pVIII$_{M\text{-}5/28L}$-Met which was 5220 Da. In the sample grown in the presence of 10 mM Aha there was no secondary peak at -5 Da that might correspond to the incorporation of Aha. This control strain indicated that incorporation of Aha, and the appearance of a -5 Da peak on the spectra, can be attributed to replacement of methionine with Aha present on pVIII$_{A9M}$, pVIII$_{S13M}$ and Wt M13 strains.

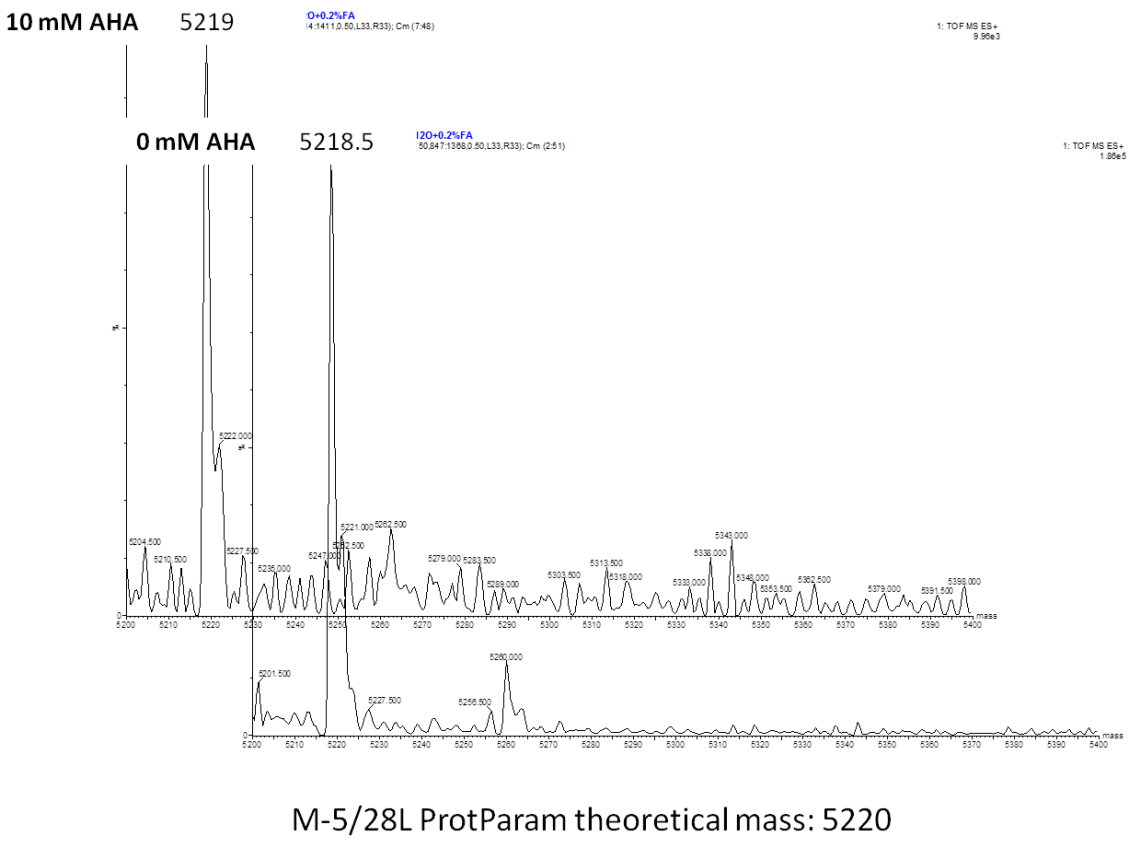

Figure 3.14: Deconvoluted ESI-TOF mass spectrum of $pVIII_{M\text{-}5/28L}$ run on a Waters Q-TOF instrument. The raw spectrum was deconvoluted using MassLynx™ 4.0 Global software with a resolution of 0.5 Da.

In summary, analyses of the mass spectrometry results show that the media growth conditions developed for residue specific UAA into M13 here could be used to incorporate an azide on pVIII of M13. In each of Wt, $pVIII_{A9M}$ and $pVIII_{S13M}$ M13 samples that were grown in the presence of Aha, pVIII-Aha was detected in each of their mass spectra. The masses of these peaks were in agreement with the mass of pVIII where a single methionine residue had been replaced by Aha with no other modifications occurring. The pVIII-Aha species was not detected in any of the spectra where M13 was grown in the absence of Aha. Furthermore, pVIII-Aha was not detected for the $pVIII_{M\text{-}5/28L}$ mutant even when grown with 10 mM Aha. This was consistent with there being no methionine residues on $pVIII_{M\text{-}5/28L}$.

Between the WT, $pVIII_{A9M}$ and $pVIII_{S13M}$ strains, the relative intensities of the pVIII-Aha peak to the pVIII-Met peak in the spectra were 10-13%. It is important to be careful in assuming that the relative intensities on a mass spectrum correspond to the relative amounts in the actual sample. For example,

when one chemical species within a mixture ionizes more readily than other compounds it will give a much higher signal on the spectrum and reduce the signal from other analytes. Experimentally, it has been shown that reducing the flow rate also reduces suppression effects (83). Since the two molecules pVIII-Aha and pVIII-Met are very similar, and a nano ESI source was used for these experiments one would expect the comparison to be more accurate in this case. A dye-labelling approach was used as well to estimate the incorporation efficiency of Aha into pVIII. Lastly, the presence of methionine sulfoxide seen in the mutants $pVIII_{A9M}$ and $pVIII_{S13M}$ serves as a clue suggesting that methionine at this position was more solvent-accessible, and therefore, more susceptible to oxidation. From these results, one can conclude that the conditions developed here that Aha has successfully replaced methionine in a percentage of pVIII subunits. The exact percentage of pVIII-Aha subunits and their distribution along the length of M13 are examined in the following chapter.

4. Chapter 4 - M13-Aha characterization and bioconjugation reactions

4.1 Introduction

Bacteriophage M13 was engineered to display azides onto the pVIII major coat protein through residue specific unnatural amino acid (**UAA**) incorporation. After confirmation of Aha incorporation by using mass spectrometric analyses, the reactive properties of these azide-bearing M13 phages were then examined. It was anticipated that the M13 strains A9M and S13M, where methionine had been repositioned, would react more completely than Wt M13. This was due to the prediction that Aha would be more exposed if it replaced methionine at positions A9M and S13M on pVIII.

First, reaction with a small dye molecule was done to explore the extent to which these engineered M13 mutants could be reacted. This would include quantifying how many dye molecules could be loaded onto the M13-Aha constructs produced. Additionally, the nature of the dye would allow calculation of the labelling efficiency and therefore the ability to obtain an estimate of how many pVIII-Aha there were per phage. The prior mass spectrometry results indicated that a large proportion of pVIII subunits still had methionine incorporated over Aha. In addition to utilizing the dye molecule to characterize these M13 constructs, it would also demonstrate the modification capabilities of M13-Aha. For example, M13 has been used to produce photo-responsive materials or potential new imaging agents using modifications with small molecules (11, 84).

Second, M13 was labelled with gold nanoparticles (**AuNPs**), specifically utilizing the pVIII-incorporated azide, so that the spatial distribution of pVIII-Aha along the length of M13 could be visualized by transmission electron microscopy (**TEM**). It was hypothesized that pVIII-Aha subunits would be evenly distributed amongst pVIII-Met subunits in the assembled M13 phage and that the spatial organization of the tethered AuNPs would reflect that. In addition to characterizing the M13 mutants, this approach would also explore the capability of this platform to organize larger components such as inorganic particles. This would be important to demonstrate since many device and biosensor applications employ noble metal nanoparticles (85). As a specific example, M13 has been used as a scaffold in dye-

sensitised solar cells utilizing plasmonic AuNPs bound non-covalently to more negatively charged pVIII mutants (12). Expanding upon these applications of M13 by fabricating a system that can be modified orthogonally utilizing azide-specific chemistries is expected to open up additional possibilities for utilizing M13 as a multi-valent device component.

4.2 Absorbance spectroscopy of M13 phages

The initial approach to testing the reaction capabilities of the M13-Aha constructs was to react them with a dye that could be easily monitored. Ideally, if one knows the concentration of M13 and the quantity of dyes covalently reacted to it, one could obtain an estimate of how many pVIII-Aha subunits are present on each M13 particle. For this to be successful, M13 should be easily quantifiable from its absorbance spectra such that both dye absorbance values and M13 absorbance values are taken from the same spectrum to be used for labelling efficiency calculations. From previous research, bacteriophage M13 can be quantified by measuring its absorbance at 269 nm and subtracting the non-specific absorbance at 320 nm. The extinction coefficient for M13 originally came from the work of Berkowitz and Day using dry masses of M13 phages (86). A different form of this extinction coefficient can be found in **equation 1** which relates M13 titre to absorbance which will be used here (87-89). While proteins normally absorb maximally at 280 nm, assembled M13 phages have considerable contribution to their absorbance from encapsulated DNA, which is reflected in the broadness of the M13 peak.

$$[\mathrm{M13}] = \frac{(A_{269} - A_{320}) \times 6 \times 10^{16}}{N_{bp}} \qquad \textbf{(1)}$$

In **equation 1**, [M13] refers to the concentration of M13 bacteriophages in virions/mL. A_{269} and A_{320} are the absorbance values at 269 and 320 nm respectively where A_{269} represents the absorbance due to M13 phages and the A_{320} is used to correct for non-specific absorbance. The extinction coefficient is dependant up the number of base pairs (**bp**) in the genome ($\mathbf{N_{bp}}$). In the mutant M13 strains, no additions or deletions were carried out, and so the value for N_{bp} was 7666 bp, which is the size of the parent vector, M13KE (NEB, Whitby, ON, Canada). The constant 6 x 10^{16} can be derived from the extinction coefficient of 3.84 $mg^{-1} \cdot cm^{-1} \cdot mL$ for fd phage by Berkowitz and Day and additional fd phage

measurements summarized by Day and Wiseman (86, 90). The units of this constant are "$mL^{-1} \cdot$ virions $\cdot$ bp".

4.2.1 Troubleshooting of M13 non-specific absorbance

During the procedure for preparing concentrated M13-Aha stocks, the initial approach was to carry out PEG8000 precipitation of M13 phages followed by centrifugation and fully retain the pellet, which contained precipitated phages as per standard methods (91). The resulting M13-Aha stocks in 1x phosphate-buffered saline (**PBS**) were cloudy with an insoluble white precipitate. This precipitate will be referred to as the insoluble fraction. After removing this insoluble fraction by briefly centrifuging, one could recover fully soluble M13 phages from the supernatant. The resulting supernatant was confirmed to contain M13 phages by spot-plating M13 on plate colonies of *E. coli*. Titres as high as 10^{13} pfu/mL were observed in this fraction. Removing the insoluble precipitate was necessary in order to properly characterize the M13 constructs and to solve the issues seen initially with the negative control reactions with M13-Aha M-5/28L.

The insoluble fraction obtained from PEG precipitation was run on Tricine SDS-PAGE and was compared to what was recovered in the soluble fraction of the M13 preparation. In addition to producing zones of turbidity on bacterial lawns, the supernatant fraction clearly contained M13 phages from the banding pattern seen on the Tricine SDS-PAGE gel. The pVIII band could be clearly seen at 7.5 kDa and was enriched in comparison to the pellet fraction (**Figure 4.1A**). For pIII, the bands at both 37 and 53 kDa are near what was expected for minor coat protein pIII. The banding pattern from the soluble fraction closely matched what was seen in **section 3.4**. The insoluble fraction produced a smear of protein when run on Tricine SDS-PAGE. In addition to contaminating proteins there were also phage-associated peaks seen in the insoluble fraction. In particular, a strong band seen at 37 kDa in the pellet fraction might correspond to pIII and suggests that some M13 phages are lost during this extra purification step.

The absorbance spectra of the insoluble and soluble fractions were also compared. One thing that was clearly noticeable in the insoluble fraction absorbance spectra was a high amount of non-specific absorbance and the M13 peak was not well-defined (**Figure 4.1B**). In comparison, the soluble fraction

had a M13 peak that was well-defined and the non-specific absorbance was largely reduced. The absorbance from M13 could be clearly seen from the broad peak with a very shallow maximum at 261 nm. This extra clean-up step was required for producing a higher quality phage preparation with less contaminating material, and was used in preparing subsequent M13 stocks for dye-labelling experiments.

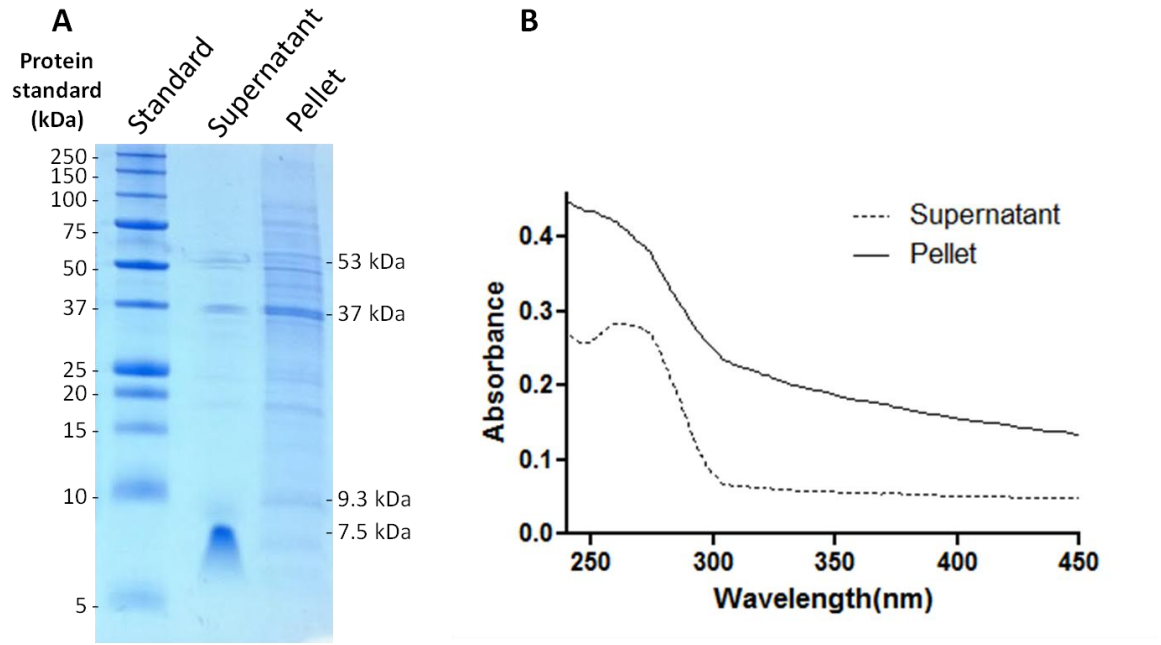

Figure 4.1: Comparison of pellet and supernatant fractions after removing insoluble particles from the final M13 phage stock. (A) Tricine SDS-PAGE of soluble and insoluble fractions from A9M M13 phage preparation stained with Coomassie R250. (B) Absorbance spectrum of soluble and insoluble fractions in 1x PBS.

4.2.2 M-5/28L M13 control reaction for dye-labelling experiments

The dye that was chosen to serve as a label for attachment to M13-Aha was 5(6)-carboxytetramethylrhodamine (**TAMRA**). TAMRA has an absorbance maximum at 556 nm and shoulder below 556 nm (**Figure 4.2A,B**). This shoulder is a characteristic of the TAMRA spectrum (92). The chemistry that was utilized to react with M13-Aha was the strain-promoted azide-alkyne cycloaddition (**SPAAC**) which utilizes an aza-dibenzocyclooctyne (**DIBAC**) reactive group (**Figure 4.2C**). This was developed by Bertozzi and colleagues for facile and mild external labelling of live cells (61). Unlike the Cu(I)-catalysed cycloaddition, the SPAAC reaction can be carried out in the absence of Cu(I). This allows conjugation reactions with Cu(I)-sensitive components such as live cells or quantum dots (61, 93). The two dibenzo- moieties were found to increase the kinetics of this reaction, and the nitrogen in the ring

structure was found to increase water solubility (51). M-5/28L M13 was used as a control since it was shown in **section 3.6** not to incorporate Aha. Therefore any background absorbance or unexpected side reactions could be corrected for or avoided before testing A9M and S13M M13 strains.

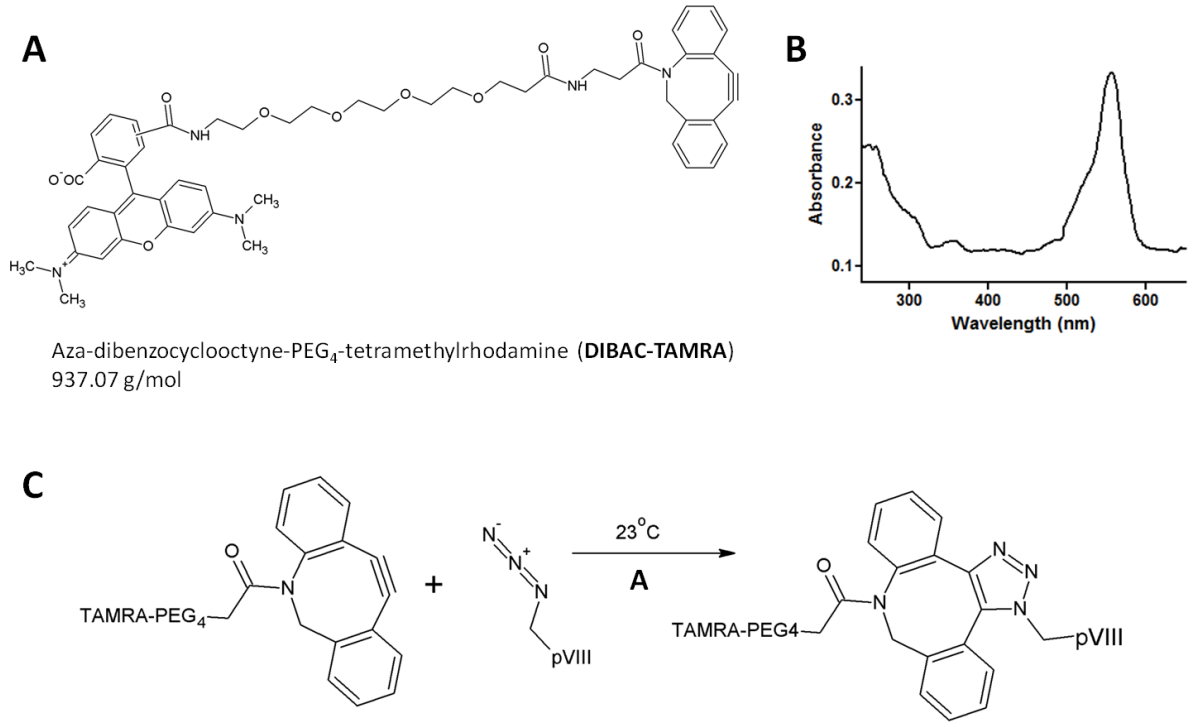

Figure 4.2: Dye-labelling conditions for the SPAAC reaction with M13-Aha. (A) Structure and mass of DIBAC-TAMRA which was used to label M13-Aha. (B) Absorbance spectrum of DIBAC-TAMRA in 1x PBS (10 mM Na_2HPO_4, 1.8 mM KH_2PO_4, 137 mM NaCl, 2.7 mM KCl, pH 7.4). (C) Reaction scheme for SPAAC labelling of pVIII subunits.

As alluded to in **section 4.2.1**, it was essential to include an additional purification step to remove the insoluble material from M13 preparations before using them as a reagent in SPAAC reactions. Prior to the inclusion of this extra purification step, DIBAC-TAMRA labelling of $pVIII_{M\text{-}5/28L}$ produced dubious results. When $pVIII_{M\text{-}5/28L}$ was reacted with DIBAC-TAMRA without first removing the insoluble fraction, this negative control reaction suggested that a high degree of labelling had occurred. **Equation 2** was used to estimate the concentration of M13 phages after reaction with DIBAC-TAMRA from the absorbance spectrum. Since DIBAC-TAMRA also absorbs at 269 nm, **equation 1** was modified to consider contribution from the absorbance of the dye at 269 nm to avoid over-estimating the

concentration of M13 phages. The correction factor (**CF**) was estimated from the absorbance spectrum of DIBAC-TAMRA and calculated as the fraction DIBAC-TAMRA absorbance at 269 nm over its maximum absorbance at 556 nm (A_{269}/A_{556}). The value of CF was estimated to be 0.65.

$$[\text{M13}] = \frac{(A_{269} - A_{556} \times CF - A_{320}) \times 6 \times 10^{16}}{N_{bp}} \quad \textbf{(2)}$$

Equation 3 was used to equate the concentration of M13 viruses to pVIII subunits. From the estimated concentration of M13 in viruses/mL (**[M13]**), one could determine the molarity of pVIII subunits (**[pVIII]**). The value used for the number of pVIII subunits per phage was 2700 pVIII per M13 virus (15).

$$[\text{pVIII}] = [\text{M13}] \times \frac{2700\ \text{pVIII}}{\text{M13}} \times \frac{1000\ mL}{L} \times \frac{1\ mol\ \text{M13}}{6.02 \times 10^{23}\ \text{M13}} \quad \textbf{(3)}$$

The labelling efficiency was defined as the number of dye molecules per pVIII subunit, expressed as a percentage (**equation 4**). The extinction coefficient ($\boldsymbol{\varepsilon_{dye}}$) of 65000 $M^{-1}cm^{-1}$ was used for TAMRA (94). Subtracting A_{590} was done to correct for non-specific absorbance to avoid over-estimating the labelling efficiency.

$$labelling\ efficiency = \frac{(A_{556} - A_{590})}{\varepsilon_{dye} \times [\text{pVIII}]} \times 100\% \quad \textbf{(4)}$$

Using **equations 2-4**, it was estimated that there was a 6.4% labelling efficiency (**Figure 4.3A**). A labelling efficiency of 6.4% was too high to be explained as reaction with the minor coat proteins, pIII, pVI, pVII or pIX. If all 65 of the methionine residues on the minor coat proteins of a single M13 phage were solvent-accessible and only those residues reacted with DIBAC-TAMRA, that would only account for a maximum of 2.4% labelling efficiency. Realistically, the contribution from minor coat protein labelling would be less than this since not all of those residues would be solvent-accessible and the incorporation efficiency of Aha was not 100%. Additionally, since M-5/28L M13 grown in the absence of Aha also had a high TAMRA signal, it seemed likely that the presence of the dye in these samples was not due to the reaction of DIBAC-TAMRA with any azides present in M-5/28L M13.

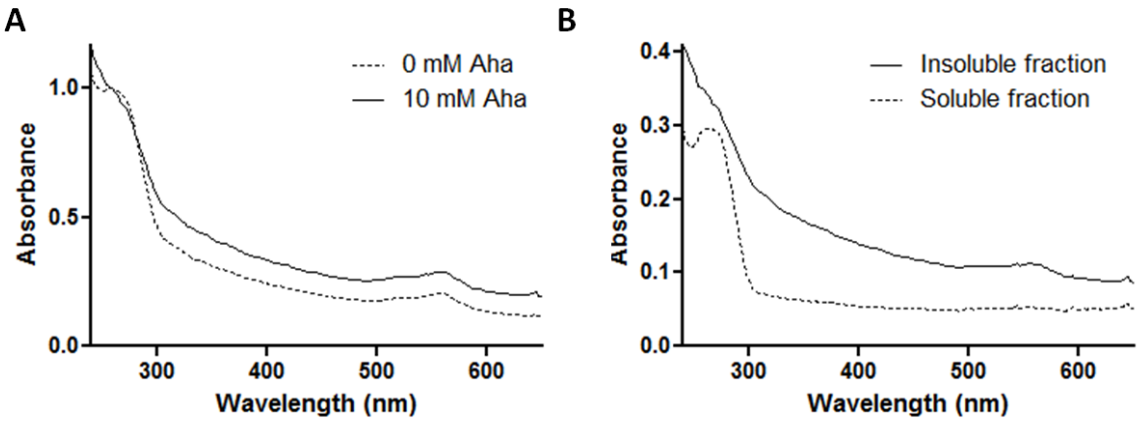

Figure 4.3: Troubleshooting the control reaction for the SPAAC reaction with DIBAC-TAMRA and M-5/28L. (A) The resuspended pellet from PEG precipitation was directly reacted with DIBAC-TAMRA. M13 M-5/28L at 10^{13} pfu/mL was reacted with 30 µM DIBAC-TAMRA for 24 hours. Unreacted DIBAC-TAMRA was removed by fractionation using a Pall Nanosep® 10 kDa MWCO column and the absorbance of the retained M13 phages were read in 1X PBS. (B) M13 phages collected from PEG precipitation were further purified by centrifuging for at 15000 *g* for 1 min and retaining the supernatant. This supernatant containing soluble M13 phages was reacted as described above.

Removing the insoluble fraction prior to reaction with DIBAC-TAMRA greatly reduced the absorbance at 556 nm in the M-5/28L M13 spectrum after reaction (**Figure 4.3B**). This suggests that the post-reaction removal of the dye by spin filtration was more successful at removing un-reacted DIBAC-TAMRA. After improving the M13 sample preparation, the labelling efficiency of M13 M-5/28L grown in 10 mM Aha was reduced to a 1.3 ± 0.9% labelling efficiency. Similarly, for M-5/28L M13 prepared in the absence of Aha, the estimated labelling efficiency was 1.1%. The TAMRA absorbance detected for 10 mM Aha M-5/28L M13 sample likely corresponded to a combination non-specifically bound dye and dye that had reacted to the minor coat proteins of M13. Importantly, troubleshooting this control reaction was an essential step in developing the correct approach to sample preparation prior to SPAAC reaction. By using M-5/28L to troubleshoot this reaction, one can be more confident that contribution to absorbance due to non-specifically bound dye or contaminants are reduced in the A9M and S13M samples.

4.2.3 Coupling of M13 strains to DIBAC-TAMRA using the SPAAC reaction

The two engineered M13 strains, A9M and S13M, along with Wt M13 were reacted with DIBAC-TAMRA after replication in the presence of 10 mM Aha. The reaction was carried out over 24 hours using the conditions outlined in **section 2.6**. The reaction was terminated by removal of DIBAC-

TAMRA using a Pall Nanosep® 10 kDa MWCO column (Sigma-Aldrich, Milwaukee, WI, USA) to fractionate the products. As the Nanosep® column contains a membrane that has a 10 kDa size exclusion pore size, it was expected that M13 phages, which are ~12.6 MDa (estimated from coat-proteins only), would not be filtered through and the smaller DIBAC-TAMRA would be removed effectively. To control for non-specifically bound dye and to ensure that the wash steps adequately removed unreacted dye, M13 phages grown in the absence of Aha were also reacted with DIBAC-TAMRA and given the same clean-up treatment on these spin-filtration membranes.

In comparing the spectra of post-reacted samples of A9M M13 and S13M M13, grown either in the presence of 10 mM Aha or without Aha, it was apparent that the post-reaction removal of DIBAC-TAMRA was sufficient to remove the bulk of the non-reacted dye (**Figure 4.4A,B**). In comparison, the A9M and S13M M13 that were grown in the presence of Aha did have a strong TAMRA peak that remained after washing. Using **equations 2-4** for labelling efficiency, the strains A9M and S13M were reacted equally well at 14 ± 2 % and 13 ± 2 % labelling efficiencies respectively (**Table 4-1**). This corresponded to approximately 360 dye molecules reacted to each M13 phages scaffold.

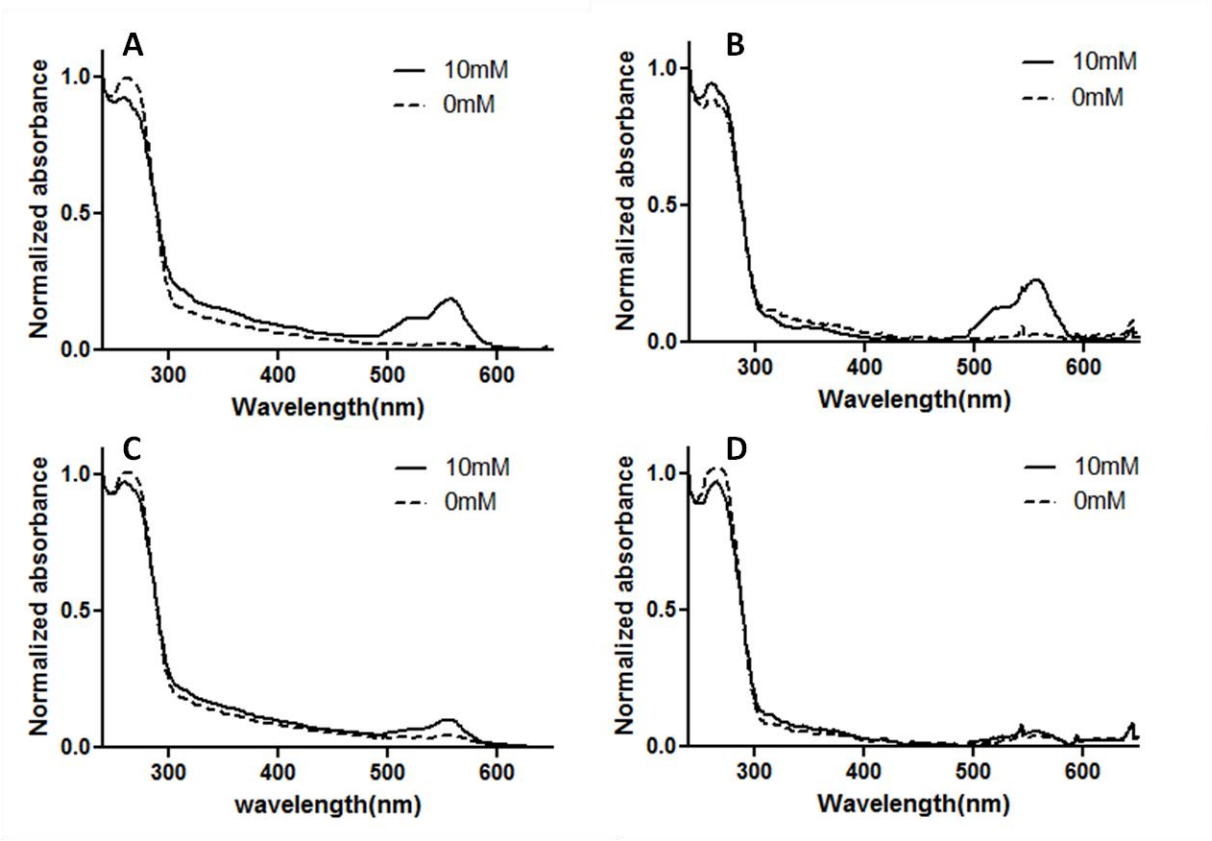

Figure 4.4: Normalized absorbance spectra of M13 strains reacted with DIBAC-TAMRA via SPAAC reaction. Reactions were carried out as described in the Methods. (A) A9M M13 grown in either 0 or 10 mM Aha post-reaction. (B) S13M M13 grown in either in 0 or 10 mM Aha post-reaction. (C) Wt M13 grown in either in 0 or 10 mM Aha post-reaction. (D) M-5/28L M13 grown in either in 0 or 10 mM Aha post-reaction.

Wt M13 was also reacted with DIBAC-TAMRA after amplification with 10 mM Aha. The TAMRA-associated absorbance peak at 556 nm was much smaller in comparison to the M13 absorbance peaks than either A9M or S13M preparations (**Figure 4.4C**). Wt M13 was labelled significantly less at 5 ± 1% labelling efficiency. While Met28 on $pVIII_{WT}$ was predicted to have low solvent-accessibility, M13 has some flexibility in solution (95). It is possible that the flexibility of M13 allowed a percentage of azides to be exposed enough for reaction with DIBAC-TAMRA. From labelling M13 strains with fluorescent dye, the necessity of repositioning the methionine residue was apparent. A9M and S13M both were labelled significantly better than Wt M13 suggesting better solvent-accessibility of the azide in those mutants. Lastly, the absorbance spectra for M-5/28L M13 after reaction with DIBAC-TAMRA were not very different from each other, regardless of whether M-5/28L was prepared with Aha (**Figure 4.4D**). In order to increase the accuracy of the dye-labelling estimates, the labelling efficiency measured for M-

5/28L was subtracted from the labelling efficiencies for A9M, S13M and Wt M13 to correct for non-specific dye absorbance and reaction with the minor coat proteins detected in the negative control (**Table 4-1**). Therefore, a more conservative estimate of the number of azide functionalities presented on each M13-Aha particle was approximately 340 azide groups per M13.

Table 4-1: Summary of labelling efficiencies of DBCO-TAMRA dye to pVIII-Aha mutants. Errors are shown as standard deviation.

Strain	Labelling efficiency (%)	Corrected labelling efficiency (%)
A9M	14 ± 2	13 ± 2
S13M	13 ± 2	12 ± 2
WT	5 ± 1	4 ± 1
M-5/28L	1.3 ± 0.9	n/a

4.2.4 Estimation of quantity of pVIII-Aha subunits per M13 bacteriophage

In the ideal case, one would like to directly relate the labelling efficiency for M13-Aha constructs to the number of pVIII-Aha subunits per phage. This required the assumption that DIBAC-TAMRA reacted to completion with available pVIII-Aha subunits. If the reaction does not go to completion, then estimating the number of pVIII-Aha subunits per phage from the dye labelling efficiencies would result in an underestimate of the degree of Aha incorporation. To assess the reaction progress of M13-Aha constructs with DIBAC-TAMRA at 24 hours of reaction, the mutant strain A9M M13 was analysed by mass spectrometry following labelling with DIBAC-TAMRA. At this point, it was found that while A9M and S13M both handled well, A9M typically produced in higher yields when grown with 10 mM Aha and so it was used for this analysis.

In the A9M M13 prepared in the absence of Aha, there were no peaks on the mass spectrum that one might expect for reaction to DIBAC-TAMRA. The major peak was seen at 5280 Da and corresponded to the expected mass of pVIII-Met (**Figure 4.5A**). Additionally, there were no pVIII-Aha peaks at 5275 Da which reflected the absence of Aha in that sample. In the A9M phages prepared with 10 mM Aha, there was a peak on its mass spectrum that corresponded well with what was expected for covalent attachment of DIBAC-TAMRA to $pVIII_{A9M}$-Aha (**Figure 4.5B**). The expected mass of DIBAC-TAMRA is 937.07 Da and $pVIII_{A9M}$-Aha had a mass of 5275 Da. Therefore, the expected MW of a pVIII-

TAMRA conjugate was 6212 Da. The peak 6212 Da in the mass spectrum was attributed to the formation of a pVIII-TAMRA conjugate. As highlighted in the inset, the pVIII-Aha peak largely disappeared among the background signal indicating that the pVIII-Aha subunits reacted to near completion over the 24 hour reaction (**Figure 4.5B; inset**). Therefore, for A9M M13, the labelling efficiency determined above was likely a good approximation of how many pVIII subunits had Aha incorporated.

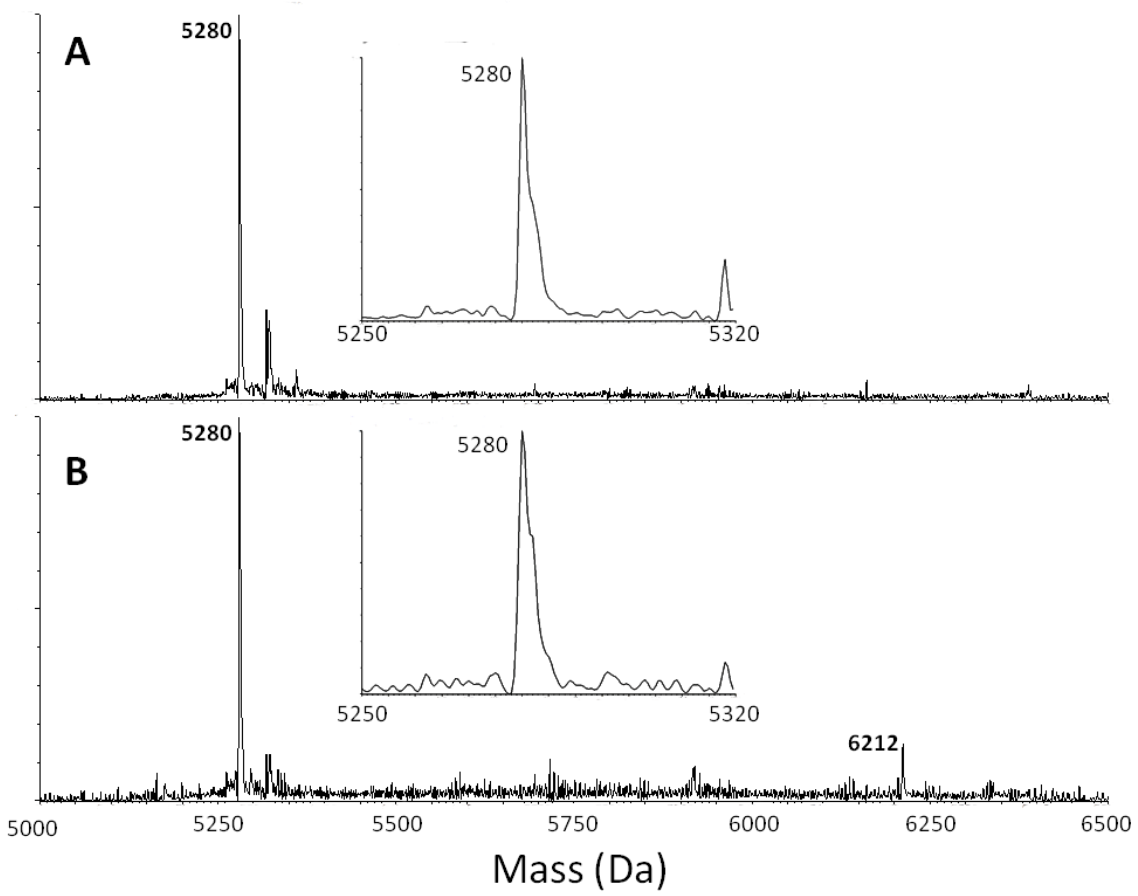

Figure 4.5: Deconvoluted mass spectra of A9M M13 phages reacted with DIBAC-TAMRA as described in the Methods. (A) A9M phages were grown in the absence of Aha and reacted with DIBAC-TAMRA. (B) A9M phages grown with 10 mM Aha were reacted with DIBAC-TAMRA. The insets magnify the section of each spectrum from 5250 to 5320 Da.

In an UAA incorporation study previously reported with adenovirus, a "pulse"-labelling type approach was used where completely methionine-deficient and Aha-containing media was added for 6 hours post-infection, followed by growth in methionine-containing media. In this adenovirus paper, their reported levels of incorporation efficiency were estimated at 10 % incorporation using Aha at 32 mM (48). In contrast to M13, adenovirus has a lytic life cycle in which the host cell dies in the process of

releasing viruses (96). This type of labelling approach differed greatly from that which was required with this thesis work. One of the requirements for M13 replication was satisfying growth of the *E. coli* host with a combination of Aha and methionine, since unlike adenovirus, M13 does not lyse its host bacterium. This was confirmed in **section 3.5** where no increase in M13 yield could be detected during 4.5 hours of replication without methionine.

While the addition of methionine to the growth media was necessary for M13-Aha production, it may also function as an additional tool for fine-tuning of Aha incorporation in M13. One of the major steps in residue specific UAA incorporation is charging the Aha onto tRNA by methionyl-tRNA synthetase (**MetRS**). For Aha, the k_{cat}/K_m for the methionyl-tRNA synthetase is 1/390 of that for methionine (35). By adjusting the availability of methionine and Aha in the growth media, which are both competing for MetRS, the relative quantities of Aha-tRNA and methionyl-tRNA might be controlled. This then would be expected to define the incorporation efficiencies using ER2738 MetE as the host stain. The ability to pre-determine or control the number of azides per M13 phage would be very useful. If one were using M13-Aha as a scaffold for a particular component in a device, one would be interested in testing a range of component concentrations to optimize device function for example. This approach might enable such fine-tuning of M13-Aha to be done.

Alternatively, there has been research done regarding a series of MetRS mutants that are capable of incorporation of a different azide-containing UAA, *L*-azidonorleucine (**Anl**). Some of the MetRS mutants constructed by Tanrikulu *et al.* had 3.2-fold preference for Anl over methionine (97). Since the M13-Aha constructs in this thesis work have already been designed to incorporate Aha in place of methionine, construction of an *E. coli* ER2738 strain that expresses one of the Anl-MetRS could be applied to the same M13 mutants. Given the preference of these MetRS mutants for Anl, one might be able to increase the incorporation efficiency of azides into pVIII of M13. This would require changes to the media conditions such that Anl was present instead of Aha and might result in more complete azide-labelled M13 phages.

4.3 Transmission electron microscopy of M13 phages

4.3.1 Construction of pVIII-biotin M13 phages via the modified Staudinger ligation

In order to visualize the distribution of pVIII-Aha subunits along the length of M13, biotin-M13 constructs were prepared. The initial approach to labelling M13-Aha phages with biotin was to utilize the modified Staudinger ligation (58). The reactive moiety used in this reaction is a triarylphosphine (**TAP**) conjugated to a PEG-linker and biotin (**Figure 4.6A**). The reaction conditions used were similar to the SPAAC reaction (**Figure 4.6B**). Also of note, unlike the SPAAC reaction, there is a loss of nitrogen gas and methanol, and gain of water during this reaction. Therefore, when analysing the mass spectra of post-reacted products, one must consider a loss of 42 Da resulting in an overall net gain of 750.92 Da to the pVIII-Aha mass of 5275 Da. The expected mass of a pVIII-biotin conjugate produced this way would be 6025.9 Da.

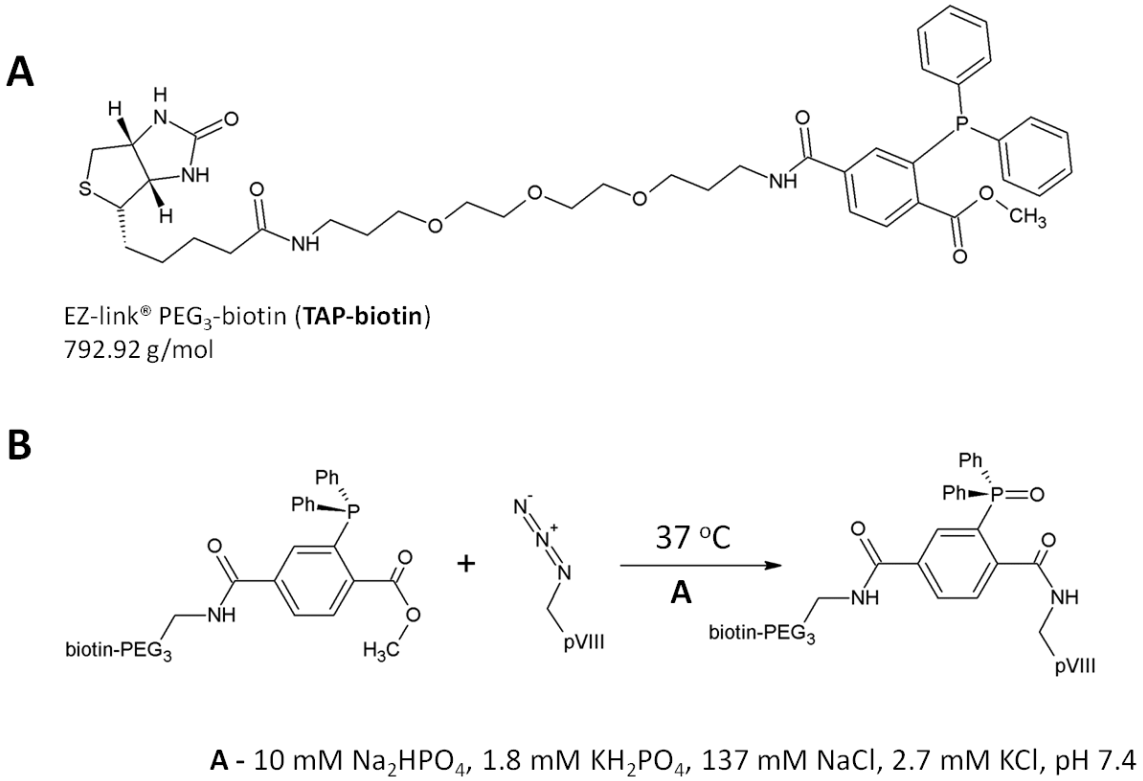

Figure 4.6: Biotin-labelling reagent for modified Staudinger ligation. (A) Structure and mass of TAP-biotin which was used to label M13-Aha. (B) Reaction scheme for the modified Staudinger ligation for labelling of pVIII subunits with biotin.

M13 A9M grown either in the absence or presence of 10 mM Aha was reacted via the modified Staudinger ligation with TAP-biotin. The mass spectrum of A9M without Aha had a major peak present at 5279 Da which likely corresponded to pVIII-Met as seen previously (**Figure 4.7A**). The signal appearing at 5295.5 Da was likely methionine sulfoxide formation (+16 Da). Additionally, a peak was seen at 5916 Da which may have corresponded to an adduct of 637 Da. Given that an ionic species of similar mass was seen when flushing the instrument with solvent only, this likely corresponded to a contaminant. The mass spectrum of A9M produced in the presence of 10 mM Aha had a major peak present at 5279 Da which likely corresponded to pVIII-Met (**Figure 4.7B**). The contaminant at +637 Da to the primary peak was again seen here. A peak at 6025 Da corresponded closely to the expected mass of pVIII-Aha reacted to TAP-biotin via the modified Staudinger ligation. This suggested that pVIII-Aha was conjugated to biotin, although the signal was low at 4.8 % of the pVIII-Met signal. Additionally, unlike with the SPAAC reaction, pVIII-Aha was detected in this spectrum at 5274.5 Da after reaction. The intensity of the pVIII-Aha signal was approximately 5.2 % of the pVIII-Met signal.

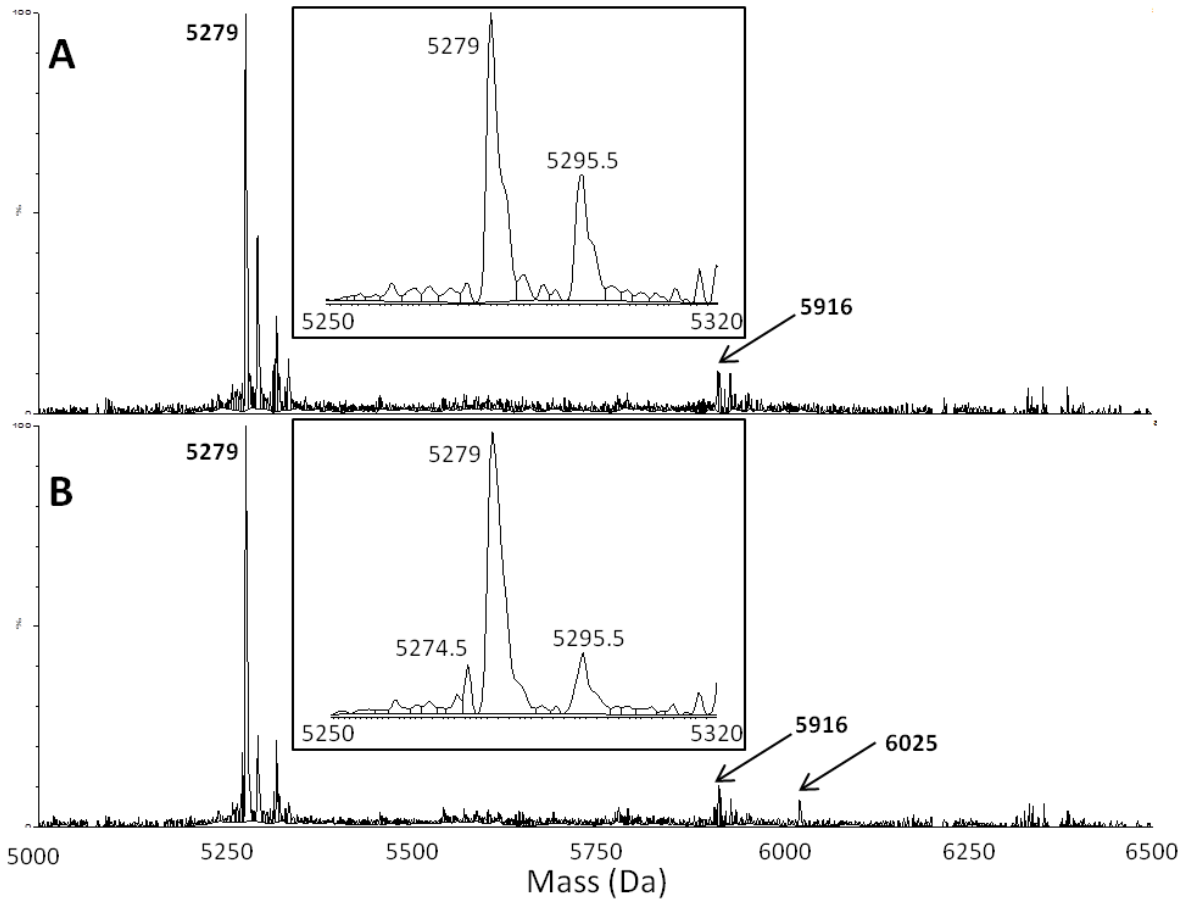

Figure 4.7: Deconvoluted mass spectra of A9M M13 phages reacted with DIBAC-TAMRA as described in the Methods. (A) A9M phages were grown in the absence of Aha and reacted with DIBAC-TAMRA. (B) A9M phages grown with 10 mM Aha were reacted with DIBAC-TAMRA. The insets magnify the section of each spectrum from 5250 to 5320 Da.

It seemed likely that while pVIII-Aha does react via the modified Staudinger ligation, over 24 hours, it does not react to completion. This was evidenced by the presence of both a pVIII-biotin and pVIII-Aha peaks on the spectrum. One issue that has been noted with the modified Staudinger ligation is the slow reaction kinetics and propensity for air oxidation of the reagents (60). Given longer periods of time, the TAP-biotin reagent might react to completion. Alternatively, one could compensate for the low second-order rate constant by increasing the reactant concentrations (60). In the case of M13-Aha, this would require additional scale-up of culture size. Overall, while this approach may be feasible, the SPAAC reaction utilizing the DIBAC reactive group was found to be more suitable for labelling of M13-Aha constructs.

4.3.2 Construction of pVIII-biotin M13 phages via the SPAAC

The SPAAC reaction was also applied to the visualization of the distribution of Aha along the length of M13 by TEM. DIBAC-biotin was reacted to Aha-M13 strains and then labelled samples were visualized on TEM (**Figure 4.8**). As was done in **section 4.2**, the reaction was terminated by removal of DIBAC-biotin. The DIBAC-biotin conjugates have a PEG linker of approximately 22 Å to facilitate binding of streptavidin. Streptavidin-conjugated gold nanoparticles (**SA-AuNPs**) were bound non-covalently to the biotin-conjugated M13 phages. In this way the positioning of pVIII-Aha subunits could be visualized indirectly based on where the AuNPs bind.

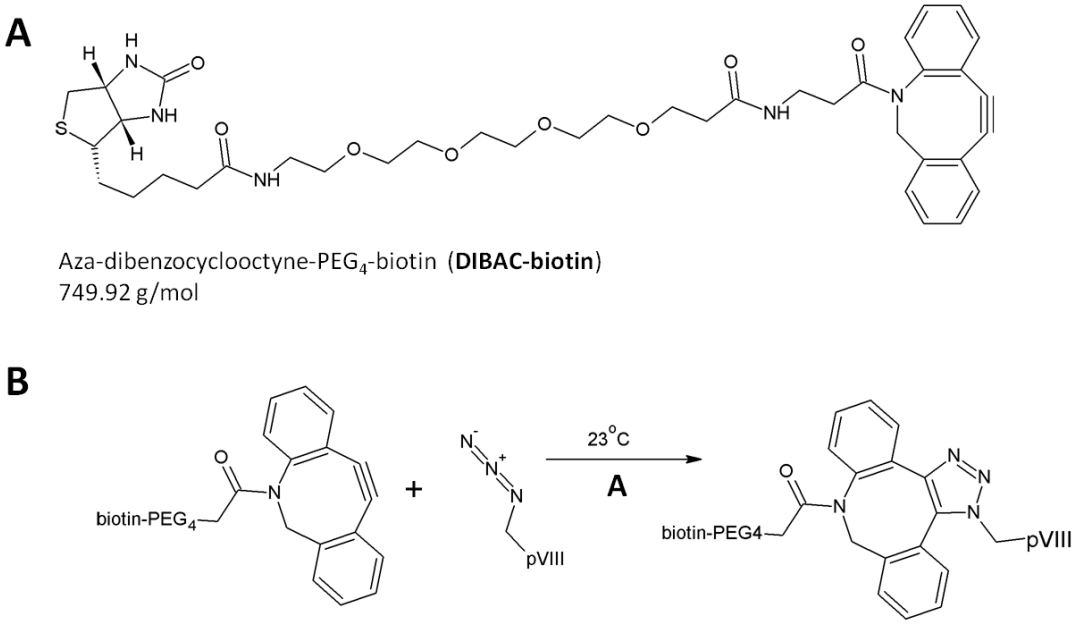

Figure 4.8: Biotin-labelling conditions for the SPAAC with M13-Aha. (A) Structure and mass of DIBAC-biotin which was used to label M13-Aha. (B) Reaction scheme for SPAAC labelling of pVIII subunits with biotin.

Electrospray ionization mass spectrometry (**ESI-MS**) confirmed that DIBAC-biotin was covalently bound to A9M and S13M pVIII-Aha as expected, but could not be detected for Wt M13. Unlike the mass spectra obtained from the Waters Q-TOF ESI-TOF instrument in **section 3.6**, these spectra were obtained on a ThermoScientific Q-Exactive Orbitrap instrument equipped with an ESI source. The higher resolution of this instrument allowed the exact masses of pVIII mutants to be

determined and so when predicting the theoretical masses of different pVIII mutants, monoisotopic masses had to be considered. This is the mass calculated for a peptide or protein assuming all amino acids were composed of the lightest isotopes for each atom.

A9M M13 amplified with Aha and reacted to DIBAC-TAMRA was analysed using ESI-MS results. The expected mono-isotopic mass of A9M was 5276.79 Da. This corresponded well with the primary peak at 5276.8 Da (**Figure 4.9**). Methionine sulfoxide formation of pVIII-Met was observed at 5292.8 Da in this sample. At 6021.1 Da there was a peak that corresponded to the expected mass of the pVIII-biotin conjugate. No pVIII-Aha peak was detected in this spectrum at -5 Da to the primary peak. This spectrum clearly indicated that A9M M13-Aha was covalently reacted to DIBAC-TAMRA and the lack of a pVIII-Aha peak suggested a low amount of un-reacted pVIII-Aha in the sample.

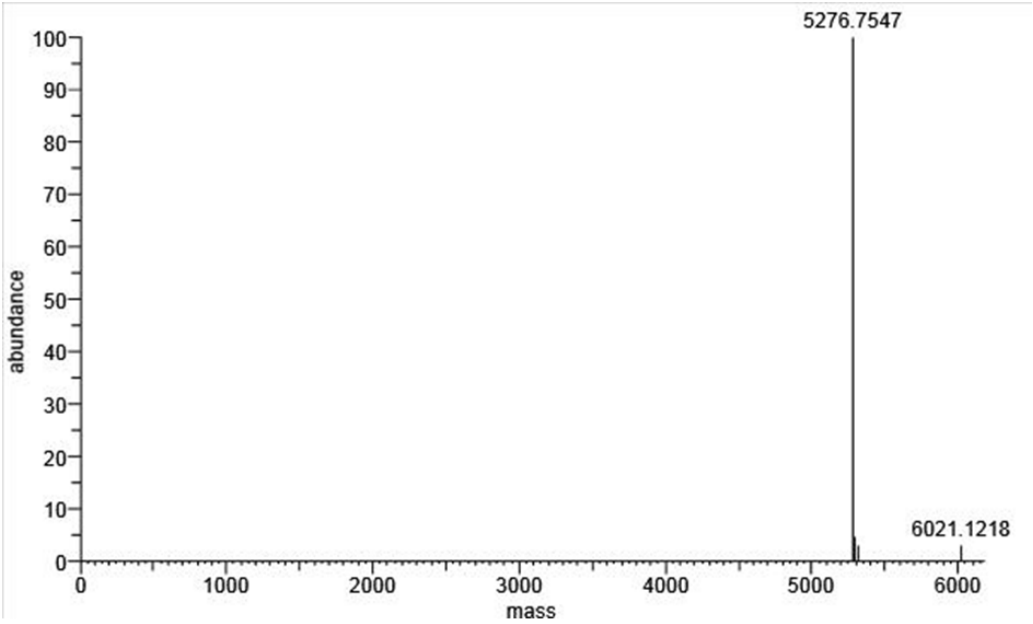

Xtract Masses Table				
Monoisotopic Mass	Sum Intensity	Number of Charge State	Average Charge	Delta Mass
5276.755	3149007	4	5.16	0
5292.769	151252.6	2	5.44	16.0145
6021.122	98396.78	2	5.57	744.3671
5317.731	95047.35	1	5	40.9761

Figure 4.9: Deconvoluted mass spectrum of A9M-Aha reacted with DIBAC-biotin via the SPAAC reaction. This spectrum was obtained utilizing a FisherScientific ESI-orbitrap instrument.

S13M M13 amplified with Aha and reacted to DIBAC-TAMRA was analysed by ESI-MS. The expected mono-isotopic mass of S13M was 5260.80 Da. This corresponded well with the primary peak at 5260.8 Da (**Figure 4.10**). Methionine sulfoxide formation was observed in this sample at 5276.7 Da. At 6005.1 Da there was a peak that corresponded to the expected mass of the pVIII-biotin conjugate. No pVIII-Aha peak was detected in this spectrum at -5 Da to the primary peak. As with A9M, this spectrum clearly indicated that S13M M13-Aha was covalently reacted to DIBAC-TAMRA and that there was a low amount of unreacted pVIII-Aha remaining.

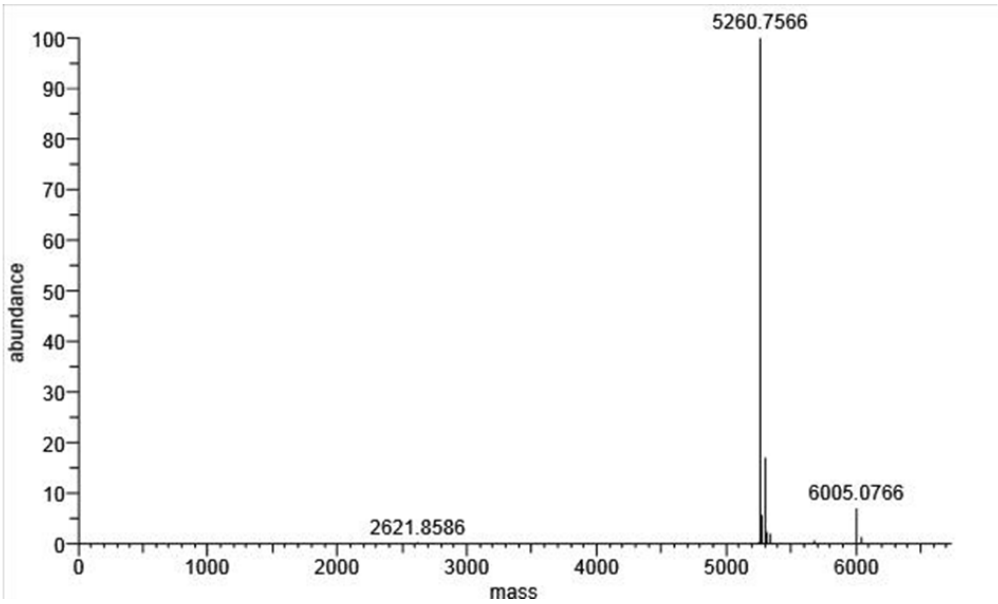

Xtract Masses Table				
Monoisotopic Mass	Sum Intensity	Number of Charge State	Average Charge	Delta Mass
5260.757	392651.7	5	5.5	0
5298.687	66872.06	5	5.88	37.93
5302.737	34293.72	4	5.19	41.9808
6005.077	28467.27	3	5.96	744.32
5276.725	22778.67	3	5.76	15.9684
5314.661	9226.71	3	5.89	53.9041
5340.662	8095.19	2	5.52	79.9051
5282.713	7219.71	3	5.99	21.9559
6043.064	5354.79	2	6.39	782.3075
5674.941	3279.11	1	6	414.1848
5245.722	2548.4	1	5	-15.0348
2621.859	2106.77	1	3	-2638.9
5336.663	1287.01	1	6	75.9063

Figure 4.10: Deconvoluted mass spectrum of S13M-Aha reacted with DIBAC-biotin via the SPAAC reaction. This spectrum was obtained utilizing a FisherScientific ESI-orbitrap instrument.

Wt M13 amplified with Aha and reacted with DIBAC-TAMRA was analysed by ESI-MS. The expected mono-isotopic mass of Wt pVIII was 5235.74 Da. This corresponded well with the primary peak at 5235.7 Da (**Figure 4.11**). Methionine sulfoxide formation was observed in this sample at 5250.7 Da. No peaks were observed that might be attributed to a pVIII-biotin conjugate. As well, pVIII-Aha was detected in this spectrum at 5229.7 Da. Unlike either A9M or S13M, Wt M13 did not appear to have reacted with DIBAC-TAMRA. One possibility was that a percentage of pVIII-Aha subunits did react, but was not detected in the mass spectrum due to low abundance in the sample.

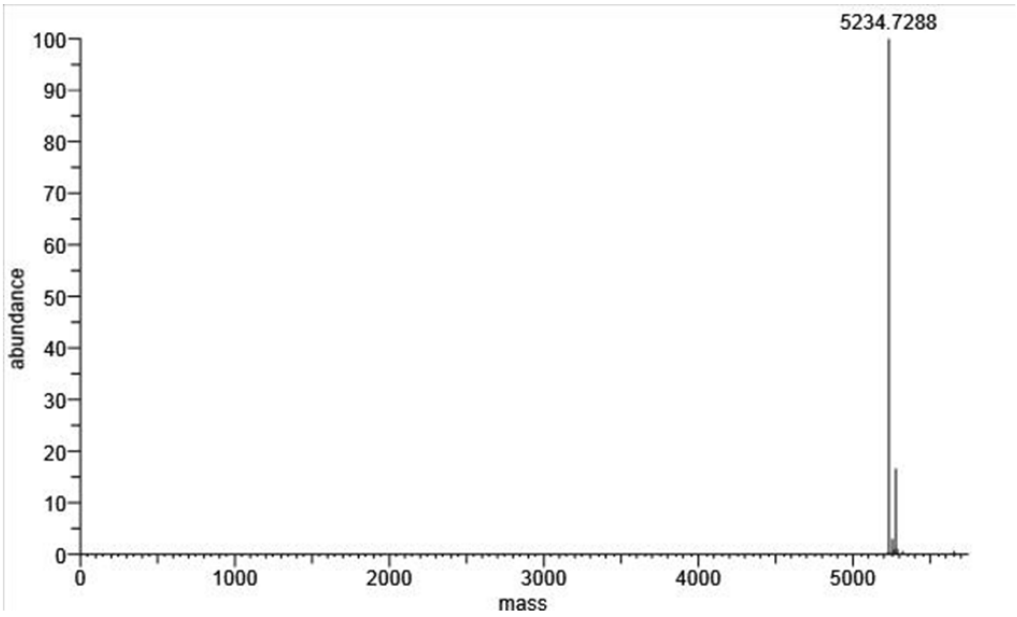

Xtract Masses Table				
Monoisotopic Mass	Sum Intensity	Number of Charge State	Average Charge	Delta Mass
5234.729	2709839	4	5.38	0
5272.674	452520.7	4	5.9	37.9451
5229.722	213084.8	3	5.59	-5.0069
5276.71	94007.57	2	5.24	41.9807
5250.735	88728.52	3	5.89	16.0066
5287.656	29179.62	2	6.35	52.9271
5267.69	29057.72	2	5.78	32.9611
5648.913	19681.5	1	6	414.1844
5314.658	19608.38	1	6	79.9287
5219.732	11151.09	1	5	-14.9968
5235.733	8635.51	1	8	1.0042

Figure 4.11: Deconvoluted mass spectrum of Wt pVIII-Aha reacted with DIBAC-biotin via the SPAAC reaction. This spectrum was obtained utilizing a FisherScientific ESI-orbitrap instrument.

4.3.3 Distribution of pVIII-Aha subunits along the length of M13 phage strains

After reacting DIBAC-biotin with the different M13-Aha constructs, the phages were prepared for TEM analysis by incubating them with bovine serum albumin (**BSA**) followed by SA-AuNPs on a copper formvar grid. The BSA was used to block the areas of the grid where there were no M13 phages and thereby prevent non-specific binding of AuNPs. This approach was done with success by Ploss, M. and Kuhn, A. to visualize M13 with Au-labelled antibodies (67). The formvar grids were stained with uranyl-acetate, an electron dense negative stain, which allows proteins that are not normally visible by

TEM to be imaged. In negative staining, the areas where there is an exclusion of dye allow electrons to pass through more easily allowing protein to be visualized (98). Since the AuNPs themselves are electron dense, they are easily visualized without staining.

A9M M13 grown in the absence of Aha was prepared for TEM analysis as described above with SA-AuNPS. The phages were visualized as ~1 µm filamentous particles of lighter colour on the TEM micrograph (**Figure 4.12**). SA-AuNPs were visualized as ~8 nm in diameter dark circles in the TEM micrograph. The white particles that can be seen spotting the image are likely the BSA that was used to block the grid. On average there were approximately 3-4 SA-AuNPs seen associated with each A9M phage. These were likely associated non-specifically with the phages as DIBAC-biotin was not expected to react with this sample.

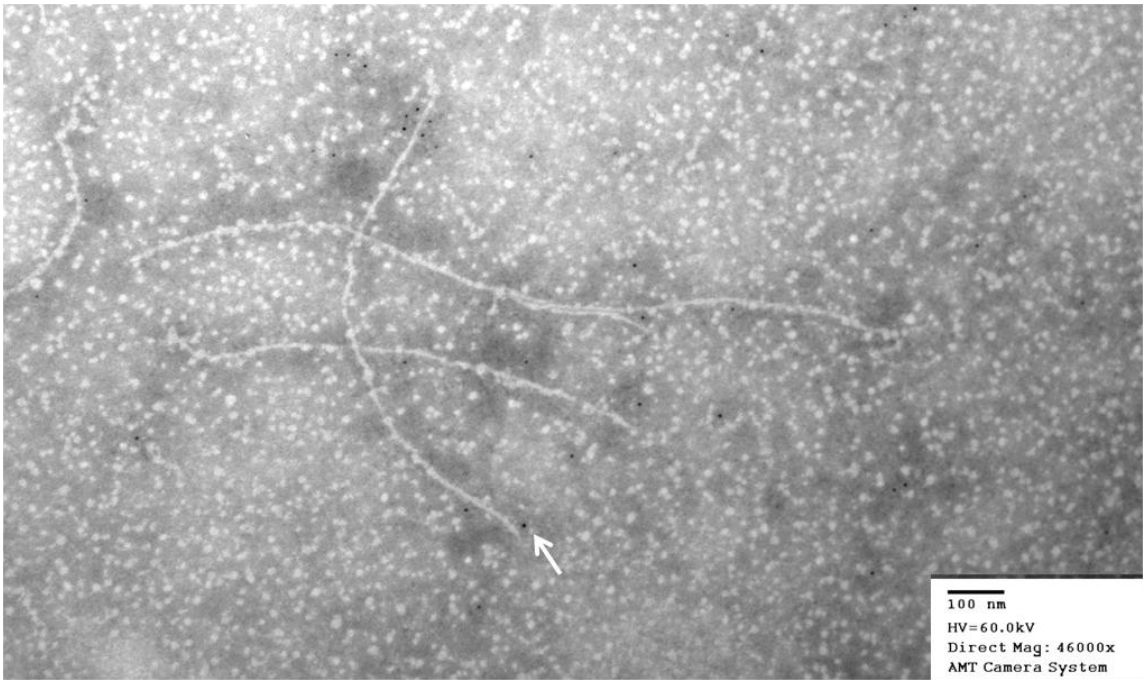

Figure 4.12: TEM micrograph of A9M M13 grown in the absence of Aha. This sample was reacted with DIBAC-biotin as outlined in the methods. The sample was prepared on a copper formvar grid which was blocked with BSA prior to stain with SA-AuNPs and 1% uranyl acetate. The white arrow shows a SA-AuNP.

A9M grown with 10 mM Aha was prepared for TEM analysis as described above with SA-AuNPS. The M13 A9M phage particles can be seen decorated with SA-AuNPs (**Figure 4.13**). On average there were 53-54 AuNPs per M13 phage particle. The AuNPs appeared to be evenly distributed along the

length of the M13 scaffold rather than concentrated in a particular region. This suggests that pVIII-Aha subunits themselves were evenly distributed along the length of M13. It is likely that this image gives an underestimate as to how many pVIII-Aha subunits there were per bacteriophage.

A thin shell can be seen surrounding SA-AuNPs which was likely the conjugated streptavidin (**Figure 4.13**). Including this shell, the particle size estimate for the SA-AuNPs was approximately 16 nm. In comparison to the estimates from dye-labelling there were less SA-AuNPs per phage than expected. One could consider several factors as to why there were less AuNPs seen bound per phage. Given the relatively large size of the nanoparticles, there are likely steric limitations whereby binding of SA-AuNPs blocked adjacent particles from binding. A crude approximation using a simulated 16 nm sphere and structure of M13 was used to approximate that 15-25 pVIII subunits may be blocked by SA-AuNP binding (**Figure 4.14**). In addition to steric effects, electrostatic effects may also be a factor. Streptavidin is reported to have a pI of 5-6 (99). Given that the SA-AuNPs were stored in 1x PBS at pH 7.4 and diluted into water, it is possible that the conjugated SA were negatively charged and may have experience some electrostatic repulsion. BSA in the blocking solution might also have blocked some pVIII-biotin subunits. Lastly, in preparing these sample grids, M13-biotin constructs were fixed to the grid prior to the addition of SA-AuNPs. If only one side of M13-biotin phages were exposed to the SA-AuNP solution, then only a fraction of pVIII-biotin subunits would be expected to be labelled with AuNPs.

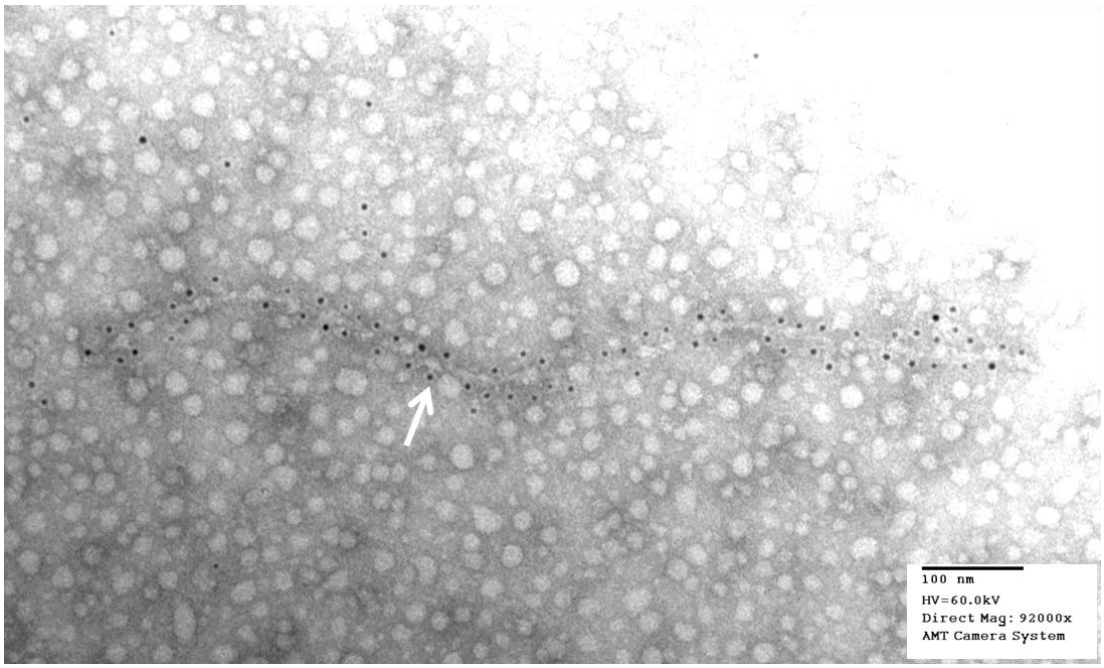

Figure 4.13: TEM micrograph of A9M M13 grown with 10 mM Aha. This sample was reacted with DIBAC-biotin as outlined in the methods. The sample was prepared on a copper formvar grid which was blocked with BSA prior to stain with SA-AuNPs and 1% uranyl acetate. The white arrow shows a SA-AuNP.

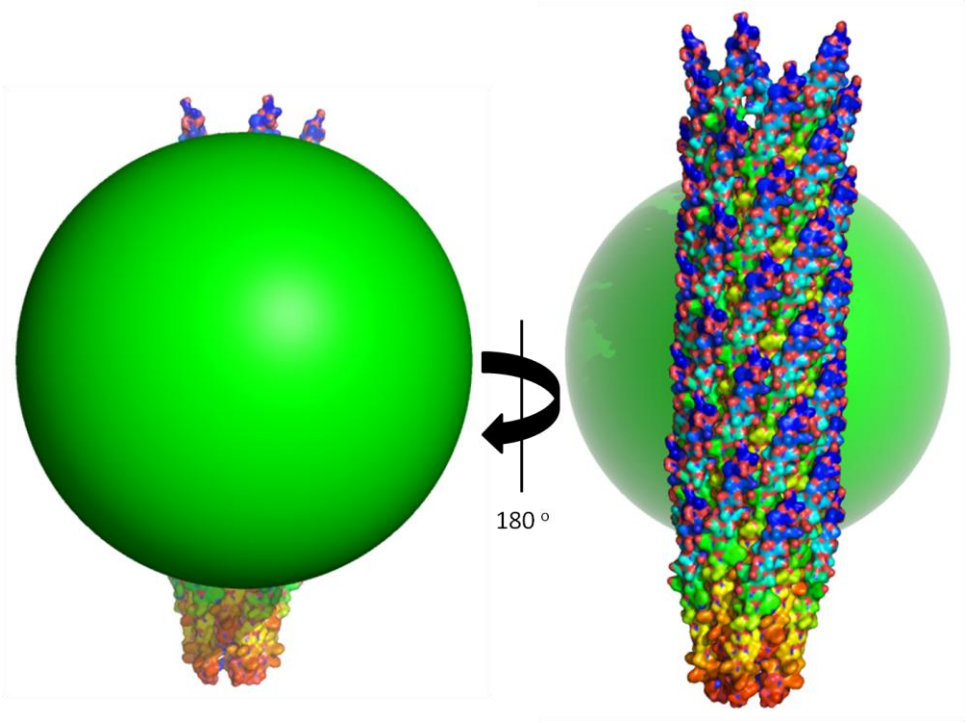

Figure 4.14: M13 segment with simulated 16 nm sphere. The structure file used comes from PDB:1IFJ (16)**.**

S13M grown in the absence of Aha was prepared for TEM analysis as described above with SA-AuNPS. The length of the M13 particles were near the expected length at approximately 1 µm (**Figure 4.15**). As was seen with A9M grown without Aha, there were few SA-AuNPs seen associated with the M13 particles. On average there were 2 SA-AuNPs seen associated per M13 phage and their interaction with M13 was likely non-covalent and independent of biotin.

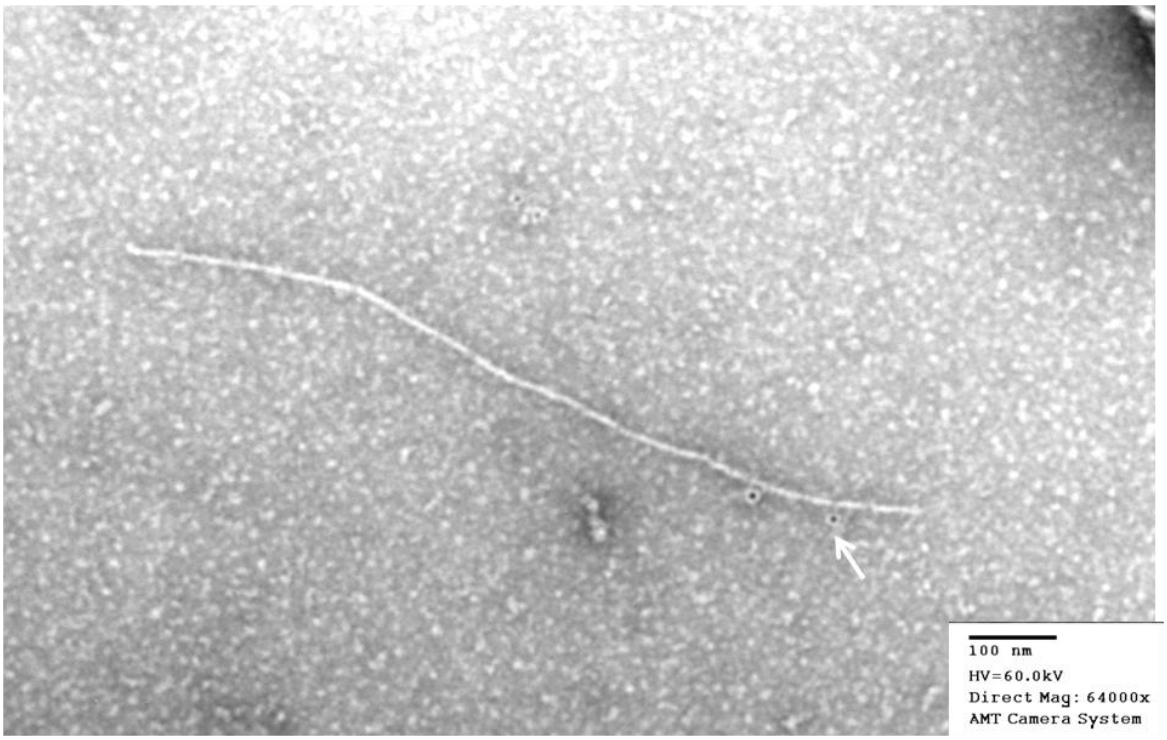

Figure 4.15: TEM micrograph of S13M M13 grown in the absence of Aha. This sample was reacted with DIBAC-biotin as outlined in the methods. The sample was prepared on a copper formvar grid which was blocked with BSA prior to stain with SA-AuNPs and 1% uranyl acetate. The white arrow shows a SA-AuNP.

S13M grown with 10 mM Aha was prepared for TEM analysis as described above with SA-AuNPs. The M13 S13M phage particles templated the organization of SA-AuNP successfully (**Figure 4.16**). The section of the TEM grid where this was imaged was not heavily stained with uranyl acetate. Despite this, the outline of M13 particles were faintly visible and at an appropriate length of about 1 µm. The SA-AuNPs were very clearly visible due to the higher contrast of AuNPs with lightly stained regions of the grid. On average there were 57-58 SA-AuNPs per M13 bacteriophage scaffold which was similar to what was observed for A9M 10 mM samples. As with A9M, it was expected that the quantity of bound

SA-AuNPs underestimated the number of pVIII-Aha subunits per phage. This was again attributed to steric limitations and the grid preparation conditions.

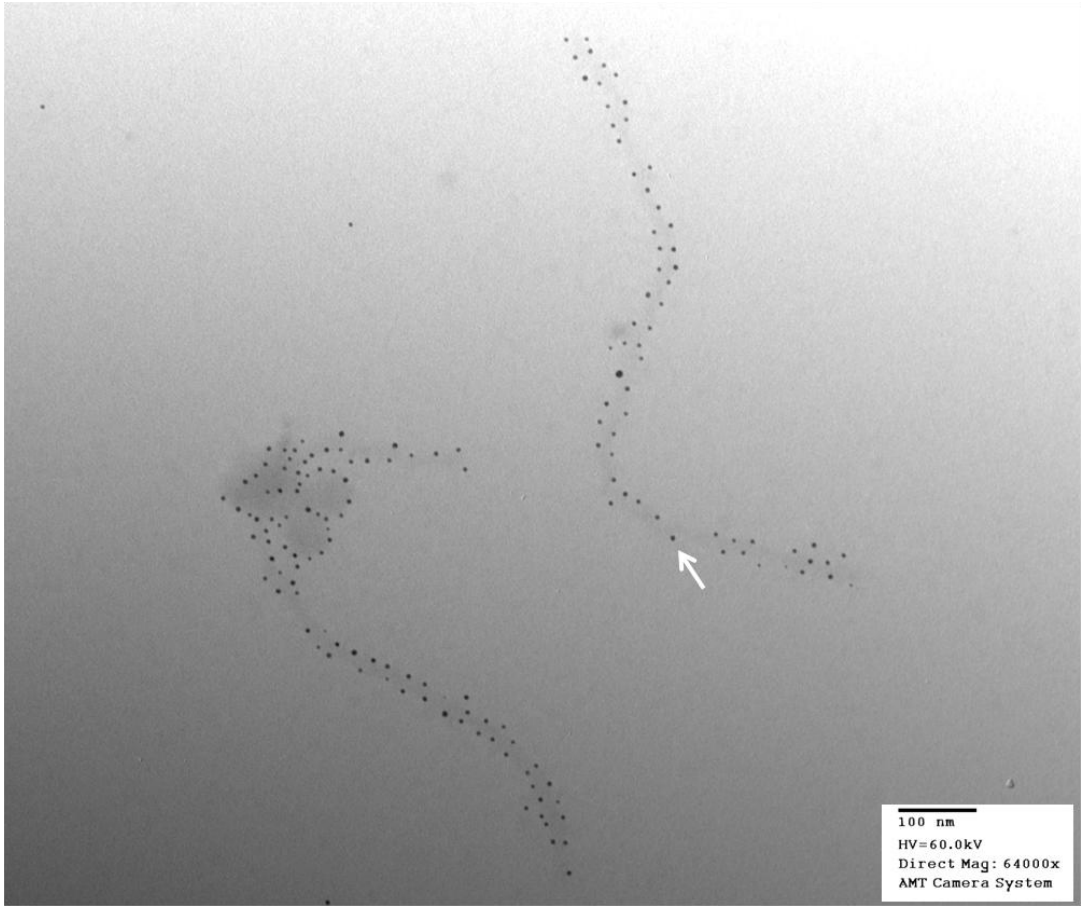

Figure 4.16: TEM micrograph of S13M M13 grown with 10 mM Aha. This sample was reacted with DIBAC-biotin as outlined in the methods. The sample was prepared on a copper formvar grid which was blocked with BSA prior to stain with SA-AuNPs and 1% uranyl acetate. The white arrow shows a SA-AuNP.

As a control to confirm that binding of the SA-AuNPs was due to binding to pVIII-Aha subunits that were reacted with biotin via the SPAAC reaction, the negative control mutant M-5/28L was grown in 10 mM Aha and also analysed by TEM. Even after growth in Aha, M-5/28L phages on average only had 5-6 SA-AuNPs in close proximity to each phage particle (**Figure 4.17**). The M-5/28L strain was expected to be incapable of templating the organization of AuNPs. From the mass spectra previously obtained for M-5/28L mutants in **section 3.6**, these constructs had no evidence of Aha incorporation into pVIII. Therefore, this sample controlled for any binding of SA-AuNPs that could possibly occur in the absence

of the SPAAC reaction with DIBAC-biotin. This control sample showed that binding of AuNPs to A9M and S13M M13-Aha samples was indeed due to the azide specific conjugation with DIBAC-biotin.

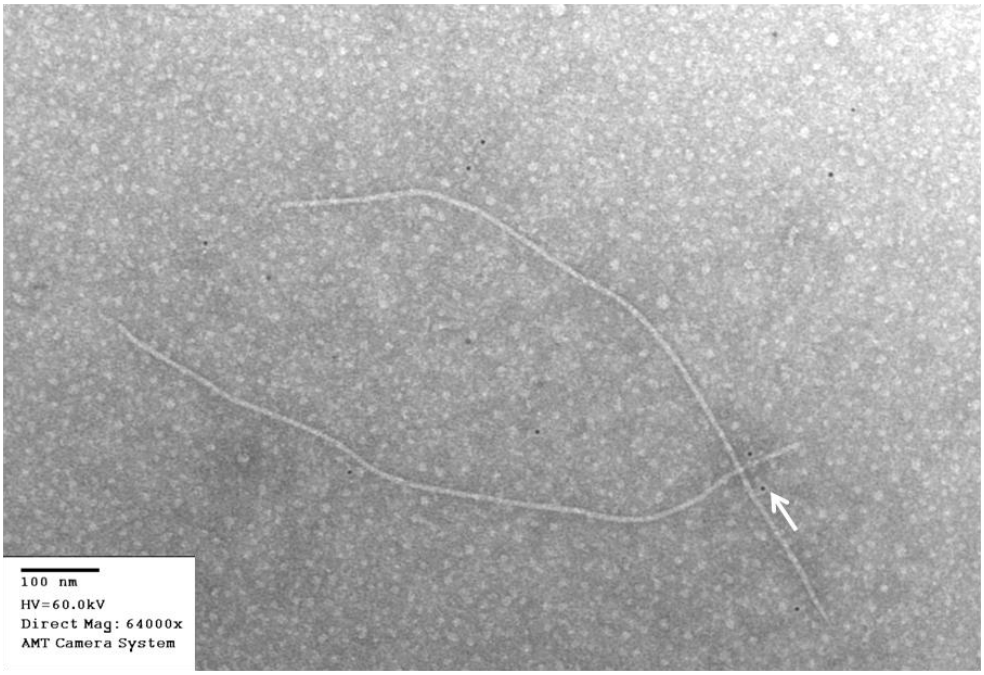

Figure 4.17: TEM micrograph of M-5/28L M13 grown with 10 mM Aha. This sample was reacted with DIBAC-biotin as outlined in the methods. The sample was prepared on a copper formvar grid which was blocked with BSA prior to stain with SA-AuNPs and 1% uranyl acetate. The white arrow shows a SA-AuNP.

Lastly, Wt M13 phages that had been grown in 10 mM Aha were reacted with DIBAC-biotin and incubated with SA-AuNPs as described above. Surprisingly, the integrity of the M13 structure itself appeared to be compromised by this treatment (**Figure 4.18**). M13 was normally observed to be fairly linear on TEM images taken, with some flexibility and slight bending. Only limited flexibility is typically expected for M13 phages (95). In these images the particles appeared to have a number of sharp bends that might suggest disruption of M13 tertiary structure. As with the dye-labelling experiments, a percentage of pVIII-Aha subunits on Wt M13 were apparently available for labelling. In this case, labelling of pVIII at Met28 may have disrupted the usually stable interactions between pVIII monomers resulting in these observed perturbations in structure. Since Met28 is near where pVIII subunits overlap, having biotin attached there might have interfered with packing of subunits. Counting the number of SA-AuNPs per Wt M13 in these samples was difficult due to inability to distinguish whether an observed particle was a single phage, or several tangled together. Therefore, only phages that could be definitively

identified as a single M13 particle were counted to determine an average AuNP-loading of 8 AuNPs per Wt M13 bacteriophage. In agreement with the dye-labelling results, the number of AuNPs associated with each Wt M13 particle was less than that observed for A9M or S13M constructs. Furthermore, since modification at Met28 appeared to affect the tertiary structure of M13, the repositioning of methionine in A9M and S13M was certainly required for engineering scaffolds that could be modified without perturbations to their structure.

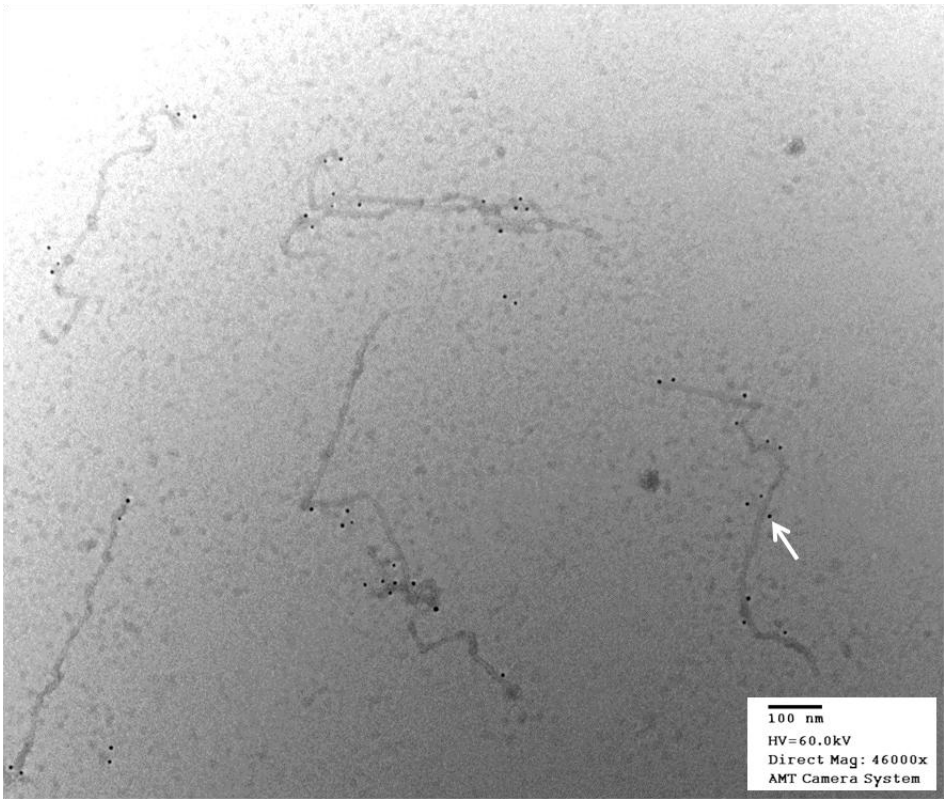

Figure 4.18: TEM micrograph of Wt M13 grown with 10 mM Aha. This sample was reacted with DIBAC-biotin as outlined in the methods. The sample was prepared on a copper formvar grid which was blocked with BSA prior to stain with SA-AuNPs and 1% uranyl acetate. The white arrow shows a SA-AuNP.

In summary, the TEM results indicated definitively the capability of the M13-Aha constructs engineered in this dissertation work to template the organization of inorganic molecules onto M13. The distribution of the pVIII-Aha were estimated to be even along the 1D length of M13 from these images. The loading of SA-AuNPs relied on actual incorporation of Aha into pVIII, rather than just its presence in the growth media, as indicated in the experiments with M-5/28L phages. The distributions of the number of SA-AuNPs per phage were similar for A9M and S13M mutants (**Figure 4.19**). These distributions

were quite wide with the occasional outliers observed in the TEM micrographs with lower than expected AuNPs bound. Rather than being due to lack of pVIII-Aha in those particles, it is possible that the TEM grid preparation procedure used to prepare AuNP-templated M13 was not fully optimized. Some examples of parameters that might be optimized to produce more uniformly templated M13 might include incubation time with AuNPs, concentration of AuNP solution used and concentration of BSA used to block the grid. In the M-5/28L control, the SA-AuNPs that were associated with the M13 particles were likely non-specifically bound. Better optimization of TEM grid preparation might be expected to reduce the non-specifically bound SA-AuNPs observed in this control. Overall, this was a successful demonstration of the capabilities of these engineered constructs to organize and selectively bind large particles.

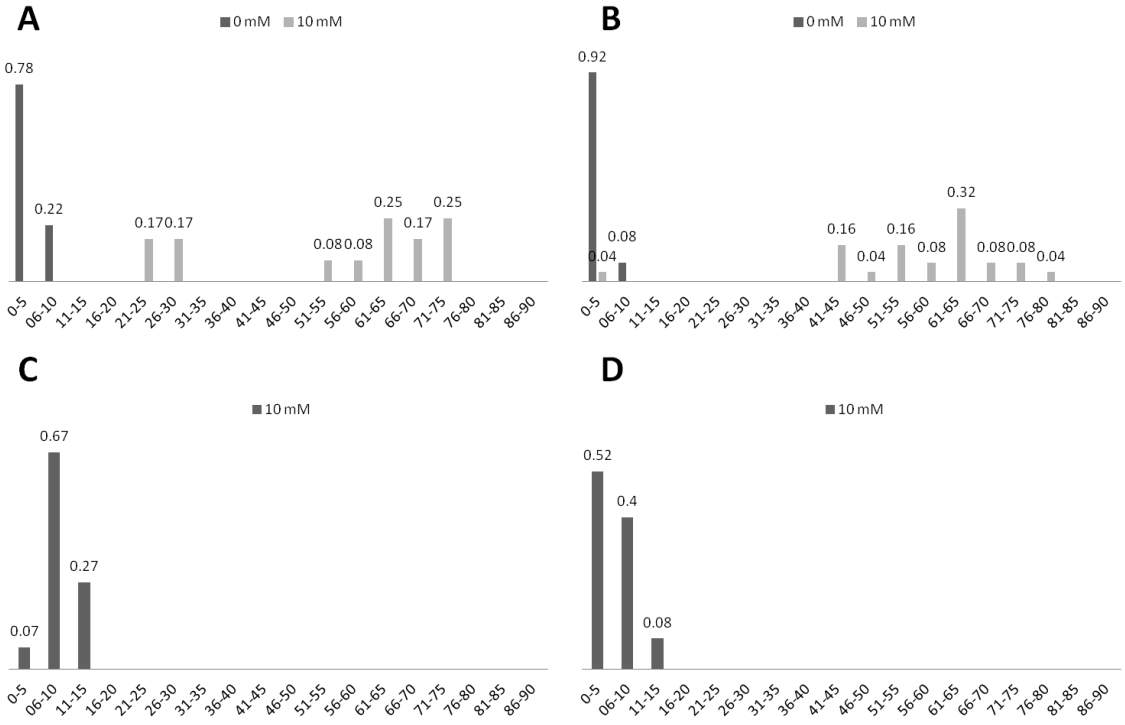

Figure 4.19: Histogram of the number of SA-AuNPs observed per M13 phage strain after reaction with DIBAC-biotin and imaging by TEM. The strains used were (A) A9M (B) S13M (C) WT 10 mM Aha (D) M-5/28L 10 mM Aha samples. The bars are expressed as frequencies of at least n=9 M13 particles counted per dataset. The legends in the figure indicate whether the M13 phages were grown with 10 mM Aha.

4.4 Summary of chapter

In developing a robust and modular scaffold one needs to be sure of the quantities of functional groups present and of the structure of the scaffold itself. The structure of un-modified M13 has been well-studied. In particular, the structural studies done by Marvin, D.A. are very detailed with respect to the geometry, symmetry and packing of pVIII subunits in M13 (74). In the current research for this thesis, it was confirmed that the overall structures of engineered mutants, A9M and S13M M13, were largely unaffected by reaction via the SPAAC reaction. In addition, it was determined in this section that using the growth conditions developed in this thesis work for Aha incorporation, one can achieve approximately 340 reactive azides groups per phage scaffold. It is expected that further optimization and experimentation with Aha:methionine ratios could allow one to fine-tune the exact number of presented azides for application of these scaffolds. The characterization of these M13-Aha scaffolds highlights the importance of re-positioning the methionine residue on pVIII. In Wt pVIII both the degree of labelling possible and the structure of the phage scaffold itself were negatively impacted by the position of Aha at Met28. It is expected that utilizing the SPAAC reaction to label M13-Aha scaffolds will furthermore be complementary and orthogonal to other commonly used M13 modifications including peptide fusions and chemical reactions with the naturally occurring amino acids found in M13.

5. Chapter 5 - Summary and future outlook

A series of *E. coli* ER2738 and M13 mutants were constructed in order to generate a phage replication system capable of Aha incorporation into the pVIII coat protein. Of the *E. coli* mutants constructed, only ER2738 MetE was found suitable as a host for M13 replication. The M13 mutants were all very tolerant to the mutations made in this study. Mass spectrometry data was used to confirm incorporation of Aha into Wt, A9M and S13M mutants. It was found that Aha could be incorporated into 10-11 % of pVIII subunits and that these displayed azides could specifically react via the strain-promoted azide-alkyne cycloaddition (**SPAAC**) reaction. The Wt M13-Aha constructs reacted via the SPAAC reaction to a lesser extent than either A9M or S13M, suggesting that availability of the azide at Met28 was low. This highlights the importance of repositioning the methionine residue on pVIII and the construction of A9M and S13M strains.

Conjugation of either 5(6)-carboxytetramethylrhodamine or biotin via the SPAAC reaction to M13-Aha constructs was also confirmed by analyzing mass spectrometric data. The Staudinger ligation was not as suitable for labelling these M13-Aha constructs. At 24 hours of reaction, the modified Staudinger ligation left a considerable amount of pVIII-Aha detected by analysis of the mass spectrometric data. It is likely that a higher concentration of M13-Aha or longer reaction times would be required for complete reaction via the modified Staudinger ligation. Neither of these requirements were desirable and the SPAAC reaction was easily carried out as an alternative. Lastly, the spatial distribution of pVIII-Aha subunits were assessed indirectly by transmission electron microscopy. It was found that pVIII-Aha subunits were evenly distributed along the length of M13. Additionally, it was found that there was an upper limit to the number of 5 nm gold nanoparticles that could be loaded onto each M13 phage due to steric and potential electrostatic considerations.

This thesis work is expected to provide the necessary information for use of these M13-Aha constructs in either bionanotechnology, or synthetic biology applications. Importantly, this report highlights the first instance of Aha incorporation into pVIII with bioorthogonal labelling capabilities.

Therefore, it would be sensible for future work to explore the capabilities of dual-labelling of M13-Aha constructs. It is expected that the azide-specific chemistry used to label Aha residues would be orthogonal to reactions with lysine residues, or N-termini for example. The ability to prepare M13-Aha constructs with pIII-fusions would also be of interest. As specified previously in this dissertation, the ability to separately engineer affinity peptides onto pIII can be done by molecular biological methods. The only foreseeable limitation to doing this might be that peptides engineered onto pIII that contain methionine might be impacted by global incorporation of Aha. This problem would only be expected to occur on a case-by-case basis. The advantage of separately manipulating pIII could be for the introduction of a motif that has affinity for a particular type of inorganic surface or cell type, allowing M13-Aha to be directed to a select area of interest. Labelling of pVIII-Aha via the SPAAC reaction could be carried out either before or after such targeting.

While a solid framework for M13-Aha is described in this thesis, there is considerable room for optimization. Areas for optimization can be distinctly separated into modifications to the host organism and modification to the replication conditions. With regards to the host bacterium, previous work has suggested that over-expression of methionyl tRNA synthetase (**MetRS**) can improve unnatural amino acid (**UAA**) incorporation for Aha (35). By transforming MetRS encoded on an expression plasmid into ER2738 MetE this could be accomplished. Furthermore, whether these M13 constructs might be applied to incorporation of *L*-azidonorleucine (**Anl**) could also be explored. The reason for expanding the approaches for engineering azide-bearing phages to include Anl are due to reports of mutant MetRS with enhanced specificity to Anl (97). Using the A9M and S13M M13 mutants generated here, this approach could result in higher azide content along the length of M13 constructs.

With the replication system described here with Aha, further optimization is still possible though. A wider range of Aha concentration in the media has not been explored, and could be one avenue by which incorporation efficiency could be increased. Experimentally examining the incorporation efficiencies obtained at different Aha concentrations might allow construction of a standard curve. A standard curve for Aha incorporation as a function of Aha concentration in growth media would be a

valuable tool for researchers utilizing the M13-Aha constructs described here, as it would allow one to engineer a known quantity of azide moieties onto M13. Overall, the construction of Aha-containing M13 bacteriophages was successfully accomplished in this research. It is expected that, as tool, these M13-Aha will complement the applications of M13 to technology already under study and allow for novel applications of M13 nano-scale scaffolds.

References

1. Seeman, N.C., and Belcher, A.M. (2002) Emulating biology: Building nanostructures from the bottom up. *Proc. Natl. Acad. Sci. U.S.A.* **99,** 6451-6455

2. Kuzuya, A., Sakai, Y., Yamazaki, T., Xu, Y., and Komiyama, M. (2011) Nanomechanical DNA origami 'single-molecule beacons' directly imaged by atomic force microscopy. *Nat. Commun.* **2,** 449

3. Uster, P.S., Working, P.K., and Vaage, J. (1998) Pegylated liposomal doxorubicin (DOXIL (R), CAELYX (R)) distribution in tumour models observed with confocal laser scanning microscopy. *Int. J. Pharm.* **162,** 77-86

4. Yu, S.M. (2012) PIEZOELECTRIC DEVICES Squeezed virus produces electricity. *Nat. Nanotechnol.* **7,** 343-344

5. Lee, L.A., Niu, Z., and Wang, Q. (2009) Viruses and Virus-Like Protein Assemblies-Chemically Programmable Nanoscale Building Blocks. *Nano Res.* **2,** 349-364

6. Mao, C.B., Solis, D.J., Reiss, B.D., Kottmann, S.T., Sweeney, R.Y., Hayhurst, A., Georgiou, G., Iverson, B., and Belcher, A.M. (2004) Virus-based toolkit for the directed synthesis of magnetic and semiconducting nanowires. *Science.* **303,** 213-217

7. Nam, K.T., Kim, D.W., Yoo, P.J., Chiang, C.Y., Meethong, N., Hammond, P.T., Chiang, Y.M., and Belcher, A.M. (2006) Virus-enabled synthesis and assembly of nanowires for lithium ion battery electrodes. *Science.* **312,** 885-888

8. Chiang, C., Mello, C.M., Gu, J., Silva, E.C.C.M., Van Vliet, K.J., and Belcher, A.M. (2007) Weaving genetically engineered functionality into mechanically robust virus fibers. *Adv. Mater.* **19,** 826-832

9. Jeong, C.K., Kim, I., Park, K., Oh, M.H., Paik, H., Hwang, G., No, K., Nam, Y.S., and Lee, K.J. (2013) Virus-Directed Design of a Flexible BaTiO3 Nanogenerator. *ACS Nano.* **7,** 11016-11025

10. Lee, B.Y., Zhang, J., Zueger, C., Chung, W., Yoo, S.Y., Wang, E., Meyer, J., Ramesh, R., and Lee, S. (2012) Virus-based piezoelectric energy generation. *Nat. Nanotechnol.* **7,** 351-356

11. Murugesan, M., Abbineni, G., Nimmo, S.L., Cao, B., and Mao, C. (2013) Virus-based Photo-Responsive Nanowires Formed By Linking Site-Directed Mutagenesis and Chemical Reaction. *Sci. Rep.* **3,** 1820

12. Chen, P., Dang, X., Klug, M.T., Qi, J., Courchesne, N.D., Burpo, F.J., Fang, N., Hammond, P.T., and Belcher, A.M. (2013) Versatile Three-Dimensional Virus-Based Template for Dye-Sensitized Solar Cells with Improved Electron Transport and Light Harvesting. *ACS Nano.* **7,** 6563-6574

13. Marvin, D.A. (1998) Filamentous phage structure, infection and assembly. *Curr. Opin. Struct. Biol.* **8,** 150-158

14. Ippenihler, K., and Minkley, E. (1986) The Conjugation System of F, the Fertility Factor of Escherichia-Coli. *Annu. Rev. Genet.* **20,** 593-624

15. Rakonjac, J., Bennett, N.J., Spagnuolo, J., Gagic, D., and Russel, M. (2011) Filamentous Bacteriophage: Biology, Phage Display and Nanotechnology Applications. *Curr. Issues Mol. Biol.* **13,** 51-75

16. Marvin, D.A., Hale, R.D., Nave, C., and Citterich, M.H. (1994) Molecular-Models and Structural Comparisons of Native and Mutant Class-i Filamentous Bacteriophages Ff (Fd, F1, M13), If1 and Ike. *J. Mol. Biol.* **235,** 260-286

17. Stopar, D., Spruijt, R.B., Wolfs, C.J.A.M., and Hemminga, M.A. (1998) Mimicking initial interactions of bacteriophage M13 coat protein disassembly in model membrane systems. *Biochemistry.* **37,** 10181-10187

18. Gao, C.S., Mao, S.L., Lo, C.H.L., Wirsching, P., Lerner, R.A., and Janda, K.D. (1999) Making artificial antibodies: A format for phage display of combinatorial heterodimeric arrays. *Proc. Natl. Acad. Sci. U.S.A.* **96,** 6025-6030

19. Armstrong, J., Perham, R., and Walker, J. (1981) Domain-Structure of Bacteriophage Fd Adsorption Protein. *FEBS Lett.* **135,** 167-172

20. Click, E., and Webster, R. (1997) Filamentous phage infection: Required interactions with the TolA protein. *J. Bacteriol.* **179,** 6464-6471

21. Bennett, N., and Rakonjac, J. (2006) Unlocking of the filamentous bacteriophage virion during infection is mediated by the C domain of pill. *J. Mol. Biol.* **356,** 266-273

22. Smith, G.P. (1985) Filamentous Fusion Phage - Novel Expression Vectors that Display Cloned Antigens on the Virion Surface. *Science.* **228,** 1315-1317

23. Parmley, S., and Smith, G. (1988) Antibody-Selectable Filamentous Fd Phage Vectors - Affinity Purification of Target Genes. *Gene.* **73,** 305-318

24. Smith, G., and Petrenko, V. (1997) Phage display. *Chem. Rev.* **97,** 391-410

25. Su, Z., Leung, T., and Honek, J.F. (2006) Conformational selectivity of peptides for single-walled carbon nanotubes. *J. Phys. Chem. B.* **110,** 23623-23627

26. Wang, S., Humphreys, E., Chung, S., Delduco, D., Lustig, S., Wang, H., Parker, K., Rizzo, N., Subramoney, S., Chiang, Y., and Jagota, A. (2003) Peptides with selective affinity for carbon nanotubes. *Nat. Mater.* **2,** 196-200

27. Whaley, S., English, D., Hu, E., Barbara, P., and Belcher, A. (2000) Selection of peptides with semiconductor binding specificity for directed nanocrystal assembly. *Nature.* **405,** 665-668

28. DALBEY, R. (1991) Leader Peptidase. *Mol. Microbiol.* **5,** 2855-2860

29. Williams, K., Glibowicka, M., Li, Z., Li, H., Khan, A., Chen, Y., Wang, J., Marvin, D., and Deber, C. (1995) Packing of Coat Protein Amphipathic and Transmembrane Helices in Filamentous Bacteriophage-M13 - Role of Small Residues in Protein Oligomerization. *J. Mol. Biol.* **252,** 6-14

30. Roth, T.A., Weiss, G.A., Eigenbrot, C., and Sidhu, S.S. (2002) A minimized M13 coat protein defines the requirements for assembly into the bacteriophage particle. *J. Mol. Biol.* **322,** 357-367

31. Mao, J.Y., Belcher, A.M., and Van Vliet, K.J. (2010) Genetically Engineered Phage Fibers and Coatings for Antibacterial Applications. *Adv. Funct. Mater.* **20,** 209-214

32. Duewel, H.S., Daub, E., Robinson, V., and Honek, J.F. (2001) Elucidation of solvent exposure, side-chain reactivity, and steric demands of the trifluoromethionine residue in a recombinant protein. *Biochemistry.* **40,** 13167-13176

33. Yoo, T.H., Link, A.J., and Tirrell, D.A. (2007) Evolution of a fluorinated green fluorescent protein. *Proc. Natl. Acad. Sci. U.S.A.* **104,** 13887-13890

34. Taskent-Sezgin, H., Chung, J., Banerjee, P.S., Nagarajan, S., Dyer, R.B., Carrico, I., and Raleigh, D.P. (2010) Azidohomoalanine: A Conformationally Sensitive IR Probe of Protein Folding, Protein Structure, and Electrostatics. *Angew. Chem. Int. Edit.* **49,** 7473-7475

35. Kiick, K.L., Saxon, E., Tirrell, D.A., and Bertozzi, C.R. (2002) Incorporation of azides into recombinant proteins for chemoselective modification by the Staudinger ligation. *Proc. Natl. Acad. Sci. U.S.A.* **99,** 19-24

36. Dieterich, D., Link, A., Graumann, J., Tirrell, D., and Schuman, E. (2006) Selective identification of newly synthesized proteins in mammalian cells using bioorthogonal noncanonical amino acid tagging (BONCAT). *Proc. Natl. Acad. Sci. U.S.A.* **103,** 9482-9487

37. Johnson, D.B.F., Wang, C., Xu, J., Schultz, M.D., Schmitz, R.J., Ecker, J.R., and Wang, L. (2012) Release Factor One Is Nonessential in Escherichia coli. *ACS Chem. Biol.* **7,** 1337-1344

38. Noren, C., Anthonycahill, S., Griffith, M., and Schultz, P. (1989) A General-Method for Site-Specific Incorporation of Unnatural Amino-Acids into Proteins. *Science.* **244,** 182-188

39. Liu, D., and Schultz, P. (1999) Progress toward the evolution of an organism with an expanded genetic code. *Proc. Natl. Acad. Sci. U.S.A.* **96,** 4780-4785

40. Feng, T., Tsao, M., and Schultz, P. (2004) A phage display system with unnatural amino acids. *J. Am. Chem. Soc.* **126,** 15962-15963

41. Wang, K., Neumann, H., Peak-Chew, S.Y., and Chin, J.W. (2007) Evolved orthogonal ribosomes enhance the efficiency of synthetic genetic code expansion. *Nat. Biotechnol.* **25,** 770-777

42. Kiick, K., Weberskirch, R., and Tirrell, D. (2001) Identification of an expanded set of translationally active methionine analogues in Escherichia coli. *FEBS Lett.* **502,** 25-30

43. Voloshchuk, N., and Montclare, J.K. (2010) Incorporation of unnatural amino acids for synthetic biology. *Mol. Biosyst.* **6,** 65-80

44. van Hest, J., Kiick, K., and Tirrell, D. (2000) Efficient incorporation of unsaturated methionine analogues into proteins in vivo. *J. Am. Chem. Soc.* **122,** 1282-1288

45. Vaughan, M.D., Cleve, P., Robinson, V., Duewel, H.S., and Honek, J.F. (1999) Difluoromethionine as a novel F-19 NMR structural probe for internal amino acid packing in proteins. *J. Am. Chem. Soc.* **121,** 8475-8478

46. Lin, Y.A., Chalker, J.M., Floyd, N., Bernardes, G.J.L., and Davis, B.G. (2008) Allyl sulfides are privileged substrates in aqueous cross-metathesis: Application to site-selective protein modification. *J. Am. Chem. Soc.* **130,** 9642-9643

47. Bottomley, M., Robinson, R., Driscoll, P., Harlos, K., Stuart, D., Aplin, R., Clements, J., Jones, E., and Dudgeon, T. (1994) Crystallization and Preliminary-X-Ray Diffraction Characterization of both a Native and Selenomethionyl Vla-4 Binding Fragment of Vcam-1. *J. Mol. Biol.* **244,** 464-468

48. Banerjee, P.S., Ostapchuk, P., Hearing, P., and Carrico, I.S. (2011) Unnatural Amino Acid Incorporation onto Adenoviral (Ad) Coat Proteins Facilitates Chemoselective Modification and Retargeting of Ad Type 5 Vectors. *J. Virol.* **85,** 7546-7554

49. Sen Gupta, S., Kuzelka, J., Singh, P., Lewis, W., Manchester, M., and Finn, M. (2005) Accelerated bioorthogonal conjugation: A practical method for the Ligation of diverse functional molecules to a polyvalent virus scaffold. *Bioconjug. Chem.* **16,** 1572-1579

50. Saxon, E., and Bertozzi, C. (2000) Cell surface engineering by a modified Staudinger reaction. *Science.* **287,** 2007-2010

51. Debets, M.F., van Berkel, S.S., Schoffelen, S., Rutjes, F.P.J.T., van Hest, J.C.M., and van Delft, F.L. (2010) Aza-dibenzocyclooctynes for fast and efficient enzyme PEGylation via copper-free (3+2) cycloaddition. *Chem. Commun.* **46,** 97-99

52. Tang, Y., and Tirrell, D. (2002) Attenuation of the editing activity of the Escherichia coli Leucyl-tRNA synthetase allows incorporation of novel amino acids into proteins in vivo. *Biochemistry.* **41,** 10635-10645

53. Gaetke, L., and Chow, C. (2003) Copper toxicity, oxidative stress, and antioxidant nutrients. *Toxicology.* **189,** 147-163

54. Worrell, B.T., Malik, J.A., and Fokin, V.V. (2013) Direct Evidence of a Dinuclear Copper Intermediate in Cu(I)-Catalyzed Azide-Alkyne Cycloadditions. *Science.* **340**, 457-460

55. Rostovtsev, V., Green, L., Fokin, V., and Sharpless, K. (2002) A stepwise Huisgen cycloaddition process: Copper(I)-catalyzed regioselective "ligation" of azides and terminal alkynes. *Angew. Chem. Int. Edit.* **41,** 2596-2599

56. Hong, V., Presolski, S.I., Ma, C., and Finn, M.G. (2009) Analysis and Optimization of Copper-Catalyzed Azide-Alkyne Cycloaddition for Bioconjugation. *Angew. Chem. Int. Edit.* **48,** 9879-9883

57. van Kasteren, S.I., Kramer, H.B., Jensen, H.H., Campbell, S.J., Kirkpatrick, J., Oldham, N.J., Anthony, D.C., and Davis, B.G. (2007) Expanding the diversity of chemical protein modification allows post-translational mimicry. *Nature.* **446,** 1105-1109

58. Prescher, J., and Bertozzi, C. (2005) Chemistry in living systems. *Nat. Chem. Biol.* **1,** 13-21

59. Tam, A., and Raines, R.T. (2009) Protein Engineering with the Traceless Staudinger Ligation. *Methods Enzymol.* **462,** 25-44

60. Sletten, E.M., and Bertozzi, C.R. (2011) From Mechanism to Mouse: A Tale of Two Bioorthogonal Reactions. *Acc. Chem. Res.* **44,** 666-676

61. Agard, N., Prescher, J., and Bertozzi, C. (2004) A strain-promoted [3+2] azide-alkyne cycloaddition for covalent modification of blomolecules in living systems. *J. Am. Chem. Soc.* **126,** 15046-15047

62. Bernardin, A., Cazet, A., Guyon, L., Delannoy, P., Vinet, F., Bonnaffe, D., and Texier, I. (2010) Copper-Free Click Chemistry for Highly Luminescent Quantum Dot Conjugates: Application to in Vivo Metabolic Imaging. *Bioconjug. Chem.* **21,** 583-588

63. Ng, S., Jafari, M.R., and Derda, R. (2012) Bacteriophages and Viruses as a Support for Organic Synthesis and Combinatorial Chemistry. *ACS Chem. Biol.* **7,** 123-138

64. Lim, R.K.V., Li, N., Ramil, C.P., and Lin, Q. (2014) Fast and Sequence-Specific Palladium-Mediated Cross-Coupling Reaction Identified from Phage Display. *ACS Chem Biol.* **9,** 2139-2148

65. Woodcock, D.M., Crowther, P.J., Doherty, J., Jefferson, S., Decruz, E., Noyerweidner, M., Smith, S.S., Michael, M.Z., and Graham, M.W. (1989) Quantitative-Evaluation of Escherichia-Coli Host Strains for Tolerance to Cytosine Methylation in Plasmid and Phage Recombinants. *Nucleic Acids Res.* **17,** 3469-3478

66. Baba, T., Ara, T., Hasegawa, M., Takai, Y., Okumura, Y., Baba, M., Datsenko, K.A., Tomita, M., Wanner, B.L., and Mori, H. (2006) Construction of Escherichia coli K-12 in-frame, single-gene knockout mutants: the Keio collection. *Mol. Syst. Biol.* **2,** 2006.0008

67. Ploss, M., and Kuhn, A. (2010) Kinetics of filamentous phage assembly. *Phys. Biol.* **7,** 045002

68. Wall, J.D., and Harriman, P.D. (1974) Phage-P1 Mutants with Altered Transducing Abilities for Escherichia-Coli. *Virology.* **59,** 532-544

69. Caspi, R., Altman, T., Billington, R., Dreher, K., Foerster, H., Fulcher, C.A., Holland, T.A., Keseler, I.M., Kothari, A., Kubo, A., Krummenacker, M., Latendresse, M., Mueller, L.A., Ong, Q., Paley, S., Subhraveti, P., Weaver, D.S., Weerasinghe, D., Zhang, P., and Karp, P.D. (2014) The MetaCyc database of metabolic pathways and enzymes and the BioCyc collection of Pathway/Genome Databases. *Nucleic Acids Res.* **42,** D459-D471

70. Born, T., and Blanchard, J. (1999) Enzyme-catalyzed acylation of homoserine: Mechanistic characterization of the Escherichia coli metA-encoded homoserine transsuccinylase. *Biochemistry.* **38,** 14416-14423

71. Patrick, W.M., Quandt, E.M., Swartzlander, D.B., and Matsumura, I. (2007) Multicopy suppression underpins metabolic evolvability. *Mol. Biol. Evol.* **24,** 2716-2722

72. Ruckert, C., Puhler, A., and Kalinowski, J. (2003) Genome-wide analysis of the L-methionine biosynthetic pathway in Corynebacterium glutamicum by targeted gene deletion and homologous complementation. *J. Biotechnol.* **104,** 213-228

73. Borg, S. (2010) Expanding phage peptide libraries by incorporation of azidohomoalanine and use in nanotechnological applications. MSc dissertation, University of Waterloo, Waterloo, Canada

74. Marvin, D.A., Welsh, L.C., Symmons, M.F., Scott, W.R.P., and Straus, S.K. (2006) Molecular structure of fd (f1, M13) filamentous bacteriophage refined with respect to X-ray fibre diffraction and solid-state NMR data supports specific models of phage assembly at the bacterial membrane. *J. Mol. Biol.* **355,** 294-309

75. Jensen, M.A., Fukushima, M., and Davis, R.W. (2010) DMSO and Betaine Greatly Improve Amplification of GC-Rich Constructs in De Novo Synthesis. *Plos One.* **5,** e11024

76. Kibbe, W.A. (2007) OligoCalc: an online oligonucleotide properties calculator. *Nucleic Acids Res.* **35,** W43-W46

77. Shen, L., Lee, J., Cheng, S., Jutte, H., Kuhn, A., and Dalbey, R. (1991) Use of Site-Directed Mutagenesis to Define the Limits of Sequence Variation Tolerated for Processing of the M13 Procoat Protein by the Escherichia-Coli Leader Peptidase. *Biochemistry.* **30,** 11775-11781

78. Schaegger, H. (2006) Tricine-SDS-PAGE. *Nat. Protoc.* **1,** 16-22

79. Vanwezenbeek, P.M.G.F., Hulsebos, T.J.M., and Schoenmakers, J.G.G. (1980) Nucleotide-Sequence of the Filamentous Bacteriophage M13-Dna Genome - Comparison with Phage-Fd. *Gene.* **11,** 129-148

80. Gailus, V., and Rasched, I. (1994) The Adsorption Protein of Bacteriophage-Fd and its Neighbor Minor Coat Protein Build a Structural Entity. *Eur. J. Biochem.* **222,** 927-931

81. Kramer, G., Sprenger, R.R., Back, J., Dekker, H.L., Nessen, M.A., van Maarseveen, J.H., de Koning, L.J., Hellingwerf, K.J., de Jong, L., and de Koster, C.G. (2009) Identification and Quantitation of Newly Synthesized Proteins in Escherichia coli by Enrichment of Azidohomoalanine-labeled Peptides with Diagonal Chromatography. *Mol. Cell. Proteomics.* **8,** 1599-1611

82. Walasek, P., and Honek, J.F. (2005) Nonnatural amino acid incorporation into the methionine 214 position of the metzincin Pseudomonas aeruginosa alkaline protease. *BMC biochem.* **6,** 21-21

83. Schmidt, A., Karas, M., and Dulcks, T. (2003) Effect of different solution flow rates on analyte ion signals in nano-ESI MS, or: When does ESI turn into nano-ESI?. *J. Am. Soc. Mass Spectrom.* **14,** 492-500

84. Li, K., Chen, Y., Li, S., Huong Giang Nguyen, Niu, Z., You, S., Mello, C.M., Lu, X., and Wang, Q. (2010) Chemical Modification of M13 Bacteriophage and Its Application in Cancer Cell Imaging. *Bioconjug. Chem.* **21,** 1369-1377

85. Doria, G., Conde, J., Veigas, B., Giestas, L., Almeida, C., Assuncao, M., Rosa, J., and Baptista, P.V. (2012) Noble Metal Nanoparticles for Biosensing Applications. *Sensors.* **12,** 1657-1687

86. Berkowitz, S., and Day, L. (1976) Mass, Length, Composition and Structure of Filamentous Bacterial Virus Fd. *J. Mol. Biol.* **102,** 531-547

87. Bardhan, N.M., Ghosh, D., and Belcher, A.M. (2014) M13 Virus based detection of bacterial infections in living hosts. *J. Biophotonics.* **7,** 617-623

88. Velappan, N., Fisher, H.E., Pesavento, E., Chasteen, L., D'Angelo, S., Kiss, C., Longmire, M., Pavlik, P., and Bradbury, A.R.M. (2010) A comprehensive analysis of filamentous phage display vectors for cytoplasmic proteins: an analysis with different fluorescent proteins. *Nucleic Acids Res.* **38,** e22

89. Mourez, M. and Collier, R.J.. (2004) Use of Phage Display and Polyvalency to Design Inhibitors of Protein-Protein Interactions. In: Fu, H., Protein-Protein Interactions. Methods and applications. Totowa, NJ: Humana Press, pp. 213-227

90. Day, L.A. and Wiseman, R.L.. (1978) A comparison of DNA packaging in the virions of fd, Xf, and Pf1. In: Denhardt, D.T., Dressler, D. and Ray, D.S., The Single-Stranded DNA Phages. Cold Spring Harbor, NY: CSH Laboratory Press, pp. 605–625

91. Sambrook, J., E.F. Fritsch, and T. Maniatis. (1989) Molecular Cloning: A Laboratory Manual, 2nd ed. Cold Spring Harbor, NY: CSH Laboratory Press.

92. Ravdin, P., and Axelrod, D. (1977) Fluorescent Tetramethyl Rhodamine Derivatives of Alpha-Bungarotoxin - Preparation, Separation, and Characterization. *Anal. Biochem.* **80,** 585-592

93. Hao, J., Huang, L., Zhang, R., Wang, H., and Xie, H. (2012) A Mild and Reliable Method to Label Enveloped Virus with Quantum Dots by Copper-Free Click Chemistry. *Anal. Chem.* **84,** 8364-8370

94. Lungu, O.I., Hallett, R.A., Choi, E.J., Aiken, M.J., Hahn, K.M., and Kuhlman, B. (2012) Designing Photoswitchable Peptides Using the AsLOV2 Domain. *Chem. Biol.* **19,** 507-517

95. Beck, K., and Duenki, R.M. (1990) Flexibility of Bacteriophage-M13 - Comparison of Hydrodynamic Measurements with Electron-Microscopy. *J. Struct. Biol.* **105,** 22-27

96. Murali, V.K., Ornelles, D.A., Gooding, L.R., Wilms, H.T., Huang, W., Tollefson, A.E., Wold, W.S.M., and Garnett-Benson, C. (2014) Adenovirus Death Protein (ADP) Is Required for Lytic Infection of Human Lymphocytes. *J. Virol.* **88,** 903-912

97. Tanrikulu, I.C., Schmitt, E., Mechulam, Y., Goddard, W.A.,III, and Tirrell, D.A. (2009) Discovery of Escherichia coli methionyl-tRNA synthetase mutants for efficient labeling of proteins with azidonorleucine in vivo. *Proc. Natl. Acad. Sci. U.S.A.* **106,** 15285-15290

98. De Carlo, S., and Harris, J.R. (2011) Negative staining and cryo-negative staining of macromolecules and viruses for TEM. *Micron.* **42,** 117-131

99. Diamandis, E., and Christopoulos, T. (1991) The Biotin (Strept)avidin System - Principles and Applications in Biotechnology. *Clin. Chem.* **37,** 625-636